Stable Isotopes and Mineralogy of Ordovician Clays, Southern Ontario, Canada in a Proposed Deep Geological Repository

Skylar Chauvin

A thesis submitted in partial fulfillment of the requirements for the
Master's degree in Earth Sciences Specializing in Chemical and Environmental Toxicology

Department of Earth and Environmental Sciences
Faculty of Science
University of Ottawa

Abstract

The mineralogy, thermogravimetric behaviour, and δ^2H and $\delta^{18}O$ of <2μm size-fractions of Ordovician shales were analyzed from three different locations near Kincardine, Ontario. This location is the proposed site for a Deep Geologic Repository (DGR) for Low & Intermediate Level Waste. Based on powder X-ray diffraction (pXRD), the <2μm size-fraction of each unit was dominated by illite, with smaller amounts of kaolinite, and still smaller quantities of chlorite. Thermogravimetric analysis (TGA) undertaken *in vacuo* revealed multi-step weight loss patterns for these clay assemblages. Weight changes at the lowest temperatures were consistent with exchangeable cation-sensitive dehydration of surface-bound water. Stepped weight losses at higher temperatures were consistent with dehydroxylation patterns of illite, kaolinite and chlorite, as determined for standards from the Clay Mineral Society Source Clay Repository. These data guided removal of clay-bound surface water prior to extraction of hydroxyl group water when analyzing the oxygen and hydrogen isotope compositions of these low water-content shales. Clays in these Ordovician shales presumably formed during weathering of the east-coast Appalachian highlands of proto-North America. The δ^2H and $\delta^{18}O$ of the <2μm separates, however, do not plot on the clay weathering lines known for their major phases. This discrepancy is interpreted to indicate isotopic exchange (mostly of hydrogen) at temperatures typical of maximum burial at the DGR site (~90°C). The possibility of hydrogen isotope exchange between clay minerals and porewater in low water-content rocks has potential implications for preservation of original porewater isotopic compositions. This possibility should be tested in future work.

Epigraph

Shales contain water, you see
Whose isotopes rarely agree
On whence came the water
Either colder or hotter
Exchange just might be the key!

FJL

Acknowledgements

I am grateful to my co-supervisors. Ian Clark (University of Ottawa) and Fred Longstaffe (The University of Western Ontario) for the opportunities they have given me during this project. Without the initial trust that Dr. Ian Clark had in me, a young mathematician, there would have been nowhere for me to develop my scholarly abilities within a graduate school program at Ottawa – thank you Ian. Without Dr. Fred Longstaffe, I would not have had the opportunity to join his laboratory and NWMO program of research at Western, and without him I would not have completed it. Thank you for allowing me to continue in this program while still pursuing my personal development. Not to mention you also had a not so insignificant role in me meeting and falling in love with my soon-to-be wife.

Although supervisors are important, the boots on the ground deserve their own standing ovation. Their contributions ranged from teaching and trusting me with all the machinery, enabling me to run samples every 3 hours for 72 hours straight, to aiding in revivifying an old piece of machinery that has been passed around numerous MSc and PhD students. Here is a very unexhaustive list of such people: Kim Law, Grace Yau, Li Huang (all staff of Western's Laboratory for Stable Isotope Science), John Vanstone and Jon Aukema (both of Western's Chemistry electronics shop), Jon Jacobs (Western's Earth Sciences machine shop), and Yves Rambour (Western's Chemistry glass blowing shop).

This project was made possible by the generous funding provided by: Nuclear Waste Management Organization Grant – GS819 Project (FJL) and CRDPJ 477852 – 14 Project (IDC), NSERC Discovery Grant (FJL), Canada Research Chairs Program (FJL), Canada Foundation for Innovation (for infrastructure) (FJL) and Ontario Research Fund (for infrastructure) (FJL).

To my fiancée, if you're reading this it means it's almost over! You no longer have to deal with long nights with me stressfully thinking about isotopy, now it'll just be enjoyable thoughts on isotopy. You have been there to support me at all my hurdles, no matter how small. You've helped celebrate my wins and console my losses. Although Fred helped me succeed, you ensured I didn't fail, something that has made me love you even more.

Last but not least. To my family; my parents, my siblings and their partners and my in-laws to be: there are many things I could say but I am limited to a page, and thus in short, I say this: Thank you for not letting me quit.

Table of Contents

Figure List

Table List

Chapter 1. Introduction

1.1. Project Overview

The Ontario Power Generation (OPG) and the Nuclear Waste Management Organization have been exhaustively investigating the safe storage of the increasing volume of low and intermediate-level nuclear waste (L&ILW). In particular, several studies, using various techniques and methodologies and involving collaborators from various Canadian and international Universities have utilized the hydrogen and oxygen isotope measurements of porewater in order to create an isotopic profile of the proposed Deep Geologic Repository (DGR) in the Ordovician shales at the Bruce site, located near Kincardine in southern Ontario (Hobbs et al., 2008; Clark et al., 2010a,b ; Hobbs et al., 2011; Clark et al., 2013; Mazurek et al., 2013; Mazurek et al., 2015; De Haller et al., 2016). This isotopic profile has been created in order to examine the suitability (i.e., *safety*) of the geologic host formations for providing multiple natural barriers of stable rock that isolate the DGR and its contents from interaction with the overlying and underlying regions, especially aquifers and the surface environment. The oxygen and hydrogen isotope tracers can be used to identify whether meteoric water has percolated through fracture systems in the past, which would be indicative of an *unsafe* site. Likewise, such data can be used to test whether solute movement has been driven only by diffusion over long periods of geological time, which would be indicative of a *safe* location.

Accurate and precise measurements of the hydrogen and oxygen isotope compositions of porewater in low water content, low permeability rocks are very challenging. That said, the results of the currently completed isotopic studies of water movement support the viability of Ordovician shales beneath Kincardine, Ontario as a suitable location for a DGR. The specific results for hydrogen and oxygen isotope compositions of the extracted porewater obtained using

different methods, however, sometimes do not agree completely for some rock units (Mazurek et al., 2016). It would be useful to identify the potential cause(s) of these differences.

The initial motivation for this thesis was to determine whether the δ^2H and δ^{18}O of clay minerals have played a role in determining the isotopic composition of porewater in the Ordovician shale pore system. Such interaction might produce measurable differences in porewater isotopic compositions as a consequence of the very low volumetric water content (typically <5%) of the Ordovician shales. Extending this idea further, the fraction of porewater bound to clay minerals as opposed to remaining mobile or 'free' in the pore system might be sufficient to change the porewater isotopic composition depending the putative isotopic fractionation between bound and mobile porewater, and on the methods used to extract porewater for isotopic measurement and the water reservoirs that the various methods sample.

Longstaffe et al. (2017) posited that isotopic fractionation between the bound and mobile porewater and isotopic exchange with structural hydrogen and/or oxygen in clay minerals might be a contributing factor to the small differences in porewater isotopic compositions measured using different methods: (i) vacuum-distillation extraction (VDE) at the University of Ottawa, and (ii) adapted isotope diffusive exchange (AIDE) at the University of Bern. To extract porewater from the shales, the University of Ottawa developed a high-temperature (150°C) vacuum-distillation extraction (VDE) technique and its modified version known as micro-vacuum distillation extraction (μVDE). This method employs a completely closed-system sample system comprised of stainless-steel containers for sample milling fitted with high-temperature silicone septa from which extracted water is transferred directly to sample vials during the heating of the samples (Murseli et al., 2017). The University of Bern's adapted isotope diffusive exchange (AIDE) methodology is based on the diffusive exchange of water

isotopes via the vapour phase between the porewater of a rock sample and two test waters of known isotopic composition in two sealed containers at room temperatures (Hobbs et al., 2011). In this procedure there is no heating or crushing (i.e., direct extraction) of water from the sample.

To better understand how interaction with clay minerals might affect the hydrogen and oxygen isotope results for shale porewater, we have separated and characterized mineralogically and thermogravimetrically the <2μm size-fraction of Ordovician shale samples, both from the site of a proposed DGR located near Kincardine, Ontario, and from elsewhere in southern Ontario. We also examined reference clay minerals (illite, kaolinite, chlorite) obtained from the Clay Mineral Society (CMS) Source Clay Repository, which provide a baseline for clays present in the Ordovician shales. Such mineralogical and thermogravimetric characterization is needed to understand how variations in clay mineralogy and crystallinity might affect isotopic interaction with porewater. It is also required to determine the temperatures at which different fractions of water (adsorbed water, hydroxyl group water, etc.) might be released from the clay assemblages.

Having established the clay mineralogy and associated thermal properties, we examined whether isotopic exchange between clay minerals and porewater could produce the measured porewater hydrogen and oxygen isotope compositions of the Ordovician shales considered here. We modelled the possibility of such exchange at room temperature (25°C), as is utilized in AIDE, maximum burial temperatures posited for the units of interest at the DGR site (70°-90°C) and the maximum temperature (150°C) used to extract final fractions of porewater using VDE.

In short, the objectives of this thesis are:

1. Mineralogical and thermogravimetric characterization of the clay minerals from the Ordovician shales of southern Ontario, particularly those from the proposed Bruce Site DGR;

2. Hydrogen and oxygen isotope characterization of the Ordovician clay mineral assemblages;
3. Evaluation of the possibility of isotopic exchange between the Ordovician clay minerals and porewater during burial diagenesis, and
4. Identification of isotopic fractionation between water, either sorbed to clay surfaces or mobile porewater, and clay minerals, and potential consequences for porewater isotopic analysis.

As this thesis will demonstrate, progress was made concerning the first three objectives, but objective 4 remained elusive and will need to be pursued further in future work.

1.2. Nuclear Energy Research

Nuclear energy research in Canada and most of the world truly began in the mid-1900s (LLRWMO, 2012). Since then, over 2 million cubic meters of radioactive waste have been produced (LLRWMO, 2012). Since its development, nuclear energy has become an increasingly important energy source. In Ontario, for instance, 61% of yearly energy outputs are from nuclear sources (IESO, 2018). As a result of the dependency placed on nuclear energy, nuclear waste will continue to be produced, and its subsequent management will be an ongoing requirement (IESO, 2018). Currently, nuclear waste is managed through surficial storage techniques such as in spent fuel pools; however, increasing volumes of nuclear waste have made these older techniques impractical. As a result, a more recent and generally accepted method of storage invoke the use of a deep geological repository (DGR) (Figure 1.1).

Underground nuclear waste storage research was initiated in Sweden and studied at the Stripa Mine (Carlsson, 1986). Previous studies have commonly examined crystalline rock (Carlsson, 1986) and old salt mines (U.S. Department of Energy, 2000), but in recent years there has been a shift in research towards storage sites within sedimentary strata, specifically those of argillaceous composition, due to their low hydraulic conductivities (<1 x 10^{-14} m/s) and low volumetric water contents (Mazurek et al., 2016).

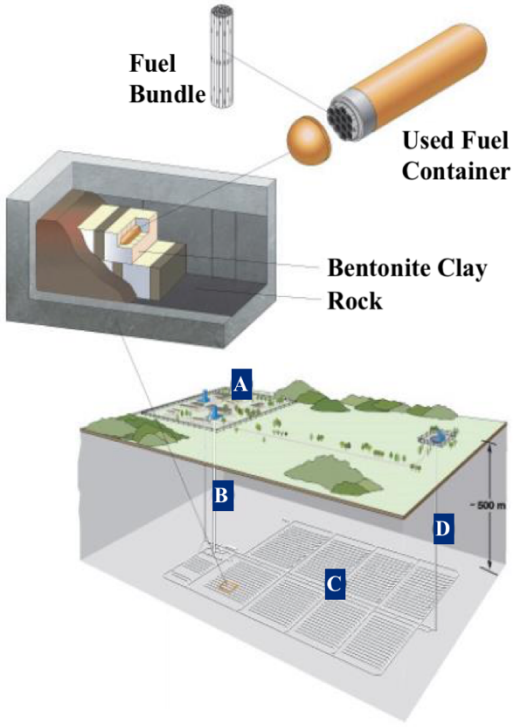

Figure 1.1 The current design for the APM project. A=Surface Facilities, B= Main Shaft Complex, C= Placement Room, and D= Ventilation Exhaust Shaft. Adapted from Noronha (2016).

The Nuclear Waste Management Organization (NWMO) has been contracted to aid with Canada's plan for the long-term management of used nuclear fuel (Noronha, 2016). It manages the waste generated by the 19 Deuterium Uranium (CANDU) reactors in Canada, as well as other waste sources through a plan called Adaptive Phase Management (APM) (Noronha, 2016).

The APM investigates containment and isolation of used nuclear fuel in centralized locations of suitable sedimentary or crystalline rock formations.

Although the APM is also examining the potential for storing high-level nuclear waste, the DGR proposed to be located in the Ordovician shales of the Bruce Peninsula is specifically for L&ILW. L&ILW is any waste that does not come directly from used nuclear fuel. Unlike high-level waste, which loses most of its radioactivity only after up to millions of years, L&ILW requires ~300 to 100 000 years to lose most if not all of its radioactivity. Sources of this lower level waste include, but are not limited to, waste from the production of medical isotopes, uranium mining and milling waste, and contaminated equipment such as protective clothing used in plant operation.

In order for DGRs to ensure that radio-nuclides cannot travel out of the storage facility, rigorous tests are done on the surrounding geological host rock to examine its ability to seal the facility from the biosphere. In this regard, it is important to characterize and understand the host rock, as it is the last line of defence in case all other containment devices fail (e.g., waste containers, bentonite clay rock, surrounding building structures). A host rock for a DGR should have strong barrier characteristics including extremely low hydraulic conductivity, complemented by a very low water content. Hydraulic conductivity is a measurement of the ease with which a fluid can move through pore spaces of soil, sediment or rock. When these characteristics, both low hydraulic conductivity as well as low water content, are found in a geological unit, the unit is classified as an aquitard. As described more fully next, the proposed L&ILW DGR Bruce Site is located within/beneath the Ordovician shale aquitards. These natural barriers represent the most promising, large-scale systems for preventing radionuclide migration into the hydrosphere and biosphere.

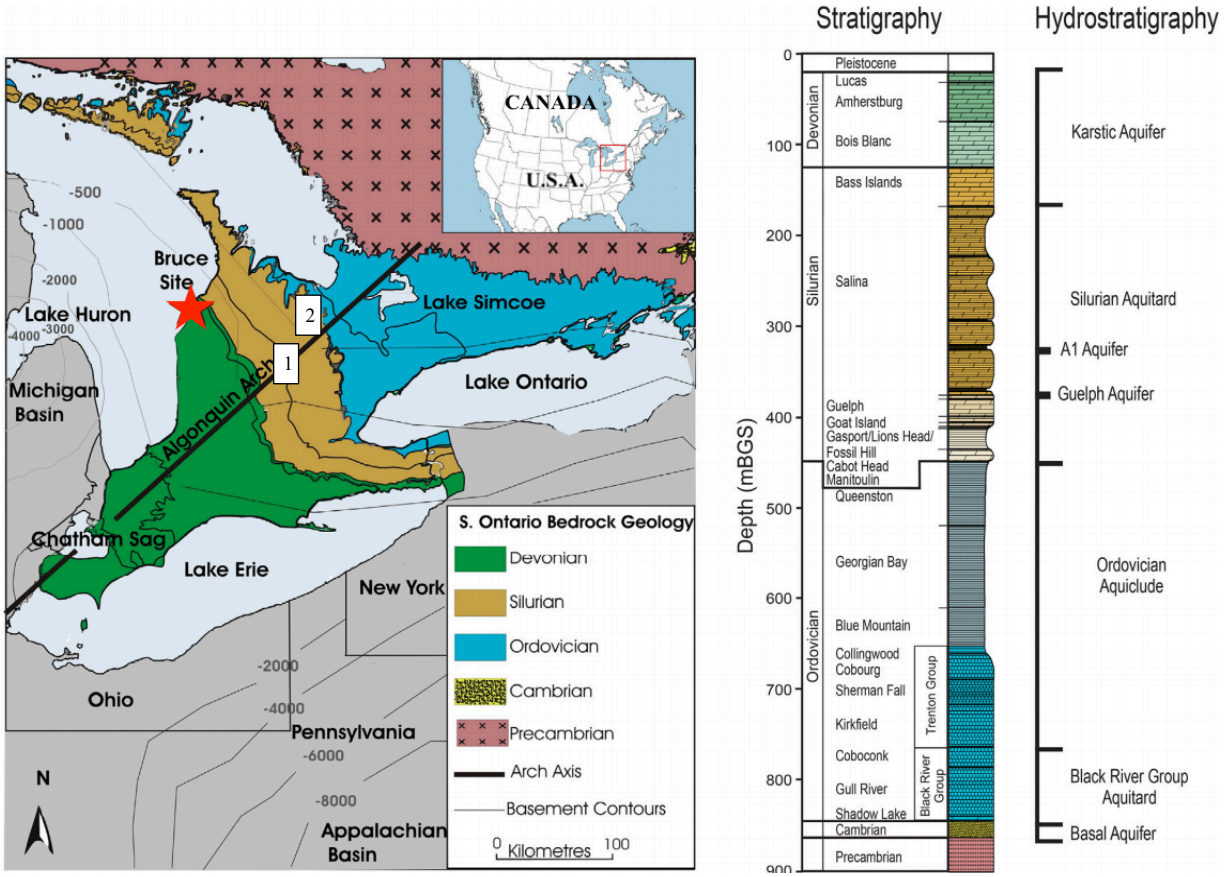

Figure 1.2. Bedrock geology, stratigraphy and hydrostratigraphy of the Michigan Basin below the Bruce site, southwestern Ontario, Canada. Contour lines for the base of the Paleozoic sediment are measured in meters with respect to the top of the Precambrian basement rock. The Bruce site, from which some samples were obtained, is indicated by the red star. Other cores sampled are indicated by [1] for the location of Wellington County where OGS-SG11-02 samples originated and [2] for the location of Dufferin County where the OGS-DHN1 129 sample originated. Adapted from Petts et al. (2017).

1.3 Bruce Site Location

The Bruce Nuclear site is located within the Michigan Basin, on the eastern shore of Lake Huron (Figure 1.2). This nearly circular intracratonic basin is 400km in diameter and 5km deep with only minor structural disruptions (Figure 1.2) (Howell et al., 1999). The basin contains a wide variety of Paleozoic and Mesozoic sedimentary rocks including carbonates, evaporites and siliciclastic units (shales, siltstones, sandstones). The Precambrian crystalline rock that underlies these sedimentary rocks varies in age from 2690 to 990 Ma and was deformed and metamorphosed during the Grenville Orogeny, ca. 1.19 Ga-0.9 Ga (Davidson 1995; Rivers 1997; Percival et al., 2007; McLelland et al., 2010).

1.4. Regional Geological Setting

During the Paleozoic Era, North America was located near or at the tropical latitudes and contained a number of inland seas. The sedimentary rocks of Cambrian to Mississippian age located in southwestern Ontario were deposited mainly in shallow marine environments. Southwestern Ontario comprises a peninsula that is situated on the Algonquin Arch, which is a north-easterly oriented Precambrian basement high. To either side of the Arch are major Paleozoic sedimentary basins, the Appalachian basin on the southeastern side, and the Michigan basin on the northwestern side (Figure 1.2). The southwestern point of the Algonquin Arch comes to an end at a structural low, the Chatham Sag, before the extension of the arch continues into the United States as the Findlay Arch. The two sedimentary basins vary in shape and sediment source. The Michigan Basin is a circular, carbonate-dominated, evaporite-bearing intracratonic basin, whereas the Appalachian Basin is an oval to elongated, siliciclastic-dominated foreland basin (Armstrong & Carter, 2010). The foreland basin was created as a result of the Taconic orogeny, ca. 490-440 Ma, which took place on the eastern edge of North America (Pavlides et al., 1968; Rodgers 1971; Rowley & Kidd, 1981; Dickinson et al., 1983; Van Staal et al., 2007).

These large-scale tectonic processes are recorded in the complex Paleozoic bedrock of Southern Ontario. Such complexities include the movements of structural elements including subsidence, arch uplift, and changes in sediment sources associated with the orogenic activity and eustatic sea level change (Armstrong & Carter, 2010).

Southwestern Ontario contains up to 1400 meters of Paleozoic sedimentary rocks, which are covered by unconsolidated glacial sediments having a maximum thickness of 200 meters. The Upper Silurian units, 400-100 meters below the surface, contain thick beds of halite and

anhydrite. These units are generally found in the Salina Group, located in the Michigan Basin and the Chatham Sag. Portions of these units have been selectively dissolved, leading to a change in groundwater salinity across many bedrock aquifers. Dissolution of these rock types has also led to the subsequent thickening or fracturing of overlying strata, which has affected groundwater flow (Armstrong & Carter, 2010). The majority of southwestern Ontario can be divided into two sections with respect to fracturing: the Niagara megablock, a heavily fractured large area flanking the Appalachian Basin, and the Bruce megablock, an even larger area northwest of the Algonquin Arch which is relatively less fractured. The Michigan Basin, and the proposed location of the DGR, are located within this Bruce megablock.

1.4.1. Bruce Site-Specific Geology

The strata of interest for the proposed DGR is the Cobourg Limestone as the host strata and the overlying Ordovician shale aquiclude. The lowest units of the Upper Ordovician are the carbonates of the Black River Group and the overlying Trenton Group. The Black River Group contains three formations: the Shadow Lake Formation, the Gull River Formation, and the Coboconk Formation. The Trenton Group contains the Kirkfield Formation, the Sherman Fall Formation, and the Cobourg Formation.

These two above mentioned groups contain sedimentary rocks deposited during a major sea level rise. The sedimentary facies within these groups represent the evolution from a supratidal and tidal flat clastic/carbonate environment to a lagoonal carbonate system. This transition was followed by an offshore, shallow water carbonate environment and finally a deep shelf carbonate environment (Al et al., 2011). These carbonates have a wide distribution due to the extensive shelf and ramp depositional environment.

The proposed DGR's potential host rock is the Cobourg Formation, which is capped by the Collingwood Member of the aforementioned formation. The Cobourg Formation represents the transition into a deep shelf setting. Due to storm deposit facies found within the Collingwood Member, however, it is believed that water never reached great depths, despite deposition at the peak of the marine transgression (Hamblin, 1999a).

The top of the Collingwood Member represents the cessation of carbonate deposition due to the collision of the continental margin with an island arc system, which occurred during the Early-Middle Ordovician Taconic Orogeny (Al et al., 2011). This tectonic event also caused loading on the above-mentioned margin by Taconic allochthons. These tectonic processes led to the westward movement of orogeny-derived clastic sediments that eventually covered the surface of the Ordovician carbonates.

These marine clastic sedimentary rocks occur in the Blue Mountain Formation, the Georgian Bay Formation, and the Queenston Formation. Due to closer proximity to the tectonic events, the quantity and age of the sedimentary rocks are greater and older in the Appalachian basin than in the Michigan basin. The tectonic processes also caused an eastward tilt of the majority of eastern Canada, causing both the Michigan basin and the Algonquin Arch to be affected by clastic deposition associated with the Appalachian Basin. Hence, Ordovician shales are pervasive across the majority of eastern Canada.

The Blue Mountain Formation is a soft, uniform blue-grey, non-calcareous shale that contains minor carbonate interbeds (Al et al., 2011). This composition is consistent with marine shale (Stott & Aitken, 1993; Hamblin, 1999a) and deposition during a marine transgression across the entire Appalachian Basin and into the Michigan Basin /Algonquin Arch Region. The non-calcareous, evaporitic sedimentary rocks present in the upper portion of the formation are

indicative of a restricted marine environment, supporting the previous observation that the Collingwood Member was deposited at the height of a transgression.

The Georgian Bay Formation overlies the Blue Mountain Formation, although a specific contact is not evident. The boundary is typically placed at the first conspicuous limestone layer (Guillet, 1977). This formation is also composed of a blue-grey, non-calcareous shale with minor beds of siltstone and limestone. The frequency and quantity of carbonate decreases with depth; these observations support the above-mentioned, shallowing upward tendency of the Ordovician shales. The Georgian Bay Formation is thus believed to represent a storm-dominated shelf succession (Williams et al., 1992; Hamblin 1999a). The carbonate seas that deposited the majority of the carbonates within the Georgian Bay Formation occasionally flooded causing lenses/fingers of carbonate rocks to be deposited in a northwesterly direction. This leads to the Blue Mountain and the Queenston formations to be eroded in these locations and the Georgian Bay deposited on the erosion surface (Al et al., 2011).

The Queenston Formation is a carbonate-rich shale unit with minor amounts of gypsum occurring along bedding planes and as fracture-fillings and nodules. The majority of the Queenston Formation is red to grey in color; the sedimentary facies, however, are characteristic of a range of depositional settings: subtidal, intertidal and supratidal. The subtidal facies is dominant at the base of the Formation where grey shales and siltstones are transitional with the Georgian Bay Formation. The middle of the Formation consists mainly of grey-red shales representing an intertidal environment. The uppermost section of the Queenston Formation is dominated by a supratidal, red-shale facies representing a significant marine regression (Al et al., 2011). This major regression led to an arid, sabkha-like environment responsible for gypsum formation within the upper section of the formation.

The Ordovician shales disconformably underlie the Manitoulin Formation, which consists of dolostone, argillaceous dolostone and minor grey shale (Armstrong & Carter, 2010). This disconformity is associated with the end of Late Ordovician-Early Silurian Cool Mode and the Late Ordovician glacial phases – as predominately recorded in Gondwanan continental fragments of Africa and South America – and a subsequent global sea level drop (Hamblin, 1999a,b; Frakes et al., 2005). Rip-ups from the Queenston Formation within the Manitoulin Formation, as well as desiccation cracks filled with the overlying Whirlpool Formation sandstone, provide corroborative evidence for the existence of this erosional surface (Hamblin, 1999a,b; Al et al., 2011).

1.5. Challenges in Isotopic Analysis of Porewater from Aquitards

As noted earlier the proposed DGR Bruce Site DGR is located within/beneath the Ordovician shale aquitards. The hydrogeology of clay-rich aquitards has been described in several studies (Hendry & Wassenaar, 1999, 2000; Hendry et al., 2004; De Haller et al., 2016). Characterization of the fluids and fluid movement within aquitards provides data that inform us about the nature – e.g., diffusion versus advection – and timing of solute movement (De Haller et al., 2016; Mazurek & De Haller, 2017). However, fluid migration in a low hydraulic conductivity and low water content porous medium is difficult to detect and to characterize. One of the few methods used for such characterization is based on examining the distribution of natural tracers such as ^{18}O and ^{2}H in porewater (Ayalon & Longstaffe, 1988; Longstaffe & Ayalon, 1990; Hendry & Wassenaar, 1999; Ziegler & Longstaffe, 2000a,b; McKay & Longstaffe, 2013; De Haller et al., 2016; Yang et al., 2016; Mazurek & De Haller, 2017). Due to the low water content (<5%), the small pore size, and the high amount of charged clay surface

area, accurate and precise measurement of tracer concentrations is difficult (Sacchi et al., 2001; Savoye et al., 2006). Studies of the Tournemire shale in France and Opalinus clay in Switzerland showed that water extraction from low water content rocks is influenced by many parameters, including extraction method, grain size and the amount of time that the sample is exposed to the atmosphere, all of which influence the concentration of ^{18}O and ^{2}H in extracted porewaters (Moreau-Le Golvan et al., 1997).

Currently, a variety of techniques are used to examine the stable isotope composition of low permeability rocks, which have been described by De Haller et al. (2016). These methods include the isotopic analysis of: 1) seepage water in confined intervals of drill holes (Pearson et al., 2003); 2) water obtained through vacuum distillation of porewater-saturated rocks (VDE) (Hobbs et al., 2008; Clark et al., 2013); 3) water recovered through advective displacement of the porewater from drill core (Mäder et al., 2014); 4) water collected by squeezing porewater-saturated rock (Mazurek et al., 2015); and water isotope compositions determined via adapted isotope diffusive-exchange (AIDE) (De Haller et al., 2016).

Another approach that combines *in vacuo* thermogravimetric analysis (TGA) and subsequent extraction of water at progressively higher temperatures may also have promise. This methodology has been used to study the isotopic compositions of clay minerals associated with hydrothermal mineralization in Japan (Marumo et al., 1995), oil sands that underwent steam stimulation in Alberta (McKay & Longstaffe, 2013) and hypogene clays in China (Yang et al., 2016). First steps for this approach have been attempted in the present research, in an effort to evaluate laboratory-induced isotopic exchange between porewater and structural hydrogen in clay minerals, and associated measurement artefacts and uncertainties related to clay-water interaction and isotopic fractionation that may affect the results produced by various methods.

The possibility also exists that original porewater isotopic compositions may have been altered during burial diagenesis. In particular, porewater trapped in low permeability, low water content, clay-rich sedimentary rocks buried for long periods of time at temperatures exceeding 70°C, such as at the proposed Bruce site DGR, may have undergone hydrogen isotope exchange with clay minerals. While oxygen isotope exchange between clay minerals and water typically does not occur below 200-300°C in the absence of dissolution-reprecipitation reactions, hydrogen isotope exchange has been shown to occur over long (geological) periods of time at temperatures as low as 40°C (Longstaffe & Ayalon, 1990). In such a scenario, porewater hydrogen isotope compositions in aquitards would then need to be considered not only in terms of water sources and processes such as mixing and diffusion, but also as the product of rock (clay)-water interaction and rock (clay)/water ratios of exchangeable hydrogen.

1.6. Summary

Low permeability, low water content sedimentary rocks are a viable option for use as geological barriers to the transportation of radionuclides. The low water content of these rocks, however, causes analysis of isotopically representative samples to be difficult. This difficulty is due in part to their low hydraulic conductivities ($<1 \times 10^{-14}$ m/s) and low volumetric water contents (<5%) (Sykes et al., 2011; Murseli et al., 2017). The low hydraulic conductivity causes difficulty because it restricts the flow of water through and therefore out of the sample during experimental extraction. The low water content requires special attention to ensure that 1) all water is collected, and 2) enough water is collected to allow for isotopic analysis.

As noted in Facella et al. (2012) one of the criteria set by the NWMO for a site to be considered as a potential site for the DGR project: "*This available land must not be located in areas with known geological and hydrogeological characteristics that would prevent the site*

from being safe." Using isotopic analysis to characterize the hydrogeology and paleohydrogeology of low water content rock units of interest has been attempted by various laboratories (Mazurek et al., 2016; Murseli et al., 2017) using different methods, which do not always produce results that are sufficiently comparable within experimental error. This difficulty may in part be a product of partitioning of porewater into water bound to clay surfaces and water that remains mobile or 'free' to move within the pore system. Likewise, it may be the case, at least for hydrogen isotopes, that the porewater compositions reflect clay-water interaction during burial, rather than the original source of the porewater.

1.7. Thesis Structure

This chapter (Chapter 1) briefly summarizes the relevant history of nuclear energy repository research in Canada and elsewhere, introduces the geology of the Ordovician shales of interest in Ontario, Canada, particularly at the DGR site, and presents the thesis research objectives. Chapter 2 describes the methodology used in the thesis, including clay separation, mineralogical characterization by powder X-ray diffraction (pXRD) and TGA, isotopic clay-water exchange experiments, and hydrogen and oxygen isotope analysis of the clay minerals and associated water. The results of these measurements are reported in Chapter 3, and discussed in Chapter 4. Chapter 4 examines the implications of our findings within the context of porewater isotopic data for the Ordovician shales reported by Clark et al. (2010a), Hobbs et al. (2011) and Mazurek et al. (2013). Chapter 5 summarizes the main findings and recommendations for future work.

Chapter 2. Sampling and Methodology

2.1. Choice of Samples

2.1.1. Clay Minerals Society Source Clays

The Ordovician shale formations of interest at the proposed DGR location contain mixtures of clay minerals as a major component (Guillet, 1977). Standard reference clay minerals were used as a reference point to begin to understand the isotopic systematics of these Ordovician clay mixtures. The reference clays were obtained from the Clay Minerals Society (CMS) Source Clay collections, which provides gently homogenized, largely monomineralic clay mineral standards of varying mineralogy (Moll, 2001). Based on their physical and chemical similarities to clay minerals present in the Ordovician shales, three CMS clay standards were selected for study: illite (IMt-1), chlorite (CCa-1), and kaolinite (KGa-1).

Illite — IMt-1

Illite – $(K,H_3O)(Al,Mg,Fe)_2(Si,Al)_4O_{10}[(OH)_2,(H_2O)]$ – is a non-swelling, 2:1 layer clay mineral whose layers are held together by electrostatic interactions with interlayer K^+ ions (Figure 2.1a). Other cations may also be present due to charge imbalances from isomorphic substitution within the 2:1layer structure. These cations typically include Fe^{2+} or Mg^{2+} exchanged for Al^{3+} in octahedral coordination or Al^{3+} exchanged for a structural Si^{4+} in tetrahedral coordination. (Brindley & Brown, 2005).

The CMS IMt-1 illite was obtained from the Middle Cambrian Silver Hill Formation, Montana, USA. This formation consists of silty and sandy carbonate rocks in the upper part of the unit and transitions to a dark argillite and thinly bedded quartzite in its lower portion (Pearson et al., 1988). Of the standards available, the physical characteristics of the IMt illite, such as its moderate crystallinity and formation during low grade metamorphism, are the most

comparable to illite in the Ordovician shales of interest in this study.

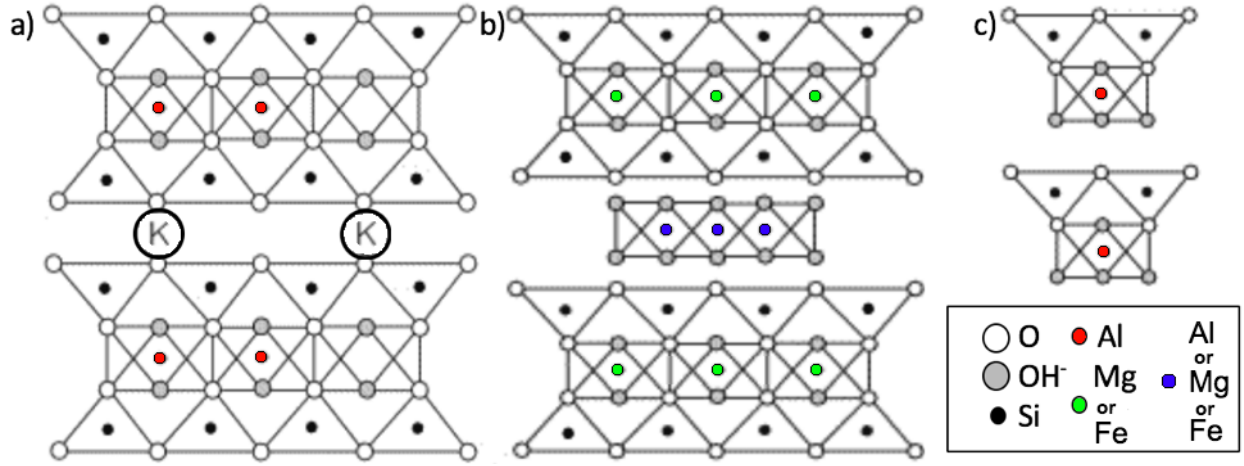

Figure 2.1.Schematic representation of a) Illite, displaying the octahedral sheets between two tetrahedral sheets, these 2:1 layer sheets are held together by electrostatic interactions with K^+ ions; b) Chlorite, displaying the octahedral sheets within the interlayer space of two 2:1 packets of tetrahedral and octahedral sheets; c) kaolinite, displaying the 1:1 ratio of the tetrahedral and octahedral sheets.

Ripidolite — CCa-1

The chlorite group – $(Mg,Fe,Al)_6(Si,Al)_4O_{10}(OH)_8$ – comprises 2:1:1 layer, non-swelling clay minerals (Brindley & Brown, 1980; Rule & Bailey, 1987). They contain a positively charged octahedral sheet within the interlayer space rather than single cations or cationic complexes (Figure 2.1b). This interlayer octahedral sheet is composed of a double layer of $(OH)^-$ ions that are coordinated with cations, such as Mg^{2+}, Fe^{2+} or Al^{3+}, in the central octahedral position. The unsatisfied charge is typically balanced by cations adsorbed to the clay surface or by the negative charge arising from the 2:1 layer (Newman & Brown, 1987). The Fe-rich CMS CCa-1 chlorite was obtained from Flagstaff Hill, El Dorado County, California, USA. This locality comprises a large body of ultramafic rock located along a major fault zone in the Sierra Nevada foothills, which was subsequently affected by low-grade metamorphism to greenschist facies during the late Jurassic or early Cretaceous time (Wells et al., 1940; Post & Plummer, 1972). This chlorite is classified as a ferroan clinochlore, also known as ripidolite, given the dominance of Fe^{2+} in the interlayer hydroxyl sheet (King & Clark, 1989). Of the available

chlorite standards, its crystal chemistry is most similar to chlorites from the Ordovician shales, which are of interest here.

Kaolinite — KGa-1

Kaolinite – $Al_4Si_4O_{10}(OH)_8$ – is an aluminous, 1:1 non-swelling clay mineral (Brindley & Brown, 1980) (Figure 2.1c). The strength of the hydrogen bonds between each 1:1layer package inhibits cations from entering the interlayer space. The CMS KGa-1 kaolinite used here is a soft kaolin from the Coastal Plain sediments of Cretaceous-Eocene age in Georgia, USA (Moll, 2001). The Coastal Plain sediments were deposited during several marine transgressions during the Cretaceous (Pruett & Webb, 1993). KGa-1 was obtained from the Cross Hodges Mine, which is located within the Tuscaloosa Formation of the Oconee Group. The Oconee Group consists of pre-Upper Eocene fluvial sediments and is dominantly kaolinitic, with rare bauxitic and smectitic lenses (Huddlestun & Summerour, 1996). Of the available kaolinite standards, KGa-1 is most similar in its crystal chemistry to kaolinite present in the Ordovician shales of interest in this study.

2.1.2. Ordovician Shale Samples from Southern Ontario

Two suites of samples were examined in the present study. The first was obtained from cores made available by the Ontario Geological Survey (OGS), through the Oil, Gas and Salt Resource (OGSR) library. The second was provided by the Nuclear Waste Management Organization (NWMO) from their core collection from the Bruce Site.

OGS Samples

Two cores were sampled from the collections of the OGSR core library, located in London, Ontario. Core choices and sampling depths were based on the OGSR core database supplemented by information in Armstrong & Carter (2010). The first sample was taken from

core OGS-SG11-02, whose drill site is located in the town of Arthur, Ontario, located ~100km southeast of the proposed DGR site (see Figure 1.2). A thickness of ~6 cm of core was taken at each of 327, 477, and 491 meters to sample the Blue Mountain Formation, Collingwood Member of the Cobourg Formation, and the Cobourg Formation proper. These samples are labelled as OGS SG11-02 327m, 477m and 491m, respectively. Due to difficulty in differentiating the Blue Mountain Formation from the overlying Georgian Bay Formation, sampling of the former was confined to the lowermost portion of this formation, just above the Collingwood Member. The second core is located in Melanchthon, Ontario, ~100km east of the proposed DGR site (see Figure 1.2). This core, OGS-Deep Hole No. 1 (OGS-DHN1), was used to sample the Queenston Formation. A 6cm sample was taken from 129m depth and labelled as OGS DHN1 129m.

NWMO Samples

The second sample suite was provided by the NWMO from cores taken at the proposed DGR site. Two cores, NWMO-DGR2 and DGR3, drilled in 2007 and 2008, respectively, were sampled. Drill cores from boreholes NWMO DGR1-DGR8 are currently preserved in wooden boxes that are shelved sequentially in a climate-controlled facility with security-controlled access at the OPG core storage facility on the Bruce nuclear site (Swanson, 2013). The Queenston Formation was sampled from core NWMO-DGR3 at its top (459m) and bottom (523m). These samples are labelled as DGR3 459m and DGR3 523m, respectively. The Georgian Bay and Blue Mountain formations were sampled from core NWMO-DGR2 at 530m and 616m, respectively. These samples are labelled as DGR2 530m and DGR2 616m, respectively. Each sample comprised a 30cm thickness of core and was immediately sealed under vacuum for delivery to The University of Western Ontario, where they were stored for six months at 5°C prior to

opening. Once opened to atmosphere, samples, when not in use, were stored in Ziplock® bags and kept refrigerated at 5°C.

2.2. Separation of the <2μm Size-Fraction

The top 1-2cm thickness of both the OGS and NWMO core samples were removed using a wet saw prior to hand-crushing and gentle grinding using a steel mortar and pestle. All OGS, NWMO and CMS samples were gently hand-crushed to a homogeneous <2mm powder, except for KGa-1, which was already in powdered, homogeneous form. All samples were then dispersed ultrasonically in distilled water. The <10μm supernate of each dispersed sample was then transferred to a 30cm high, 1L glass column where the <2μm fraction was separated following Stokes Law and standard sedimentation techniques (Jackson, 1979). Each sample underwent re-suspension and collection of the <2μm size-fraction for a minimum of five times. KGa-1, OGS SG11-02 477m and OGS SG11-02 491m required addition of sodium hexametaphosphate to disperse the clay-size-fraction.

Fifty ml of 6% sodium hypochlorite was added to the collected <2μm to induce flocculation and to oxidize any organic matter. Samples were then placed in a ~60°C water bath overnight. Following this treatment, samples were washed with distilled water via centrifugation. Each sample was then divided into three portions. One portion comprised the bleached and washed sample described above. The second portion was then saturated with a 2M solution of Ca^{2+} and the third with a similar concentration of K^{+}, after which excess amounts of the saturating solutions were removed by washing and centrifugation. All three portions were then frozen and freeze-dried. Thus, each sample then existed in three different cation saturations: Na^{+} (from the bleach treatment), Ca^{2+}, and K^{+}. In this thesis, samples that were exchanged with a

specific cation are prefixed with Na-, Ca- or K- before the sample name. See Appendix A for a more detailed description of these procedures.

2.3 X-ray Diffraction

The mineralogy and sample purity of the <2μm size-fraction were determined by powder X-ray diffraction (pXRD) of both oriented and randomly oriented aggregate samples via glass mounts and backpack mounts, respectively. These samples were analyzed at the Laboratory for Stable Isotope Science (The University of Western Ontario) using a High-Brilliance Rigaku Rotoflex RU-200B series diffractometer, equipped with a rotating anode (CoKα radiation operated at 160mA and 45 kV) and a graphite monochromator (Ziegler & Longstaffe, 2000a,b and Libbey et al., 2013). Bulk analysis was completed on samples which were freeze-fried, finely ground using a mortar and pestle, and back-packed into an aluminum sample holder to achieve random orientation. Bulk samples were then scanned from 2^o to 82^o 2θ theta at a scanning rate of 10^o 2θ /min. These results were then compared with the International Centre for Diffraction Data (ICDD) to identify mineralogy. All other samples were performed at 2^{o}2θ/min with a step size of 0.02^{o}2θ. In order to determine the clay mineralogy in detail, several sample treatments were performed prior to pXRD analysis, as described in detail by Ignasiak et al. (1983). About 15mg of each of the Ca- and K-saturated samples were pipetted onto separate glass slides in an effort to achieve a preferred orientation of clay mineral particles. The glass slides bearing the K-saturated samples were then dried overnight at 107°C and analyzed using the pXRD from 2-42° two-theta while still hot to ensure that they remained at 0% relative humidity. The K-saturated samples were then maintained at 54% relative humidity overnight through vapour exposure in a sealed chamber to a magnesium nitrate solution and then

reanalyzed immediately by pXRD from 2-42° two-theta. Following this treatment, the K-saturated samples were heated at 300°C for 4 hours, followed immediately by pXRD from 2-42° two-theta, and then heated to 550°C for 2 hours, followed by pXRD from 2-42° two-theta. The Ca-saturated samples were first analyzed after equilibration at 54% relative humidity, as described above for the K-saturated samples. These samples were then placed inside a chamber containing ethylene glycol (EG) and held under vacuum at 65°C overnight and then at room temperature for a further 24 hours. The Ca-saturated, ethylene-glycol solvated samples were then immediately analyzed by pXRD from 2-82° two-theta. Examples of how such a series of pXRD patterns aid in detailed determination of clay mineralogy are provided in Ignasiak et al. (1983), Libbey et al. (2013) and McKay and Longstaffe (2013).

2.4. Thermogravimetric Methods

A Linseis 81 Thermobalance, with an upgraded computer/software control package, was used in this study to measure weight loss during heating of the <2μm size-fractions. Several upgrades and modifications to the Linseis 81 system were necessary, as are detailed in Appendix B. Standardization and reproducibility of the unit for all analytical conditions employed were verified using calcium oxalate hydrate, a characteristic thermally sensitive material within the temperature range of interest. Standard curves were obtained for the reference material before and after analysis of the CMS, NWMO, and OGS samples to test for accuracy and reproducibility.

To perform the analyses, 15mg of each Ca, K-, and Na-saturated sample were placed in an alumina ceramic crucible and analyzed both *in air* and under active vacuum (*in vacuo*) after purging the system of air for 20 minutes. Comparison of TGA behaviour *in air* versus *in vacuo*

for all standards and samples in this study was used to guide the temperature of water and hydroxyl group extraction from the clays during isotopic analyses, all of which are conducted *in vacuo*. All samples were analyzed using a heating rate of 10°C/min from room temperature (~20°C) to ~950°C, as per common TGA procedures (Guggenheim & Van Groos, 2001). The TGA patterns for each sample were produced by comparison with an empty crucible, with all data collection and processing performed using Linseis STA (Simultaneous Thermal Analysis) Platinum series software (Bahri et al., 2017).

Periodic bi-monthly cleaning of the TGA system and its crucibles was performed by heating for 3 hours at 1000°C. This procedure ensures that weight loss unrelated to the sample does not occur during analysis. Between samples, crucibles were washed thoroughly in a sonication bath followed by manual rinsing with acetone.

2.5 Microscopy

The NWMO samples were examined petrographically in order: (i) to verify and complement the mineralogical results obtained by pXRD, (ii) to examine the microfabric of the shales, and (iii) to obtain semi-quantitative chemical data for identifiable mineral phases. For this purpose, eight uncovered polished thin sections (30μm thick) cut perpendicular to bedding and four uncovered polished thin sections (30μm) cut parallel to bedding were prepared by Vancouver Petrographics, Ltd. The thin-sections were examined using both optical light microscopy in plane and cross-polarized light, and electron microscopy. The optical light microscopy was performed using a Nikon Eclipse LV100 POL. Prior to electron microscopy, samples were coated with ~20nm of carbon. The electron microscopy was performed at Western's Earth and Planetary Materials Analysis laboratory using a JEOL JXA-8530F

Hyperprobe operating at 15kV accelerating voltage, 50nA probe current, and 10ms dwell time per pixel with pixel size at 2.5μm. Ca, Fe, K, Si and Mg were mapped using the wavelength dispersive spectrometers (WDS), while Ti, Na, O, Al, and S were mapped using energy dispersive spectroscopy (EDS).

2.6. Stable Isotope Methods

Isotopes are varieties of the same element that have the same number of protons and electrons but differ in their number of neutrons. Stable isotopes are those whose abundances do not change through radioactive decay, at least within our ability to measure rates of radioactive decay. The stables isotopes examined in this study are those of hydrogen (^{1}H, ^{2}H), and the most common of oxygen (^{16}O and ^{18}O). As summarized recently in Clark (2015), the relative abundances of heavy versus light stable isotopes of an element in any compound typically vary in a predictable fashion as a function of temperature, chemical composition and structure, nature of phase transitions, bonding, reaction rates (if equilibrium between reacting/isotopically exchanging phases is not established), and so on – all driven by the differences in masses between the heavy versus light isotopes of a given element or molecule (isotopologue) that contains that element. These differences are typically referred to as mass-dependent fractionation.

Stable isotope ratios are most commonly expressed using δ-notation (e.g., δ^{2}H, δ^{18}O) in parts per thousand (‰) relative to an internationally accepted standard (Equation 2.1), which in the case of hydrogen and oxygen isotopes, as used in this thesis, is Vienna Standard Mean Ocean Water (VSMOW):

$$\delta E = (R_{sample} - R_{standard})/ R_{standard} \qquad \text{(Eq. 2.1)}$$

where E = the isotope in question, in this case hydrogen (^{2}H) or oxygen (^{18}O), and R = $^{2}H/^{1}H$ or $^{18}O/^{16}O$, respectively.

Hydrogen and oxygen isotope analyses were performed on the K-saturated, <2μm size-fraction for structural oxygen, hydroxyl hydrogen and in the few cases possible, hydrogen in water sorbed on the <2μm size-fraction. The hydrogen isotope composition of the two waters used for isotopic exchange experiments was also performed. All stable isotope analyses were carried out in the Laboratory for Stable Isotope Science (LSIS) at the University of Western Ontario and all internal laboratory standards have been calibrated on the VSMOW-SLAP scale following protocols of Coplen (1996).

2.6.1. Structural Oxygen Isotope Analysis of the K-saturated, <2μm Clay Size-Fraction

Structural oxygen isotope compositions were obtained following standard procedures described by Clayton & Mayeda (1963) and Borthwick & Harmon (1982), as outlined in Huggett et al. (2017). About 8mg of sample was weighed into spring-loaded sample holders and heated at 150^{o}C for 12 hours under dynamic pumping. Samples were subsequently top-loaded into nickel reaction vessels and underwent 150°C heating for an addition 2 hours under dynamic pumping. Chlorine trifluoride was then added to the nickel reaction vessels and vessels were sealed and reacted for 16 hours at 580°C to release the silicate-bound oxygen. The oxygen was subsequently recovered and quantitatively converted to CO_2 for oxygen isotope analysis. All oxygen isotope results were measured using a VG Optima dual-inlet stable-isotope-ratio mass-spectrometer (IRMS).

2.6.2. Hydroxyl Group Hydrogen Isotope Analysis of the <2μm Clay Size-Fraction, Torch Method

Prior to extraction of structural hydrogen from the K-saturated, <2μm size-fraction, all samples were heated to remove adsorbed and interlayer water. The K-saturated <2μm samples

were chosen to facilitate the most effective removal of sorbed water during heating (Derkowski et al., 2012). To do so, samples were first dried in a 65°C oven overnight and subsequently ~65mg of each sample weighed and loaded into a quartz tube and outgassed from two hours to overnight at 200°C. Samples were then heated using a gas-fueled oxygen torch for ~15 minutes during which the released H_2O was cryogenically trapped. Gas released from the samples as H_2 was first oxidized via copper oxide at 550°C to form H_2O, which was then captured by the liquid nitrogen cryotrap. The collected water was then reacted with powdered chromium at 900°C to produce H_2. The H_2 was subsequently trapped onto charcoal via a liquid nitrogen cryotrap. The H_2 was analysed using a Thermo Scientific Delta^{plus} XL IRMS.

2.6.3. Clay-Water Hydrogen Isotope Exchange Experiments

To examine: (i) the possibility that hydroxyl hydrogen in the <2μm size-fraction was exchangeable with surrounding porewater at burial temperatures, and (ii) potentially detect isotopic discrimination between bound and mobile water, a H-isotope exchange experiment was undertaken using the K-saturated, <2μm samples of all NWMO samples and the CMS Source Clay illite IMt-1. Approximately 100mg of each chosen sample was placed in the bottom of Pyrex® side-arm tubes while the side arm portion was filled with 10ml of ^{2}H-enriched water (Heavy, δ^2H= +810±3‰) or low-^{2}H water (Light, δ^2H= –309±5‰). The water was then frozen to avoid loss and associated isotopic fractionation during subsequent evacuation of the side-arm tubes. Once under vacuum and sealed, the side-arm tubes containing sample and water were placed in a water bath at 68°C for 70 days, with the exception of DGR3 523m Heavy, which was removed from the water bath at 63 days. Along with these samples, an experiment was also conducted using the CMS Source Clay kaolinite KGa-1, which was left to equilibrate with ambient water vapour in the laboratory at 20°C for 2 days.

The NWMO and CMS illite IMt-1 samples were then transferred to a Plas-Lab Inc. Model 855 anaerobic chamber, which was subsequently purged with dry nitrogen until the relative humidity was 10%. Only then were the side-arm tubes opened, the clay samples weighed (~100mg) and transferred into a quartz-wool filled quartz tube. The quartz tube was then sealed with Parafilm® for transportation to the vacuum line. A similar approach was taken to preparing the KGa-1 sample for isotopic analysis in the anaerobic chamber and sample transfer to the vacuum line.

The initial plan was to then attach each sample to the vacuum line, evacuated the line, and then heat the <2μm size-fraction in stepwise fashion to release hydrogen at temperature intervals likely to be most closely associated with surface / mobile water, bound water and hydroxyl groups, as also demonstrated by the TGA data (see Chapter 3: Results). This approach was first undertaken with KGa-1. Efforts were made to collect hydrogen in the form of H_2O and/or H_2 at room temperature (~20°C), ~20-100°C, 100-200°C, 200-300°C, 300-400°C and 400 to 1000°C, following Marumo et al. (1995) and McKay and Longstaffe (2013), provided that sufficient amounts of these volatiles were released from the sample at each step. The evolution of H_2O and/or H_2 at each step was monitored, and the time to completion noted. Any free H_2 was converted to, and combined with released water as described above, and then reconverted to H_2 gas, also as described above. Yields of hydrogen were measured at each step. If the yield was too low to enable measurement by IRMS, gas collected at the next temperature step was added to that collected earlier, until sufficient gas was obtained for hydrogen isotope analysis. The hydrogen isotope analyses were performed using a Micromass Prism II IRMS.

The same approach was then attempted for the sample of NWMO DGR3 523m K<2μm that had been exposed to the Heavy exchange water. The hydrogen isotope results for this

sample, however, demonstrated a carry-over of ^{2}H-enriched hydrogen from lower to higher temperature intervals of the stepwise heating process (see Chapter 3 - Results). As a result, efforts to conduct stepwise hydrogen isotope analyses for the remaining samples were abandoned.

2.6.4. Hydrogen Isotope Analysis of Exchange Waters

The hydrogen isotope compositions of the two exchange waters prepared for the exchange experiment (Heavy = +810±3‰; Light = –309±5‰) were obtained using the same approach as described above for analyzing water released from the clay minerals. About 3μl of water was injected through a reusable rubber septum, where it was then heated, using a heat gun, and trapped in a liquid nitrogen trap. The water was reacted with powdered chromium at 900°C to produce H_2, which was subsequently trapped onto charcoal via a liquid nitrogen cryotrap, and then analysed using a Thermo Scientific Delta^{plus} XL IRMS.

2.6.5. Hydrogen Isotope Analysis of the <2μm Clay Size-Fraction using a High Temperature Conversion Elemental Analyser (TC-EA) and IRMS

Several samples of the <2μm clay size-fractions were also analyzed using a Thermo Scientific High Temperature Conversion Elemental Analyser (TC-EA) coupled in continuous flow mode to Thermo Scientific Delta^{plus} XL IRMS. Use of this approach to clay hydrogen isotope analysis was first described by Sharp et al. (2001), although there have been several improvements since that time. This process allows for sample sizes of <2-3mg with a water content of 5-10% (Bauer & Vennemann, 2014). Samples are weighed into silver capsules and subsequently crimped closed after drying overnight in a vacuum at 200°C. Samples are then placed into an autosampler directly above the TC-EA. To release the H_2 hydroxyl groups contained in the clay minerals, the TC-EA is equipped with a ceramic tube that contains a

smaller glassy carbon tube, glassy carbon chips, and a graphite cup, all of which are necessary for high temperature (1450°C) reduction and release of hydrogen gas fron the clay. The hydrogen gas (H_2) is swept by He carrier gas into IRMS, via a gas chromatographic column, for isotopic analysis. Isotope ratios are normalized to VSMOW-SLAP using USGS57 (biotite) and USGS58 (muscovite) (Qi et al., 2017), with the accuracy of the calibration tested using in-house standards GBS biotite and KGa-1 kaolinite.

Chapter 3. Results

3.1. Hand Samples and Microscopy

The macroscopic features of the OGS and NWMO core samples were characterized from hand samples and the rocks classified following Folk (1980). Optical and electron microscope examinations were also conducted on the NWMO core samples.

3.1.1. Upper Queenston Formation – NWMO DGR3 459m

The sample is classified as a fine-grained calcareous shale with minimal lamination (Hobbs et al., 2011). As a result of the sample's fine-grained nature, the majority of the minerals occur in the matrix, and therefore are difficult to identify in hand specimen. Some coarser grained minerals include quartz and carbonates (dolomite and minor amounts of ankerite, as confirmed by energy dispersive spectroscopy (EDS) (Figure 3.1) (Reed, 2005; Hobbs et al., 2011). Numerous shelly fragments are present. The matrix is composed of extremely fine-grained clays and carbonates. Both euhedral carbonates that have overgrown the matrix and anhedral, fine-grained carbonates within the matrix are peppered throughout the sample. The sample also contains spherical to ovoidal dark patches that occur in small groupings in all thin sections (Figure 3.2).

a)

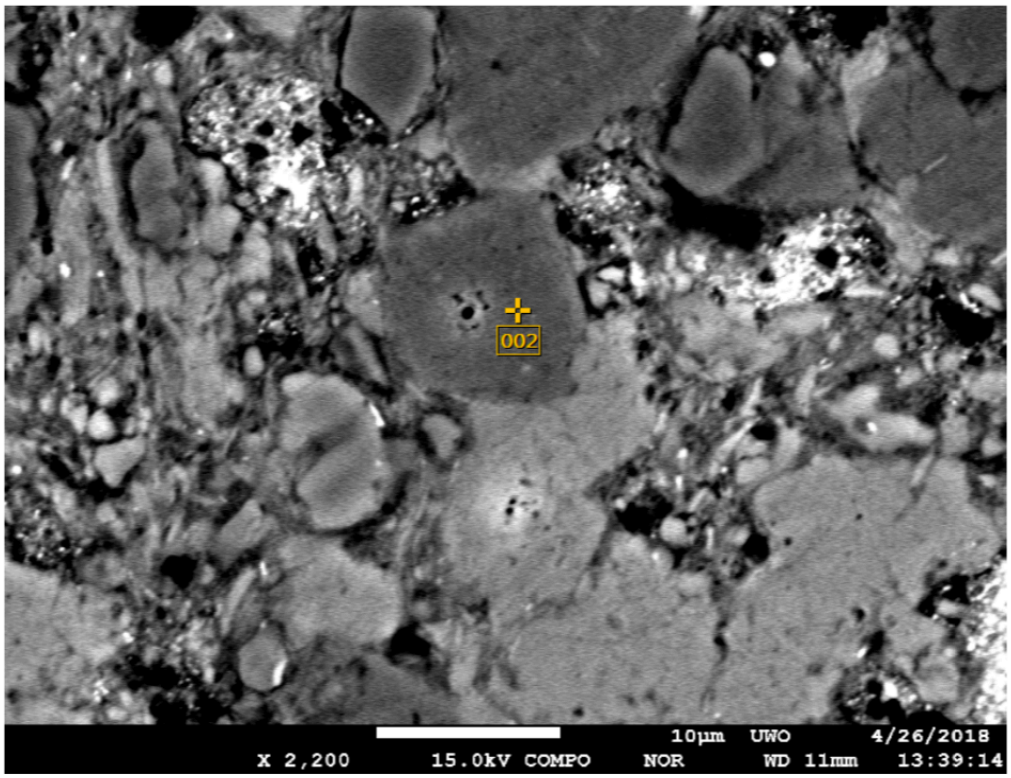

b)

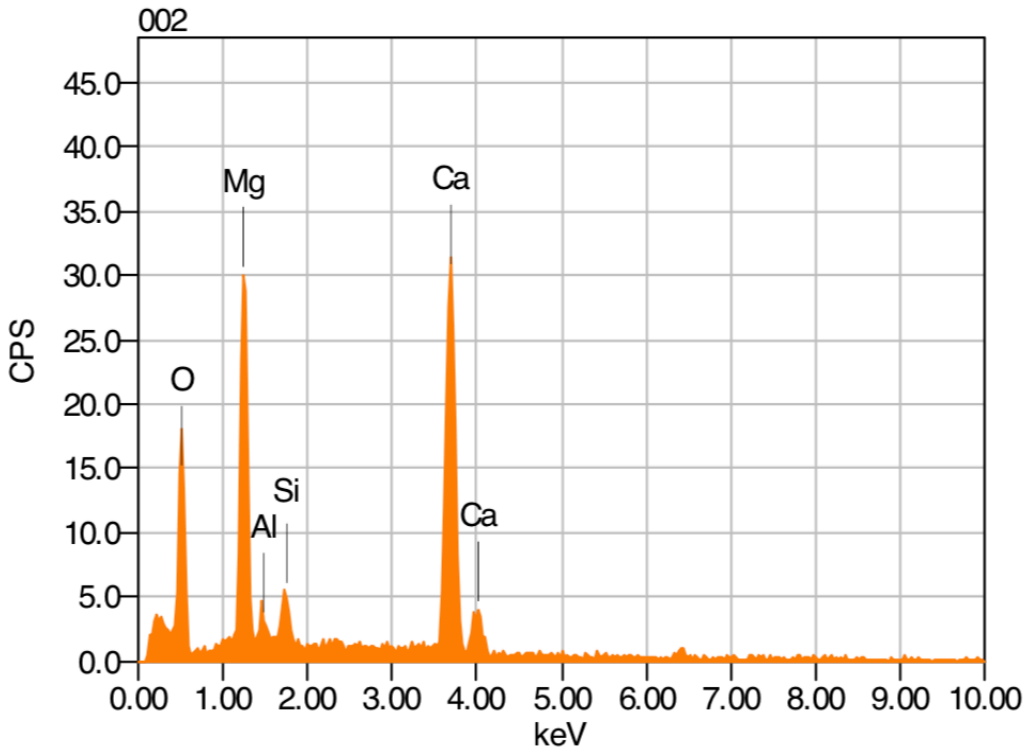

Figure 3.1. Sample NWMO DGR3 459m: (a) Backscattered electron (BSE) image; b) Energy-dispersive spectroscopy (EDS) of spot 002 shown in (a) of a dolomite crystal. Voltage at 15 kV.

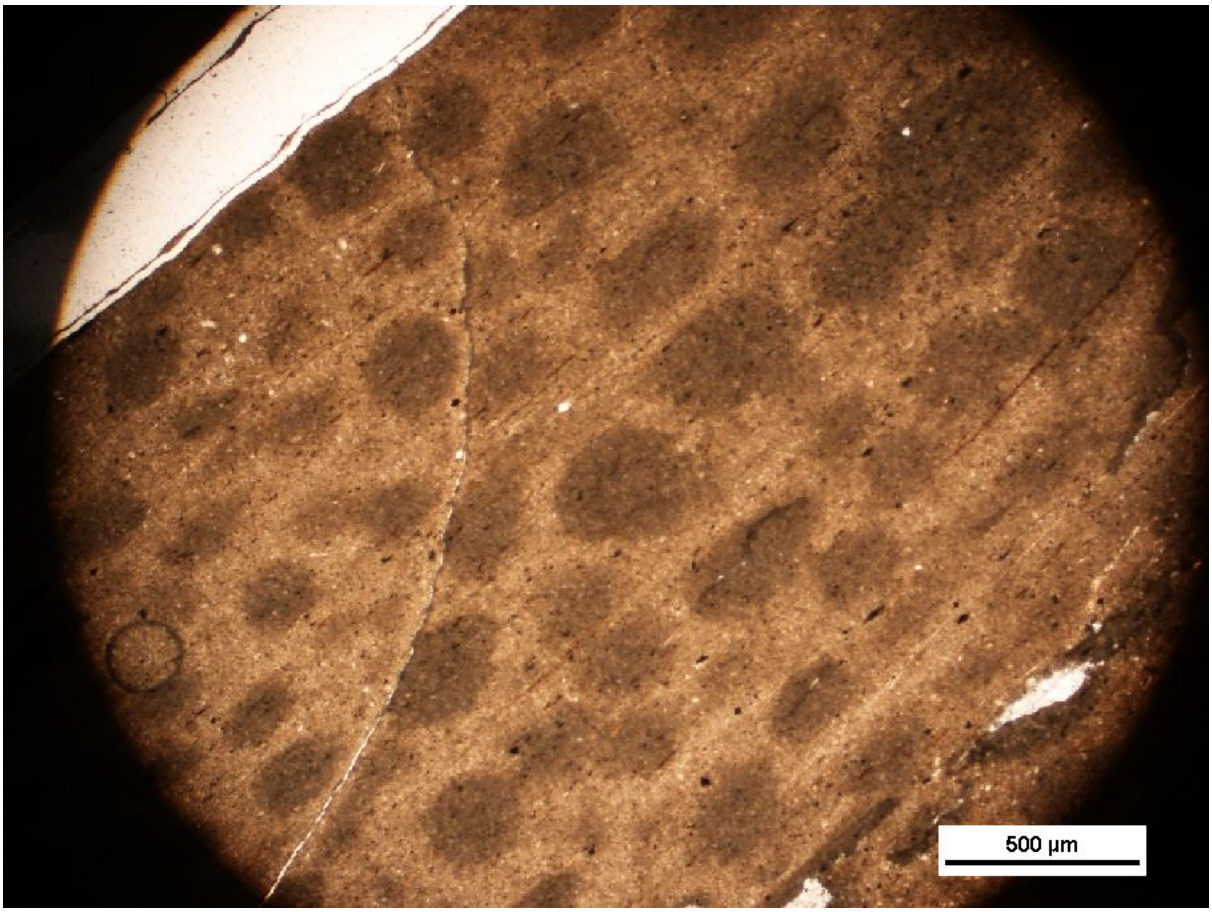

Figure 3.2. Plane-polarized, optical light image of sample NWMO DGR3 459m displaying a dark brown, ovoidal pattern, likely associated with iron-redox reactions linked to organic matter and iron sulfides.

3.1.2. Lower Queenston Formation – NWMO DGR3 523m

The sample is classified as a dark brown-red, iron-rich, very fined grained calcareous shale (Hobbs et al., 2011). Minerals and fossil fragments visible in hand-specimen are interstitial to the matrix. Visible minerals include iron sulfides (Figure 3.3), carbonates (calcite and dolomite) and quartz. Minor deformation is visible in the matrix laminae that alternate with discontinuous laminae of anhedral quartz and carbonate. Microcrystalline clays are compacted around carbonate minerals. Based on EDS analysis and Hobbs et al. (2011) and confirmed by

powder X-ray diffraction (pXRD) in this study (see below), the matrix comprises a mixture of carbonates and illite (Figure 3.4).

a)

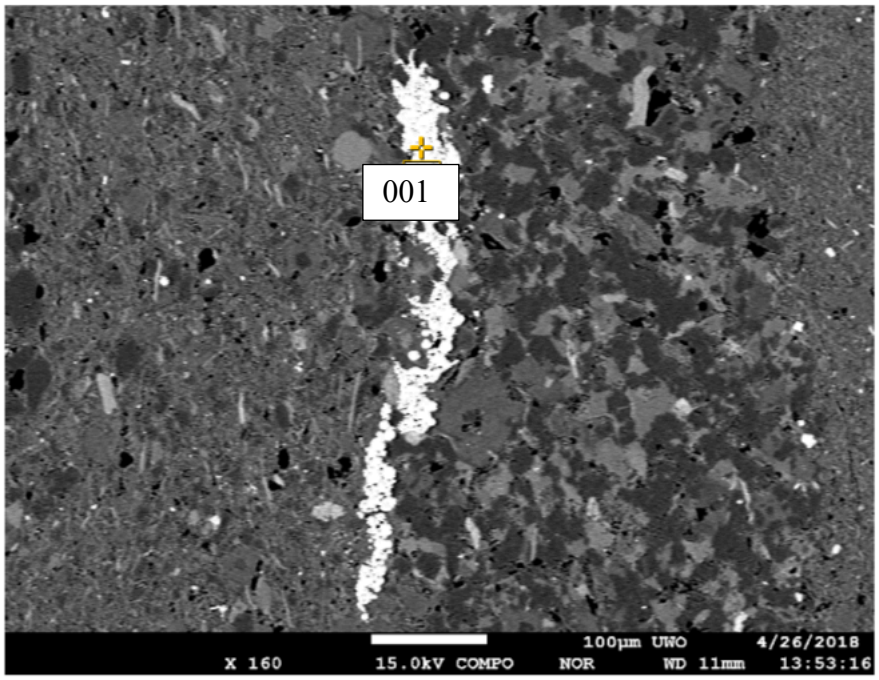

b)

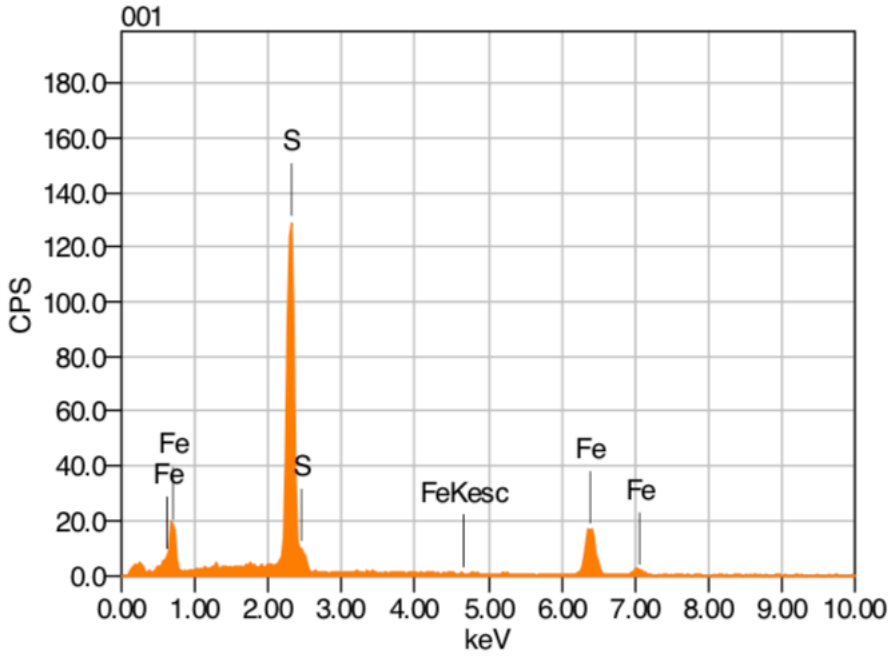

Figure 3.3. Sample NWMO DGR2 530m: (a) BSE image of iron sulfide at spot 001; (b) EDS of spot 001 shown in (a). Voltage at 15 kV.

3.1.3 Georgian Bay Formation – NWMO DGR2 530m

The sample is classified as an iron-rich, very fine-grained, dark brown, calcareous shale (Schandl , 2009; Skowron & Hoffman, 2009). Minerals visible in hand specimen and/or identifiable using the electron probe in EDS mode are interstitial to the matrix and include iron sulfides, halite, carbonates (calcite and dolomite) and quartz. Minor deformation is present in the alternating discontinuous laminae of anhedral quartz and carbonate (Schandl , 2009). Microcrystalline clays are compacted around carbonate minerals (Schandl , 2009). Based on EDS analysis the matrix is a mixture of carbonates and illite (Figure 3.4).

a)

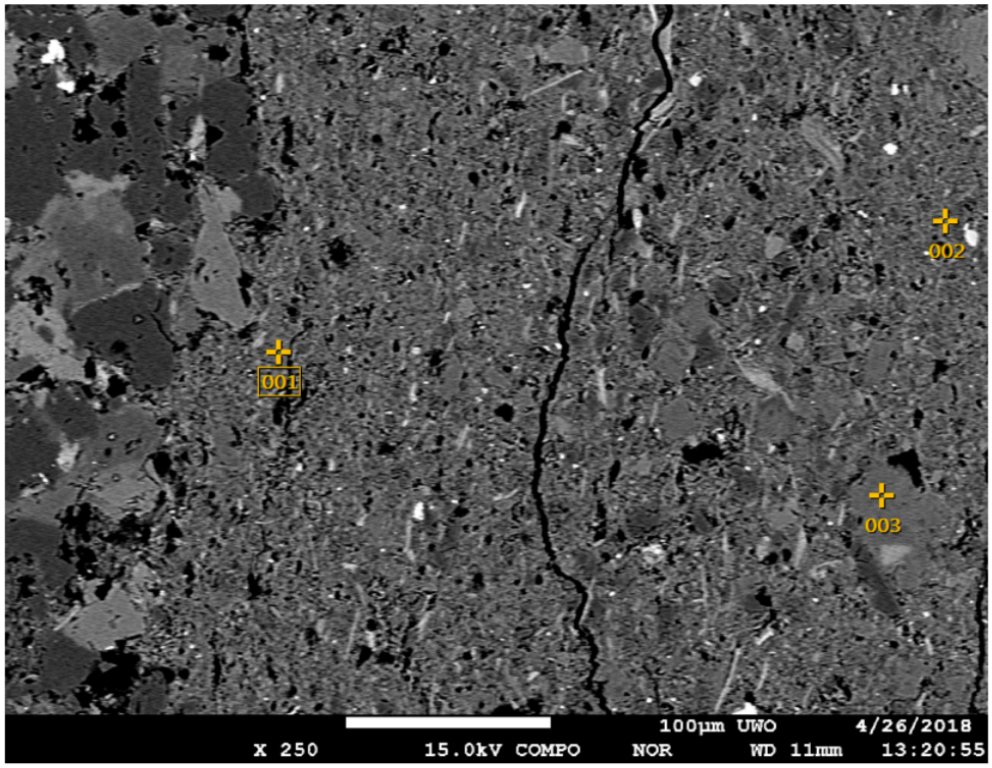

b)

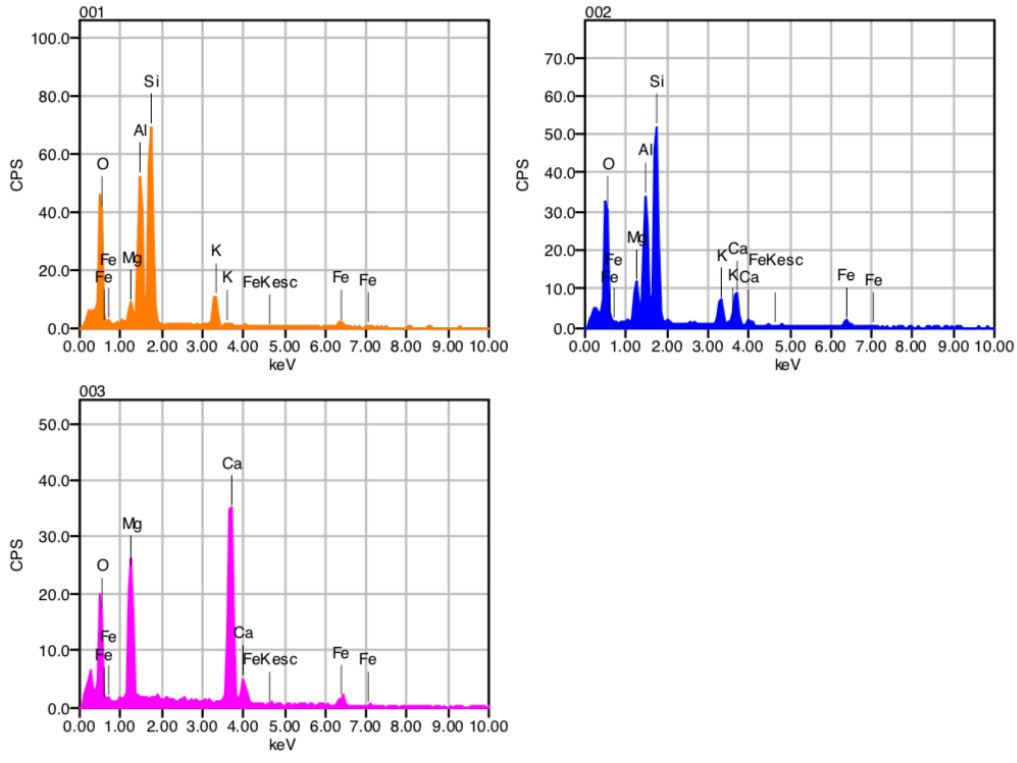

Figure 3.4. Sample NWMO DGR2 530m: (a) BSE image of fine-grained matrix; (b) EDS of illite at spots 001 and 002, and dolomite at spot 003 shown in (a). Voltage at 15 kV.

3.1.4. Blue Mountain Formation – NWMO DGR2 616m

The sample is classified as a fossiliferous limestone (Schandl , 2009; Skowron & Hoffman, 2009). It has an iron-dominated, fine-grained matrix with euhedral dolomite and large bryozoan fragments scattered through the sample (Figure 3.5). The majority of the fossils' zooecia are filled with coarse-grained carbonates, with the clay matrix seeping into any of the surficial fractures and crevices of the zooecia (Schandl , 2009). Framboidal pyrite is common throughout the sample, and typically is associated with fossil fragments (Figure 3.6).

Figure 3.5. Plane-polarized, optical light image of a bryozoan in sample NWMO DGR2 616m.

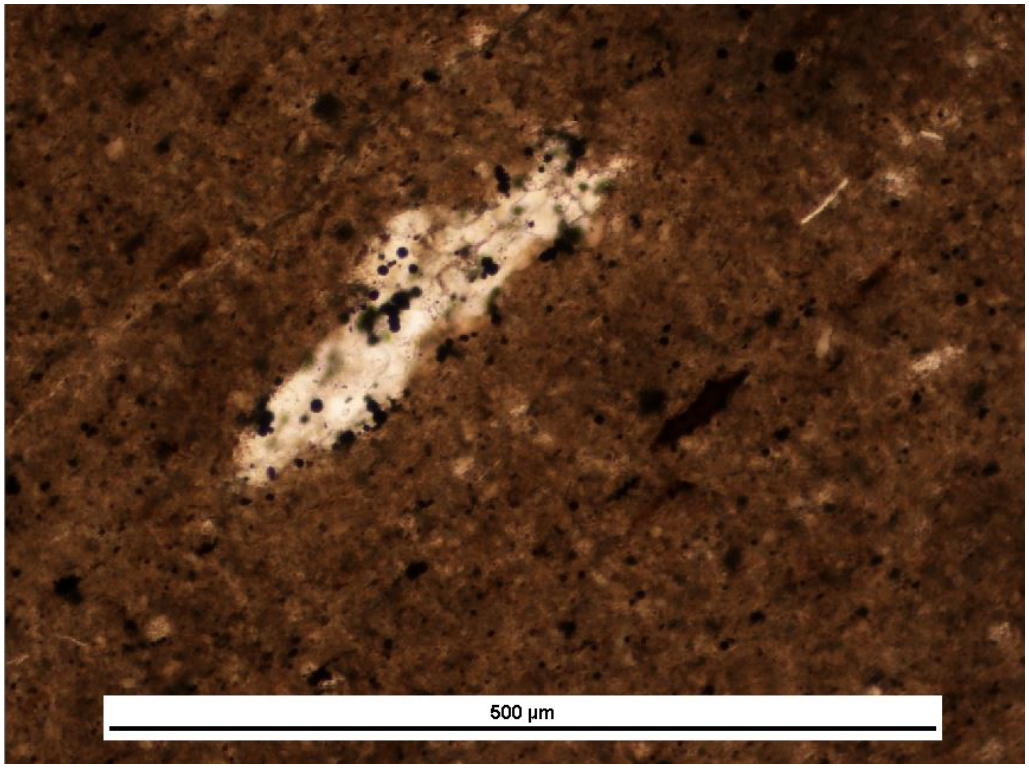

Figure 3.6. Plane-polarized, optical light image of pyrite associated with a fossil fragment in sample NWMO DGR2 616m sample.

3.1.5 Cobourg Formation – OGS SG11-02 477m and OGS SG11-02 491m

These samples are classified as a fossiliferous limestone-mudstone. Pyrite was found through the sample as an accessory mineral. Fine-grained, euhedral dolomite also occurs in aggregates in the limestones where they contain interstitial, Fe-stained clays as cement (Schandl, 2009).

3.2. Powder X-ray Diffraction (pXRD) & Thermogravimetric Analysis (TGA)

The results of pXRD and TGA are presented here for the <2μm CMS Source Clays and the Ordovician shale samples from the Queenston Formation, Blue Mountain Formation, Collingwood Member and Cobourg Formation. For an introduction to pXRD and TGA, see Appendix C. Long-term use of TGA analyzers can cause small fluctuations in the apparent

weight change in the <200°C range (Linseis Thermal Analysis, 2018). This fluctuation is normally on the scale of 15μg (0.015mg) for instruments of the vintage used in our measurements. Any fluctuation within this range at <200°C are likely instrumental artefacts. TGA weight loss curves are displayed in percentage change in mass (Delta M) with increasing temperature (°C).

3.2.1. Source Clays (<2μm)

Illite – IMt-1

The pXRD diffractograms of preferred-oriented samples of IMt-1 (illite) are characterized by strong basal diffractions at 1.0nm (001) and 0.33nm (003) and a less intense (002) basal diffraction at 0.5nm. These diffractions are unaffected by hydration or rehydration at 54% relative humidity (RH; Ca- and K-saturated samples, respectively), treatment with EG (Ca-saturated sample) or heating to 300°C and 550°C (K-saturated sample) (Figure 3.7a), as is characteristic of illite (Brindley & Brown, 1980). The 06 band pXRD analysis of randomly oriented samples confirmed the presence of a dioctahedral clay at 0.150nm, which is typical of illite.

There are variations in illite (001) peak sharpness in IMt-1 across the spectrum of pXRD patterns obtained, as determined from the peak width at one-half of the maximum peak height or "full width half maximum" (FWHM) (Figure 3.7b). The Ca-saturated 54% RH and EG samples have FWHM = ~1.1 to 1.4. Similar values are obtained for the K-saturated 0% and 54% RH samples (1.22-1.30), which reduces to 0.66 upon heating to 300°C and further to 0.62 upon heating to 550°C. These values are very typical of illite formed during weathering and/or shallow diagenesis, with lower values upon heating reflecting some crystal reorganization towards higher crystallinity.

TGA analysis of the illite was conducted both *in air* and under vacuum (*in vacuo*). *In air*, the sample lost 4% and 5% by weight during the first 200°C for Ca- and K-saturations, respectively (Figure 3.8a). The Na-saturated sample lost ~9% by weight during the first 200°C of heating. The Ca- and K-saturations lost an additional 3% and 4% by weight, respectively, throughout the remainder of the heat treatment. The Na-saturated sample lost 8% by weight from 200-500°C after which its weight remained more or less unchanged for the remainder of the heating.

In vacuo, the TGA patterns of all saturations of IMt-1 showed minor weight loss within the first 200°C, some of which may be an instrumental artefact. Between 200-400°C the Na-saturated sample lost an additional ~1% by weight whereas the Ca- and K-saturated samples did not lose weight. Once temperatures rose above 425°C all aliquots of IMt-1 – regardless of cation saturation – lost a further 5% in weight by 700°C, which is characteristic of dehydroxylation. The weight then remained stable between 700-950°C (Figure 3.8b).

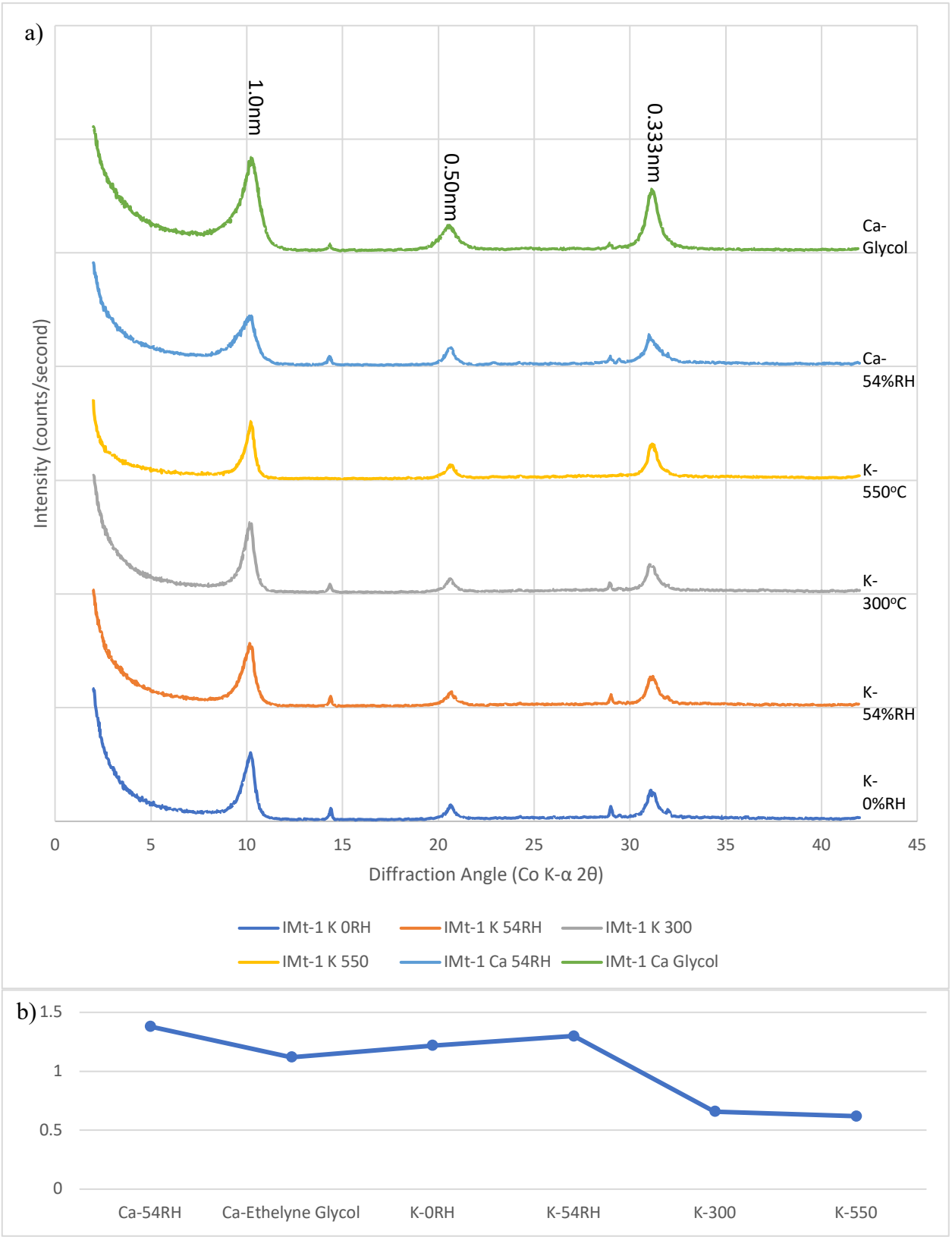

Figure 3.7. (a) Preferred orientation pXRD of <2µm K- and Ca- saturated IMt-1 after various treatments. All treatments are displayed at the same relative intensity. (b) FWHM of IMt-1 (001) after various treatments.

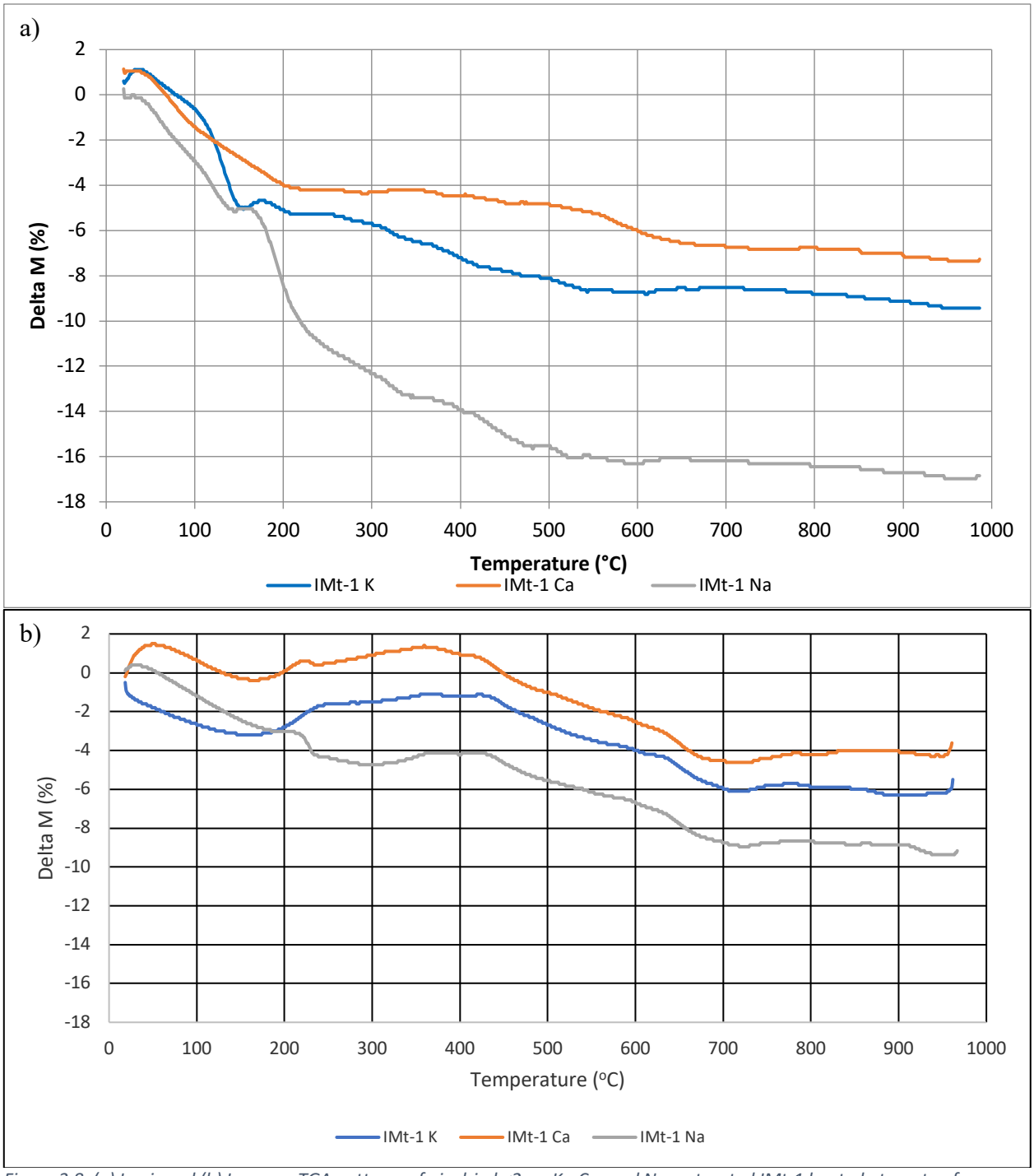

Figure 3.8. (a) In air and (b) In vacuo TGA patterns of air-dried <2µm K-, Ca- and Na- saturated IMt-1 heated at a rate of 10°C/minute.

Ripidolite – CCa-1

CCa-1 has a (001) basal diffraction at 1.4nm, with higher order basal diffractions at 0.7nm (002), 0.47nm (003), 0.354nm (004), and so on. The preferred-oriented pXRD patterns for the CCa-1 chlorite were unaffected by hydration (Ca-saturated) / rehydration (K-saturated), treatment with EG (Ca-saturation) or heating at 105°C and 300°C (K-saturated). After heating to 550°C, the (001) diffraction increased in intensity, whereas the intensity of all higher order basal diffractions decreased (Figure 3.9a), as is characteristic of many chlorites (Brindley & Brown, 1980). The pXRD analysis of the randomly oriented samples revealed a 06 band diffraction typical of trioctahedral chlorite (0.155nm).

There is little variation in the chlorite (001) peak sharpness in CCa-1, as determined using the FWHM. Values remain constant at 0.22 across all pXRD treatments (Figure 3.9b). Such low values are consistent with high crystallinity, as expected for a chlorite forged under greenschist facies conditions, and with the absence of any interstratification with swelling clay materials.

During TGA *in air*, the <2μm CCa-1 lost 3, 6, and 9% by weight for the Na-, Ca-, and K-saturations, respectively, within the first 200°C. All saturations lost 3% by weight upon heating to 500ºC after which they then lost a further 5% by weight from 500-650°C. Weights then stabilized for the remainder of the heat treatment up to 950°C (Figure 3.10a). During *in vacuo* TGA, both Na- and K-saturated <2μm fractions showed little weight change until 550°C after which they lost ~8% by weight by ~700°C. Sample weight then stabilized for the remainder of the heating. This weight loss is typical of dehydroxylation. The Ca-saturated <2μm fraction of CCa-1 displayed two weight-loss steps, the first loss of 3% occurred at ~225ºC and the second loss of 8% occurred from 550-700°C (Figure 3.10b).

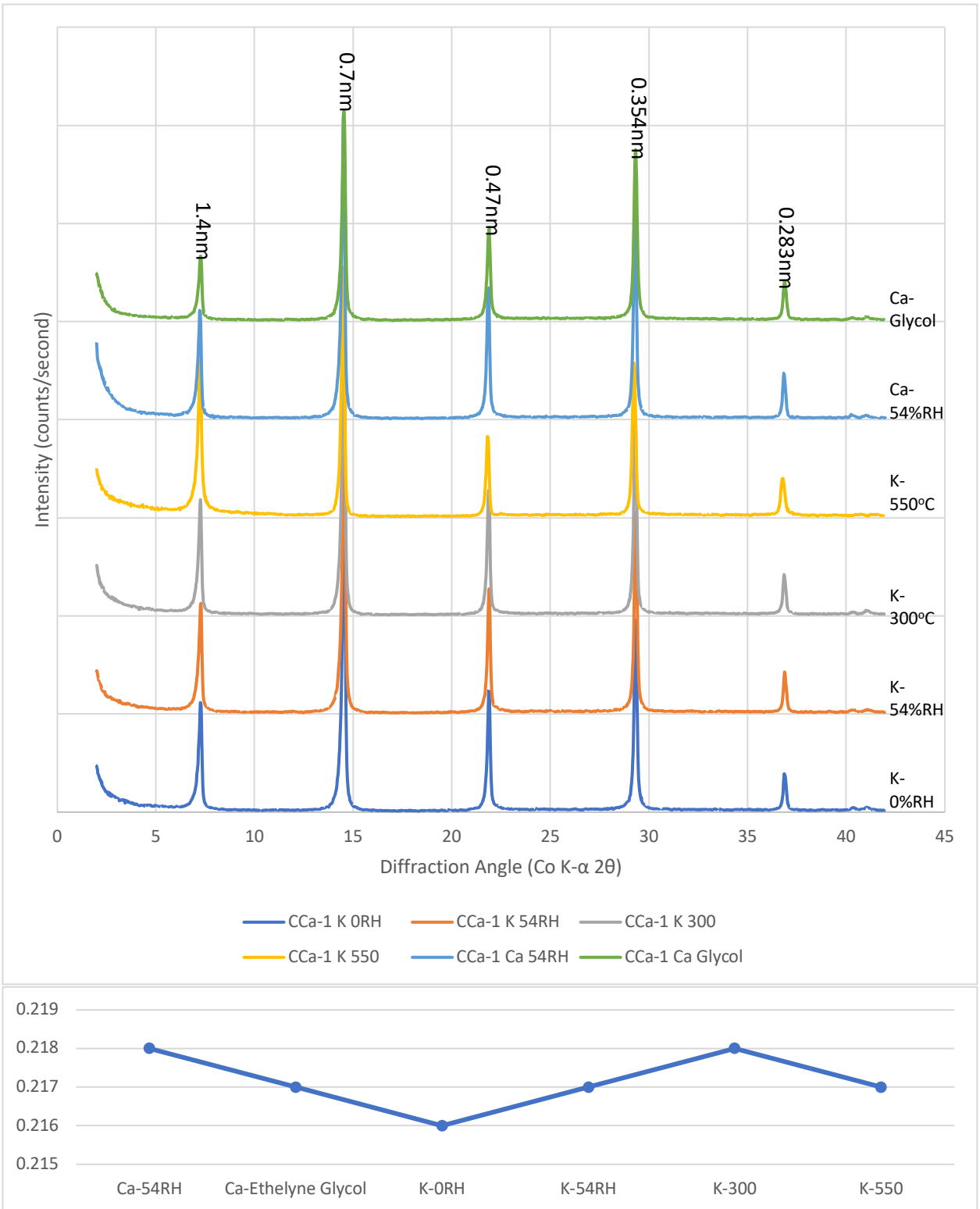

Figure 3.9. (a) Preferred orientation pXRD of <2µm K- and Ca- saturated CCa-1 after various treatments. All treatments are displayed at the same relative intensity. (b) FWHM of CCa-1 (001) after various treatments.

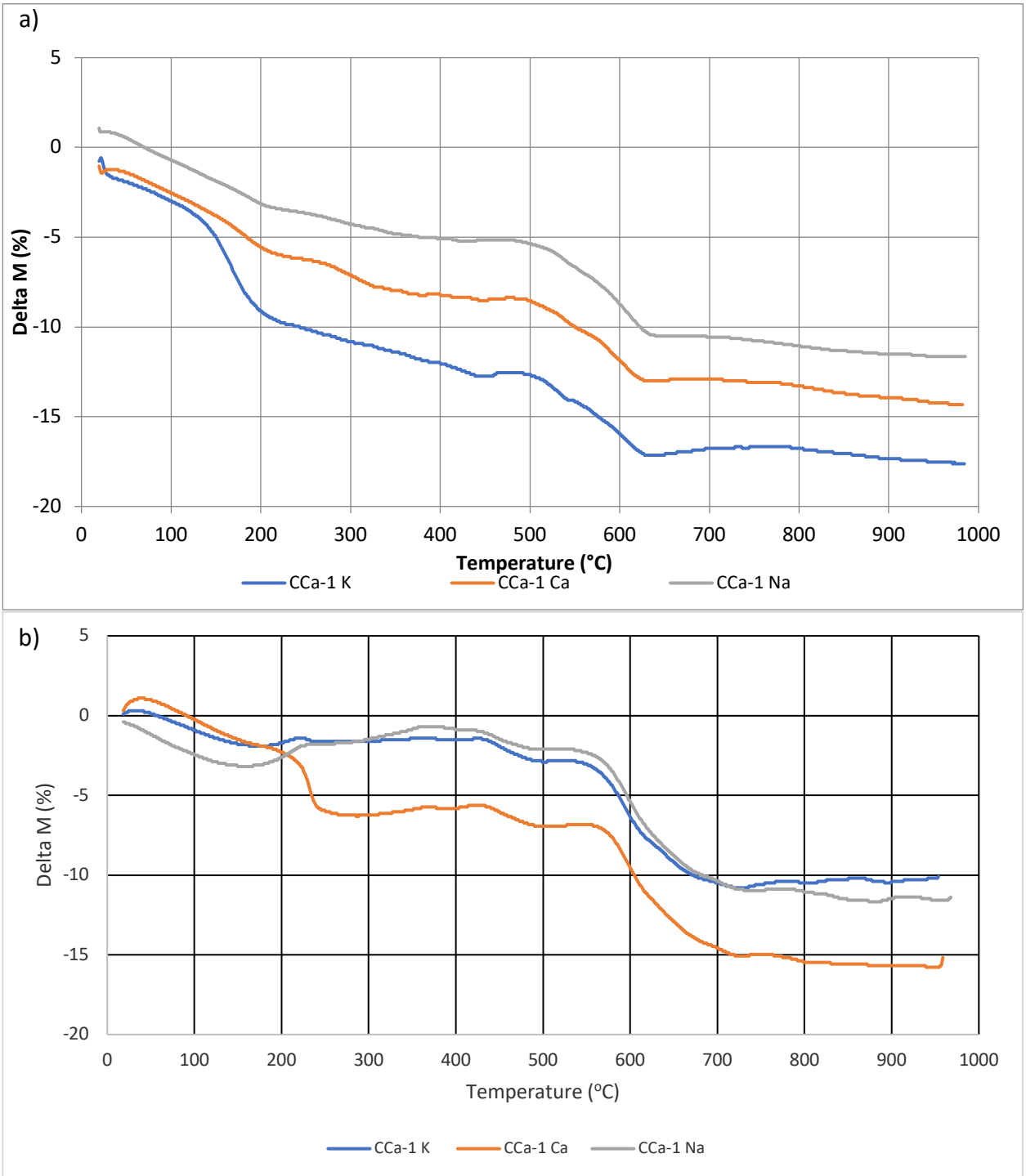

Figure 3.10. (a) In air and (b) In vacuo TGA patterns of air-dried <2µm K-, Ca- and Na- saturated CCa-1 heated at a rate of 10°C/minute.

Kaolinite – KGa-1

The preferred-oriented pXRD patterns for KGa-1 kaolinite were unchanged upon hydration (Ca-saturated) / rehydration (K-saturated, treatment with EG (Ca-saturated) or heating to 105°C and 300°C (K-saturated). Once KGa-1 was heated to 550°C, all basal diffractions disappeared (Figure 3.11a). A randomly oriented sample displayed a pXRD 06 dioctahedral band diffraction (0.149nm) typical of kaolinite.

There is little variation in the FWHM of the kaolinite (001) of KGa-1 across the spectrum of pXRD patterns obtained (0.16-0.22; Figure 3.11b). Such low values are consistent with high crystallinity, and the absence of any intercalation with other clay layers.

In air, the TGA of KGa-1 <2μm saturated samples were virtually identical for the K- and Na-saturations. Within the first 200°C of heating both saturations lost 1% by weight, after which weights remained stable until 500°C after which 12% by weight was lost within the next 100°C. The Ca-saturated sample gained 4% by weight from ~120-180°C and then did not change further up to ~375°C. Thereafter to 600°C, the sample lost 15% by weight. From 600 to 950°C there was only very minor weight change for any of the saturations (Figure 3.12a).

Unlike the *in air* sample, the Ca-saturated *in vacuo* sample showed no weight gain within the first 500°C. The *in vacuo* TGA weight loss curve for Ca-saturated KGa-1 <2μm showed a ~3% loss up to ~425°C, the Na-saturated sample showed a ~2% gain, and the K-saturated sample's weight remained unchanged. The major weight loss (~12%) in all saturations occurred between 425-700°C (Figure 3.12b), which is indicative of dehydroxylation.

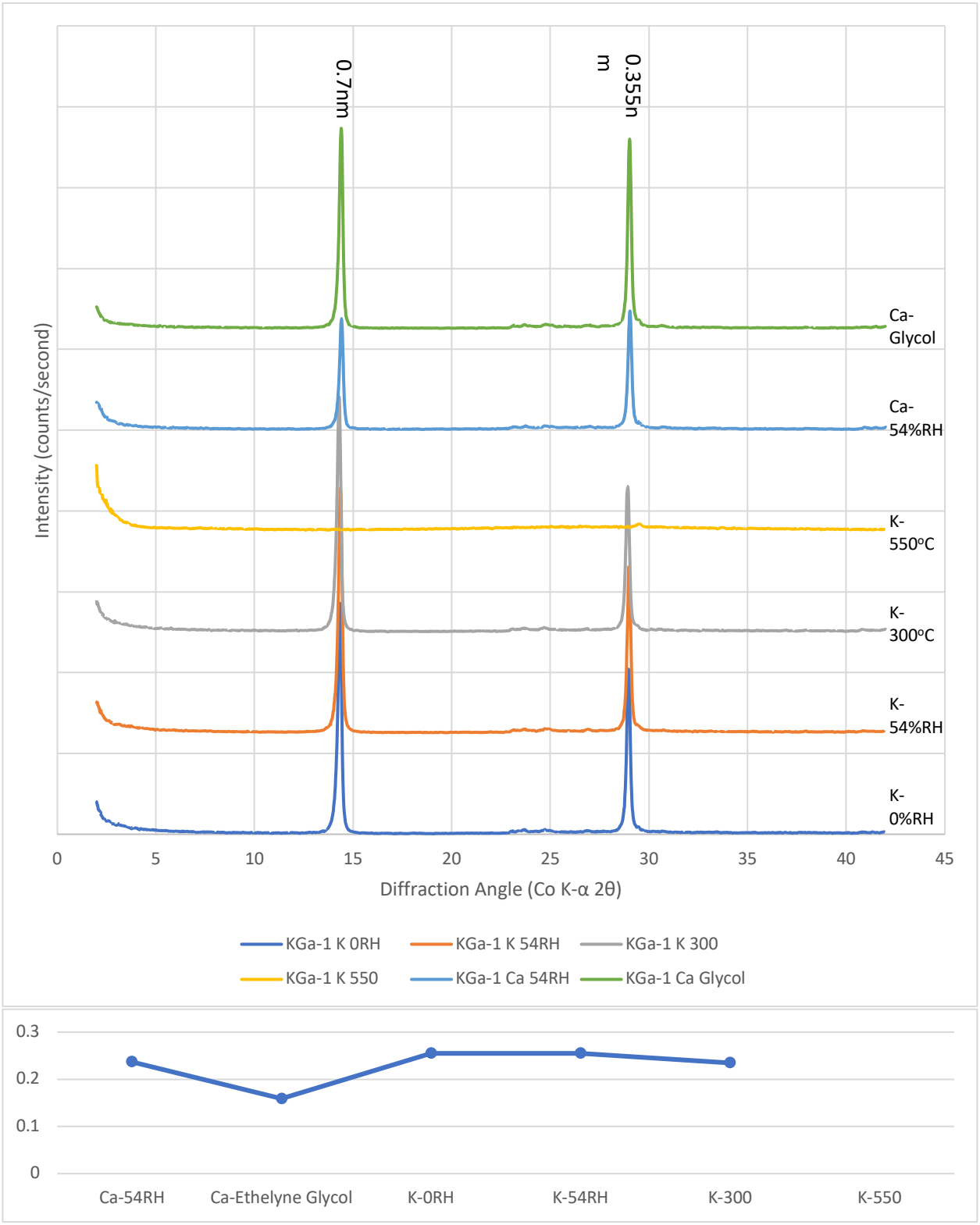

Figure 3.11. (a) Preferred-orientation pXRD of <2μm K- and Ca- saturated KGa-1 after various treatments. All treatments are displayed at the same relative intensity. (b) FWHM of KGa-1 (001) after various treatments. Data for the K-saturated 550˚C treatment was not available due to collapse the of (001) after the heat treatment.

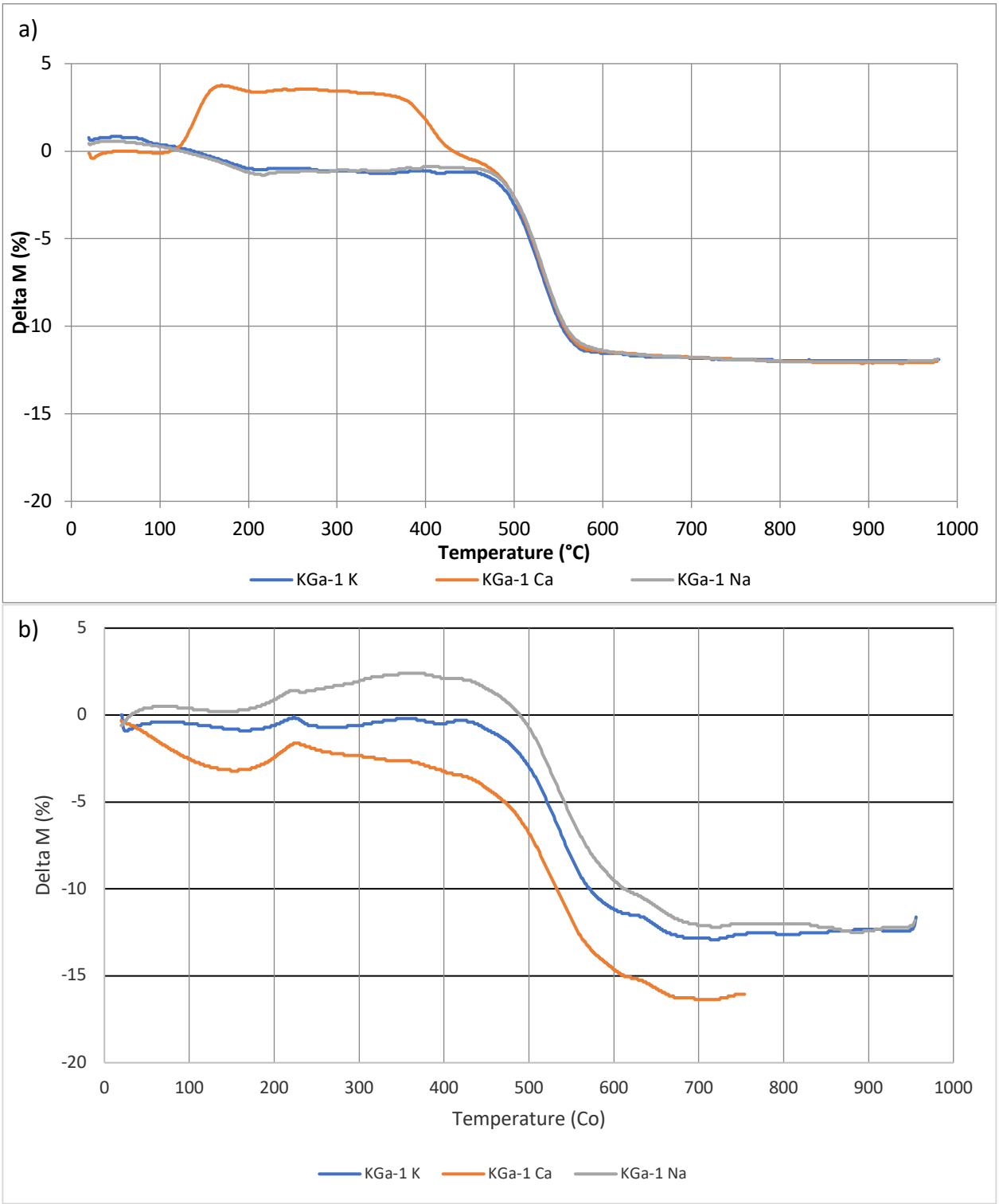

Figure 3.12. (a) In air and (b) In vacuo TGA patterns of air-dried <2µm K-, Ca- and Na- saturated KGa-1 heated at a rate of 10°C/minute.

3.2.2. Southwestern Ontario Ordovician Clays Minerals (<2μm)

The mineralogical compositions of all bulk and <2μm size-fractions of the Ordovician shale and limestone samples are summarized in Table 3.1. The relative abundances were calculated using weighted peak heights following Biscaye (1964, 1965). Identification of chloritic, illitic and kaolinitic clays was based on characteristic pXRD behaviours after various treatments of the <2μm size-fraction, as described earlier.

Queenston Formation – OGS DHN1 129m, NWMO DGR3 459m, NWMO DGR3 523m

The clay mineral assemblage (<2μm) of the Queenston Formation is dominated by illite, followed by kaolinite and then chlorite (Table 3.1; Figs. 3.13a, 3.15a, 3.17a). Non-clay minerals include quartz, plagioclase, gypsum and dolomite, with the highest abundances of these phases occurring in sample DGR3 459m (Table 3.1).

No clay samples showed significant swelling properties upon hydration at 54% relative humidity (RH) or treatment with EG, which indicates the absence of smectite group minerals. The pXRD patterns displayed a complete loss of kaolinite and/or chlorite clay basal diffractions at 0.7, 0.47, and 0.354nm upon heating to 550°C, which is typical of these phases. The illite 1.0nm (001) diffraction displayed no change upon heating to 550°C, consistent with minimal interstratification. Upon heating to 550°C, the 1.4nm chlorite (001) diffraction increased in intensity as well as shifting to a slightly lower d-spacing (Figures 3.13a, 3.15a, 3.17a). The pXRD 06 band patterns of randomly oriented <2μm material from the NWMO-DGR samples confirmed the presence of the dioctahedral clays kaolinite and illite at 1.489 and 0.150nm, respectively, and trioctahedral chlorite at 0.153nm.

*Table 3.1. Mineralogical abundances of the <2µm and bulk samples estimated using weighted peak heights of the most characteristic X-ray diffractions. Quartz abundances are based on the 0.343nm diffraction after correction for peak overlap from illite (003). n/a = not available; *= samples treated with HCl. All results are normalized to 100%.*

Sample	Formation/ Member	Size-fraction	Chloritic Clays (1.4nm)	Illitic Clays (1.0nm)	Kaolinitic Clays (0.7nm)	Quartz	Gypsum	Plagioclase	Calcite	Dolomite	Pyrite
NWMO DGR3 459m	Queenston	Bulk	3%	11%	4%	32%	2%	24%	17%	2%	3%
		<2µm	6%	45%	17%	14%	6%	9%	0%	2%	0%
NWMO DGR3 523m	Queenston	Bulk	2%	7%	4%	35%	17%	11%	18%	0%	4%
		<2µm	8%	50%	20%	10%	7%	2%	0%	2%	0%
NWMO DGR2 530m	Georgian Bay	Bulk	4%	17%	11%	53%	4%	3%	6%	0%	0%
		<2µm	7%	58%	21%	4%	7%	0%	1%	1%	0%
NWMO DGR2 616m	Blue Mountain	Bulk	4%	17%	11%	53%	5%	5%	2%	0%	2%
		<2µm	8%	52%	22%	9%	7%	1%	0%	1%	0%
OGS DHN1 129m	Queenston	Bulk	6%	14%	5%	39%	n/a	0%	28%	8%	0%
		<2µm	4%	75%	14%	0%	5%	0%	0%	1%	0%
OGS SG11-02 327m	Blue Mountain	Bulk	8%	23%	14%	45%	n/a	2%	5%	4%	0%
		<2µm	5%	70%	14%	0%	8%	2%	1%	1%	0%
OGS SG11-02 477m	Collingwood	Bulk	0%	12%	3%	22%	n/a	2%	59%	2%	1%
		<2µm*	4%	52%	9%	24%	4%	3%	0%	3%	0%
		<2µm	7%	27%	10%	13%	4%	2%	33%	2%	0%
OGS SG11-02 491m	Cobourg	Bulk	0%	0%	0%	10%	n/a	0%	86%	3%	0%
		<2µm*	5%	67%	12%	12%	3%	0%	0%	1%	0%
		<2µm	3%	14%	6%	7%	2%	0%	64%	3%	0%

There are minor variations in illite (001) peak sharpness in the DGR and OGS samples, as determined from the peak width at one-half of the maximum peak height (typically reported as "full width half maximum": FWHM) (Figures 3.13b, 3.15b, 3.17b). There are many indices of illite "crystallinity" related to FWHM, of which the most common is the 'Kübler Index' (Guggenheim et al., 2002). Lower values of FWHM are commonly interpreted to indicate higher crystallinity. As Guggenheim et al. (2002) noted, however, such measures do not describe the crystallinity of a mineral, which is a three-dimensional property. Instead, FWHM is a measure of a two-dimensional crystal property. Kübler (Kübler & Jaboyedoff, 2000) later noted that the Kübler Index is "an indirect measurement of the mean consecutive illite layers contained in the coherent scattering domains of mixed layer illite-smectite", and is best applied to the identification of the transitional zone between diagenesis and metamorphism, commonly referred to as the anchizone. In this thesis, the Kübler Index is used within that context.

Since the Kübler Index, and its values for the anchizone, were originally defined for the (001) of oriented, air-dried samples analyzed using Cu K-alpha radiation (i.e., the Ca-54% RH sample), those values have been proportionally adjusted to account for use of Co K-alpha radiation in this study, and to incorporate the recalibration of the Kübler Index reported by Warr & Ferreiro Mählmann (2015). In the present work, illite FWHM values of >1.16 are used as first estimates to demarcate the shallow diagenetic zone, 1.16-0.49 the deep diagenetic zone, 0.49-0.35 the low anchizone, 0.35-0.29 the high anchizone, and <0.29 the epizone. Ongoing work by others at Western's Laboratory for Stable Isotope Science is seeking to further test and refine this initial calibration. In addition, variations in the Kübler Index produced during various pXRD treatments provide insight into the potential for penetration by water or organic liquids in illitic clays. The Kübler Index cannot be applied directly to chlorite. The same principles, however, can

be used to assess the accessibility of the interlayer position, which is normally filled by a 'gibbsite-like' or 'brucite-like' sheet, to fluids.

For the Queenston Formation samples, the FWHM of the Ca-54% sample (~ 0.5) lies at the boundary between the deep diagenetic zone and the low anchizone (Figures 3.13b, 3.15b, 3.17b). The NWMO samples from the DGR showed no significant variation in FWHM among the various pXRD treatments. Higher values of FWHM were observed for the K-saturated pXRD patterns of the OGS sample, which are more typical of lower diagenetic grades. The FWHM for the Ca-54% RH pXRD of chlorite ranges from ~0.35 to 0.7 (Figures 3.13c, 3.15c, 3.17c). For the other pXRD treatments, one chlorite sample shows a steady decrease in FWHM with heating, another no significant change, and still another, more variable behaviour. While this likely reflects some differences in the stability of the interlayer octahedral sheet from sample to sample, there is no overall indication of significant water sensitivity of this chlorite.

Air-dried K- and Na-saturated <2μm fractions of sample DGR3 459m, from the upper portion of the Queenston Formation, showed little to no change in weight during *in vacuo* TGA for the first 550°C of heating (Figure 3.14). The Ca-saturated <2μm fraction, by comparison, lost ~5% by weight within the first 200°C of heating. All saturations lost ~9% by weight from 550-700°C.

In air TGA patterns for Queenston Formation sample OGS DHN1 129m displayed a weight loss of 2, 5, and 10% for the K, Ca, and Na-saturations of the air-dried <2μm fractions, respectively, within the first 200°C of heating. The K and Ca-saturated <2μm fraction lost an additional 4% by weight up to 700°C, after which there was no further weight loss for the remainder of the heating up to 950°C. The Na-saturated <2μm sample lost an addition 6% by weight from 200-700°C after which there was no further weight loss for the remainder of the

heat treatment (Figure 3.16a). By comparison, *in vacuo* TGA patterns displayed a weight loss of 4, 3 and 6% for the K, Ca and Na-saturations of the air-dried <2μm fractions, respectively, within the first 200°C of heating (Figure 3.16b). K and Ca- saturated <2μm fractions lost an additional 5% by weight up to 700°C, after which there was no further weight loss up to 950°C. The Na-saturated <2μm sample lost an additional 6% by weight from 200-700°C after which there was no further weight loss for the remainder of the heat treatment (Figure 3.16b).

During *in vacuo* TGA analysis, air-dried <2μm fractions from the lower portions of the Queenston Formation (sample DGR3 523m, Figure 3.18) lost ~1% by weight from 0-425°C of heating, after which 6% by weight was lost by 700°C. The weight of all <2μm fractions then stabilized for the remainder of the heating.

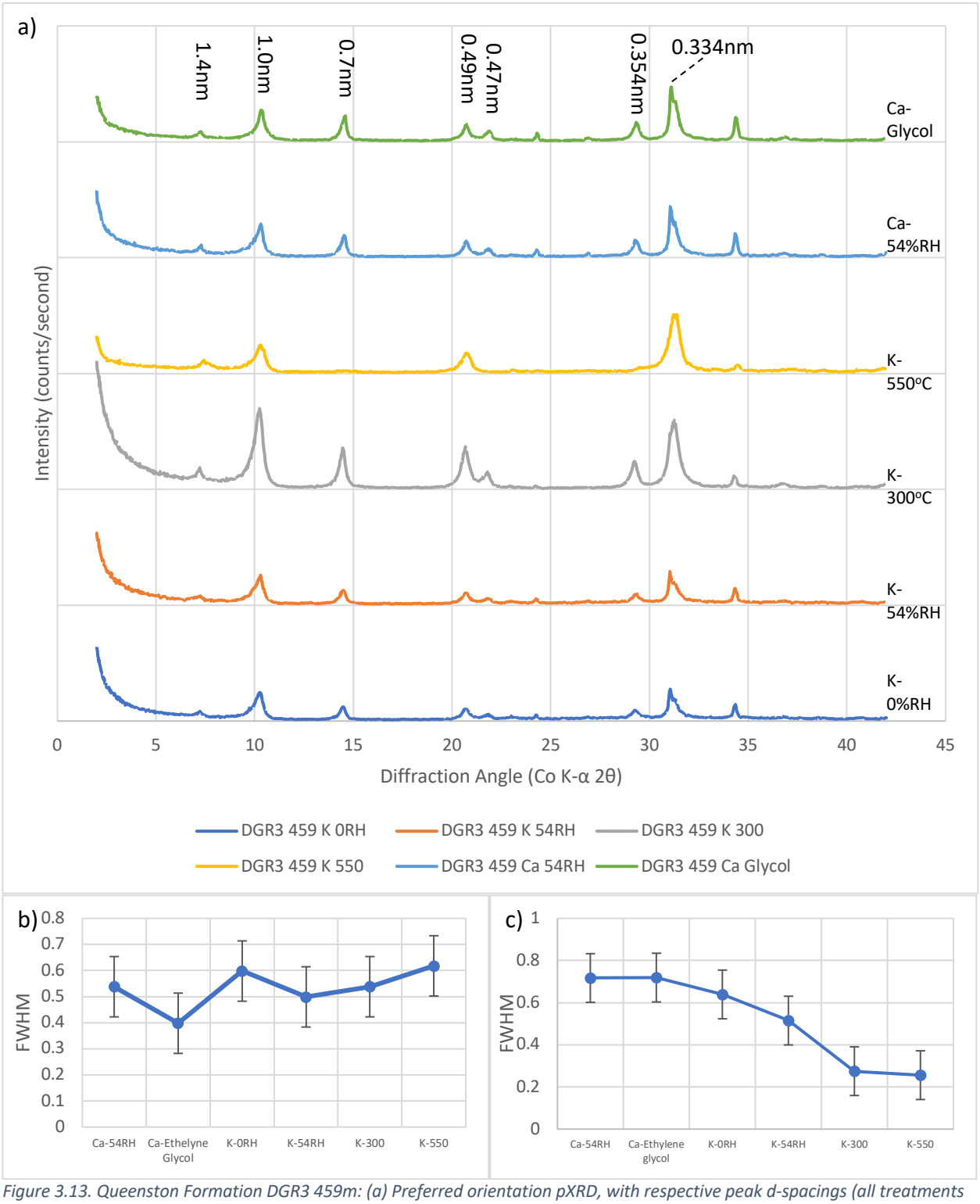

Figure 3.13. Queenston Formation DGR3 459m: (a) Preferred orientation pXRD, with respective peak d-spacings (all treatments are displayed at the same relative intensity enabling direct comparison); (b) FWHM of illite (001) (error bars represent standard deviation of FWHM of quartz (101) within each sample set); (c) FWHM of chlorite (001) peak (error bars represent standard deviation of FWHM of quartz (101) within each sample set).

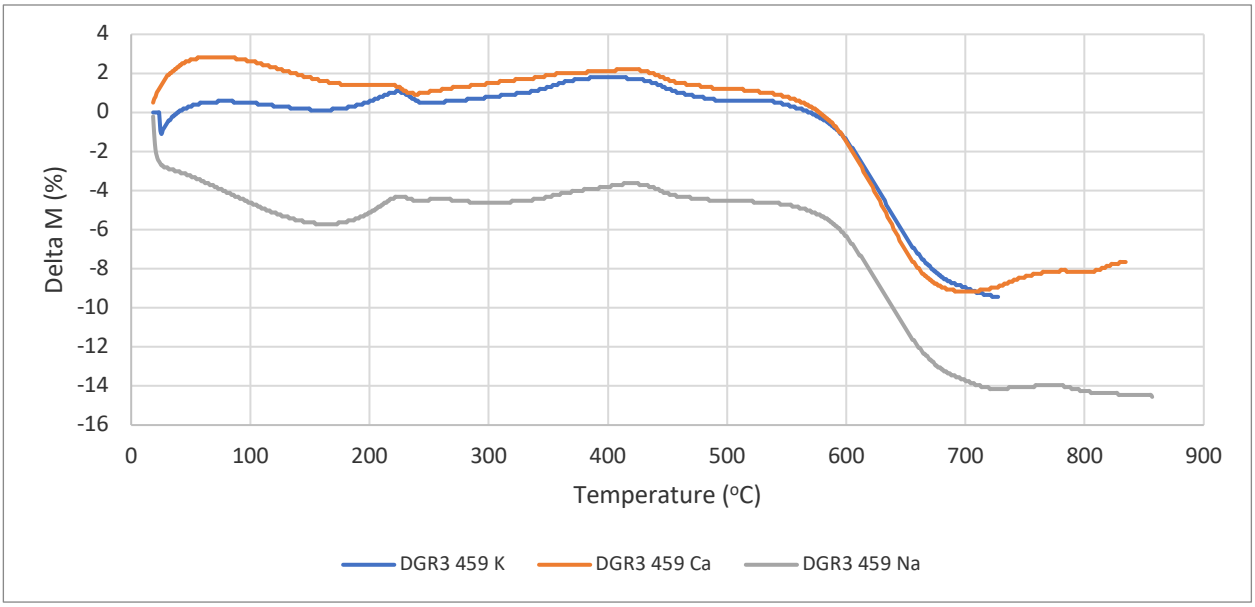

Figure 3.14. Queenston Formation DGR3 459m: In vacuo TGA patterns for air-dried <2µm K-, Ca- and Na- saturated samples heated at a rate of 10°C/minute.

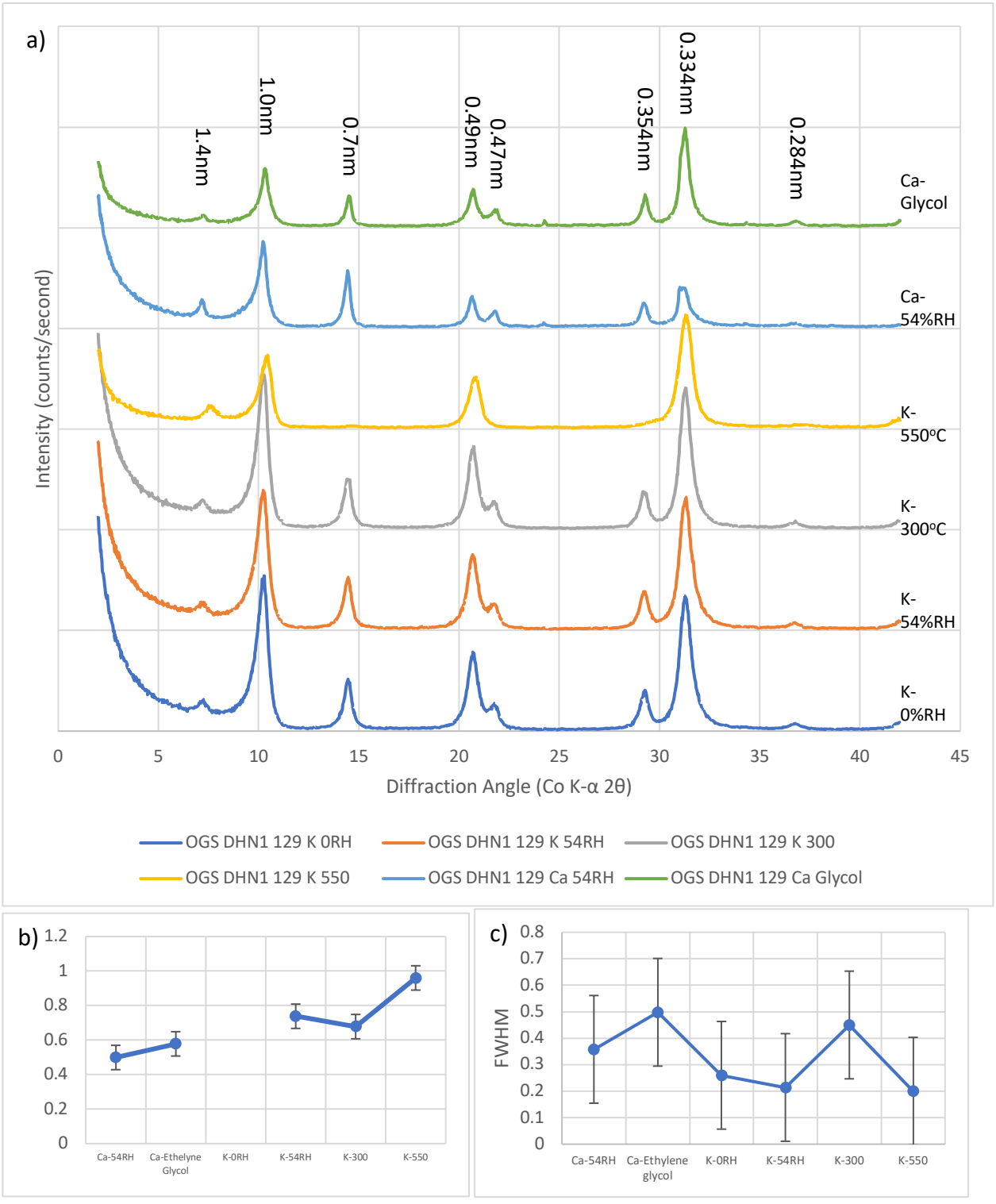

Figure 3.15. Queenston Formation OGS-DHN1 129m: (a) Preferred orientation pXRD, with respective peak d-spacings (all treatments are displayed at the same relative intensity enabling direct comparison); (b) FWHM of illite (001) (error bars represent standard deviation of FWHM of quartz (101) within each sample set) Anomalous data for the K-saturated 0%RH treatment is not shown.*; c) FWHM of chlorite (001) (error bars represent standard deviation of FWHM of quartz (101) within each sample set).*

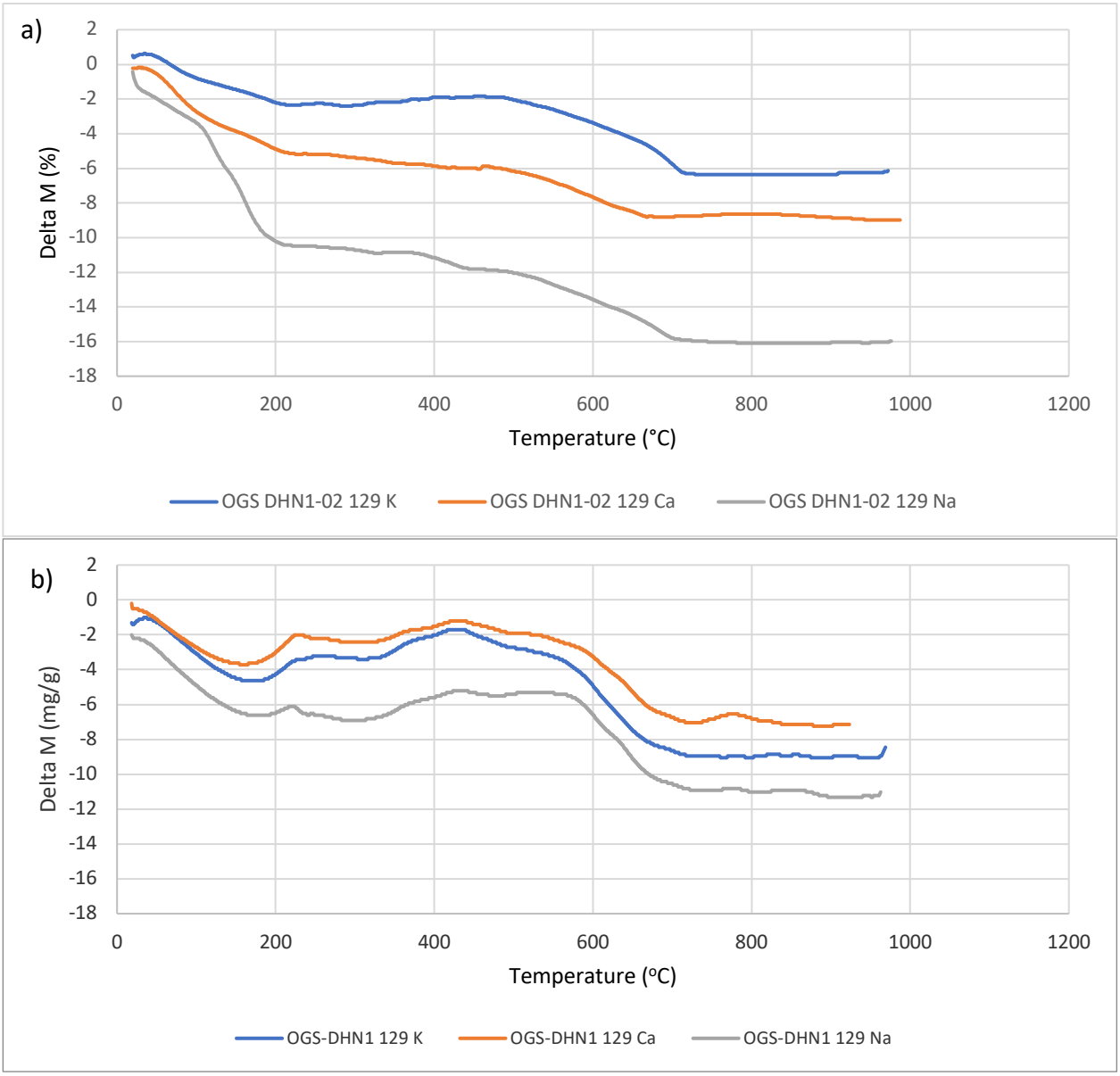

Figure 3.16. Queenston Formation OGS-DHN1 129m: (a) In air, and (b) in vacuo TGA patterns of air-dried <2µm K-, Ca- and Na-saturated OGS-DHN1 129m heated at a rate of 10°C/minute.

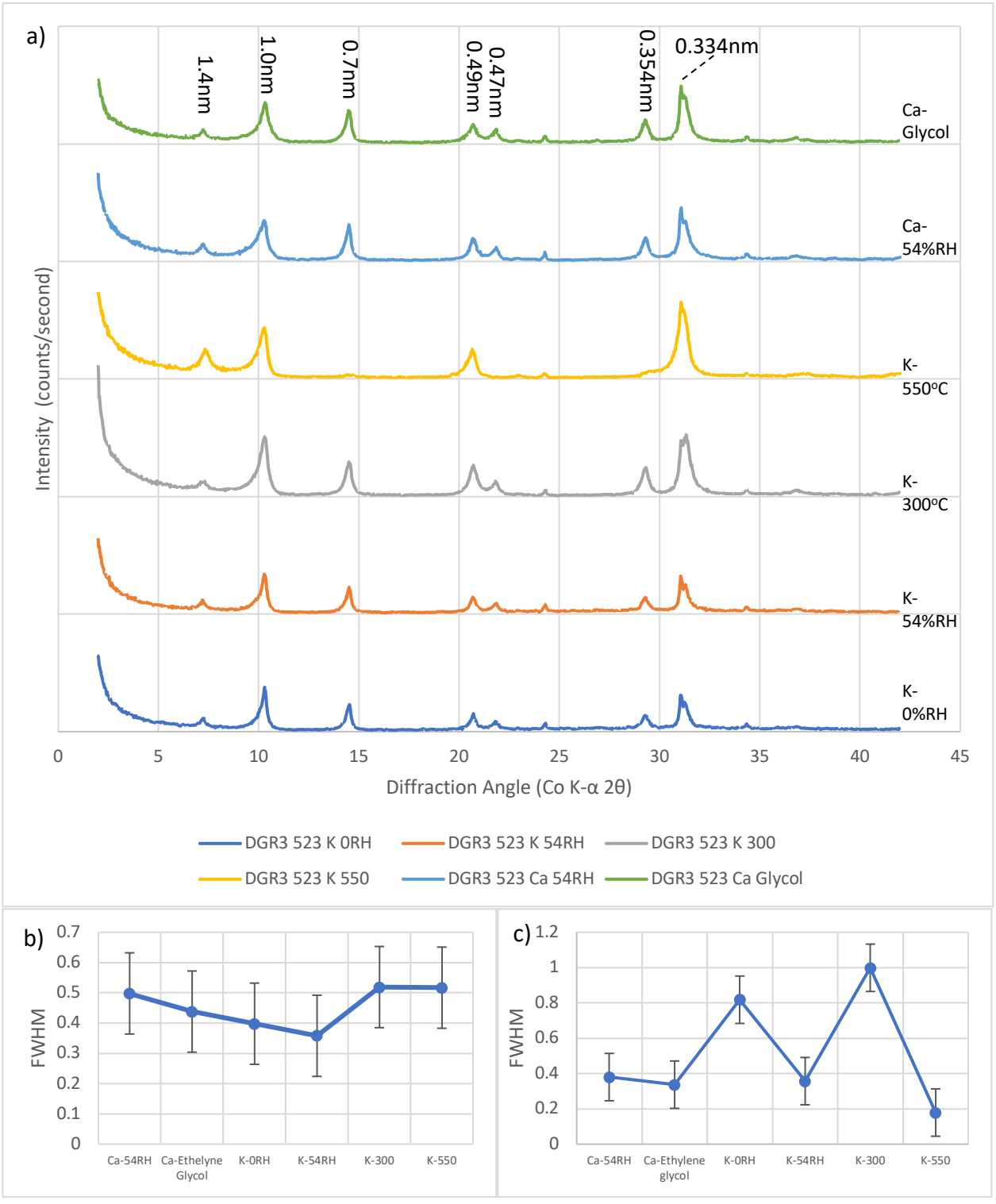

Figure 3.17. Queenston Formation DGR3 523m: (a) Preferred orientation pXRD, with respective peak d-spacings (all treatments are displayed at the same relative intensity enabling direct comparison); (b) FWHM of illite (001) (error bars represent standard deviation of FWHM of quartz (101) within each sample set); (c) FWHM of chlorite (001) (error bars represent standard deviation of FWHM of quartz (101) within each sample set).

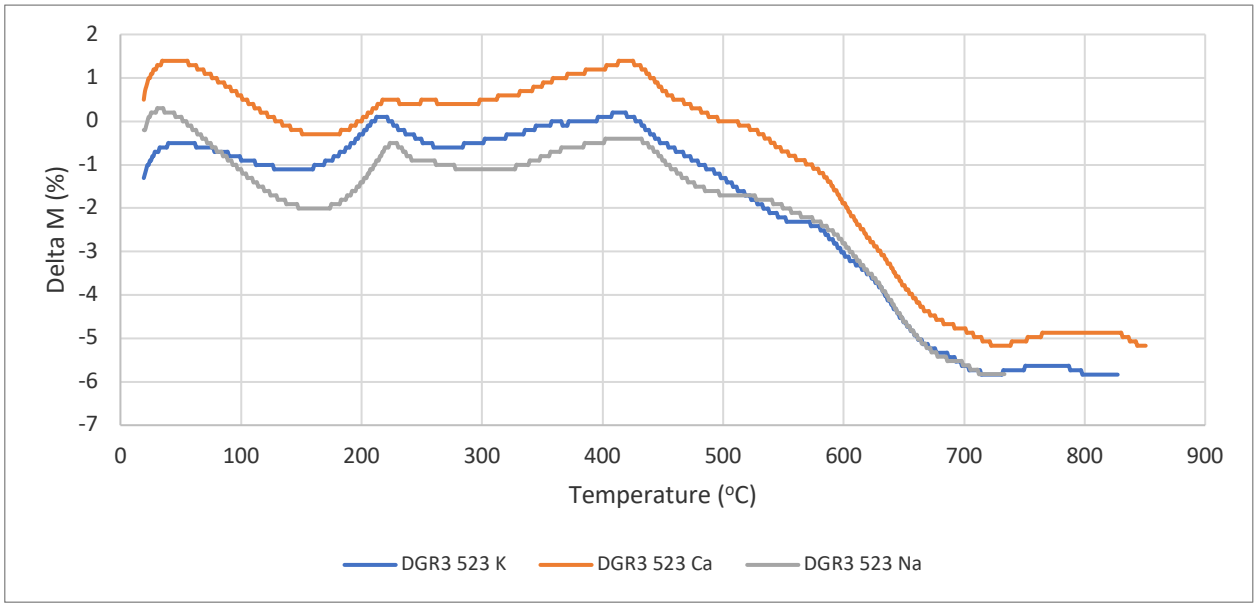

Figure 3.18. Queenston Formation DGR3 523m: In vacuo TGA patterns of air-dried <2µm K-, Ca- and Na- saturated samples, heated at a rate of 10°C/minute.

Georgian Bay Formation – NWMO DGR2 530m

The Georgian Bay Formation clay mineral assemblage (<2μm) is dominated by illite, followed by kaolinite and then chlorite (Table 3.1). The pXRD 06 band patterns of a randomly oriented sample confirmed the presence of illite (dioctahedral, 0.150nm) and trioctahedral chlorite (0.152nm). Non-clay minerals include quartz, gypsum and trace amounts of calcite and dolomite (Table 3.1; Figure 3.19) (Reed, 2005).

None of the clays showed significant swelling properties upon hydration of Ca-saturated samples at 54% RH or during EG treatment, which indicates the paucity of smectite group minerals or interlayers (Figure 3.20a). Consistent with this observation, the 1.0nm diffraction showed no change upon rehydration from K-saturated 0% RH to the 54% RH. Once the sample was heated to 300°C, there was an increase in the intensity of the illite (001). Heat treatment to 550°C, however, caused degradation of the illite (001), as indicated by its lower and broader peak (Figure 3.20a).

The illite FWHM for the Ca-54% RH sample (~1.1) lies at the boundary between the deep and shallow diagenetic zones (Figure 3.20b). There was no significant increase in the FWHM during EG treatment, indicating a low abundance of interstratified smectite layers. The availability of interlayer space to accept K^+, however, was shown by a sharp decrease in FWHM for K-saturated K-0% RH and K-54% RH (Figure 3.20b). Upon heating, however, degradation of the illite structure is demonstrated by an increase in FWHM (Figure 3.20b). The chlorite FWHM showed little variation from its average value of 0.5 across pXRD treatments (Figure 3.20c). Upon heating to 550°C, the K-saturated pattern showed the typical loss of diffractions at 0.7, 0.47, and 0.354nm. The (001) diffraction at 1.4nm also shifted to a lower d-spacing (1.28nm), typical of heating-related structural disruption similar to that observed for illite in this sample.

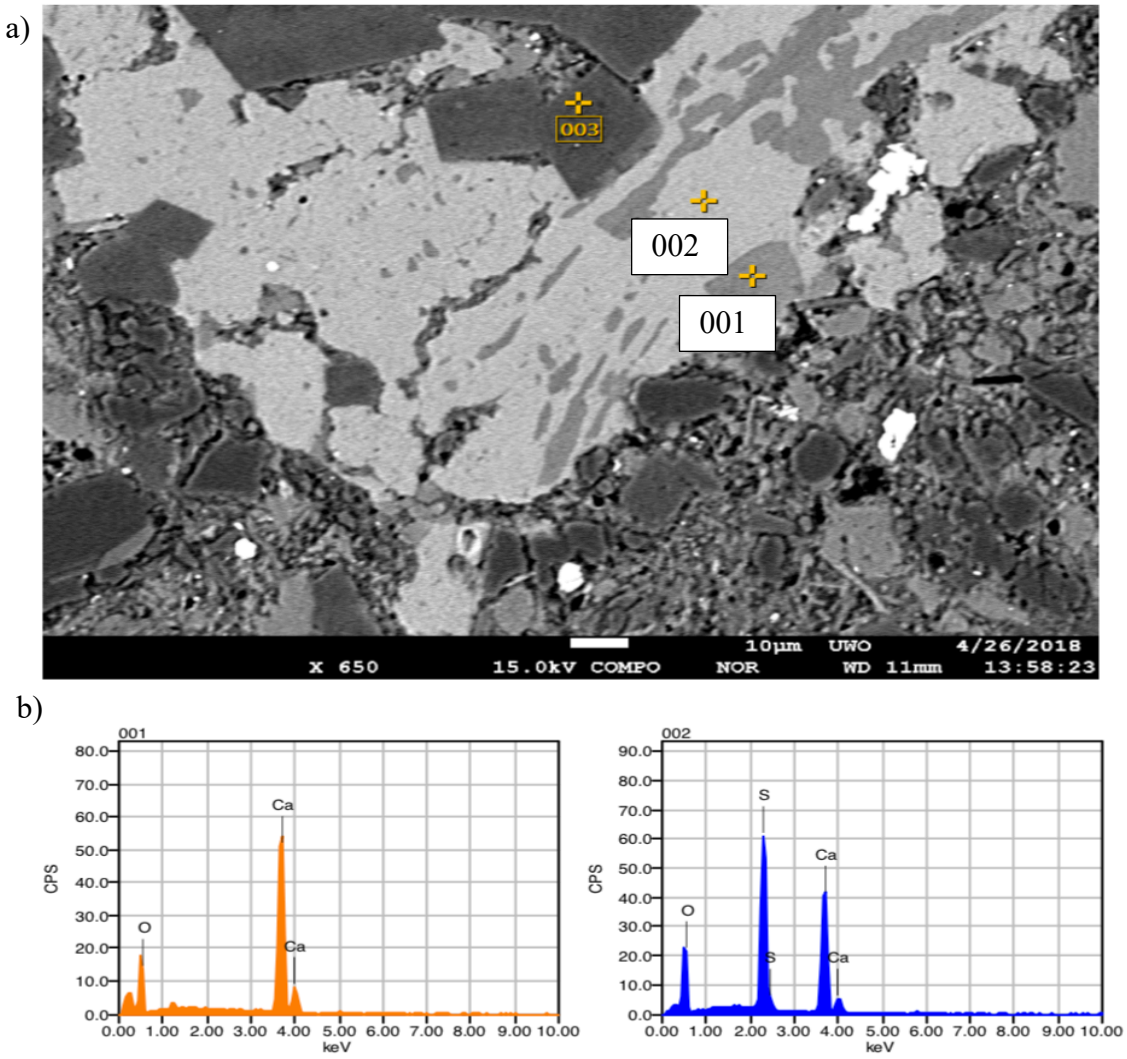

Figure 3.19. Sample NWMO DGR2 530m: (a) BSE image; (b) EDS of calcite at spot 001 and gypsum at spot 002 shown in (a) Voltage at 15 kV.

Air-dried Ca- and Na-saturated <2μm fractions of sample DGR2 530m lost ~1% by weight within the first 150°C of *in vacuo* TGA, which was then regained by 400°C. From 400-700°C, there was a 4% loss by weight after which there was only minor weight loss. K-saturated samples lost 4% by weight within the first 150°C, regaining 1.5% by 400°C. The remaining 500°C of the heat treatment resulted in a gradual weight loss amounting to 4.5% (Figure 3.21).

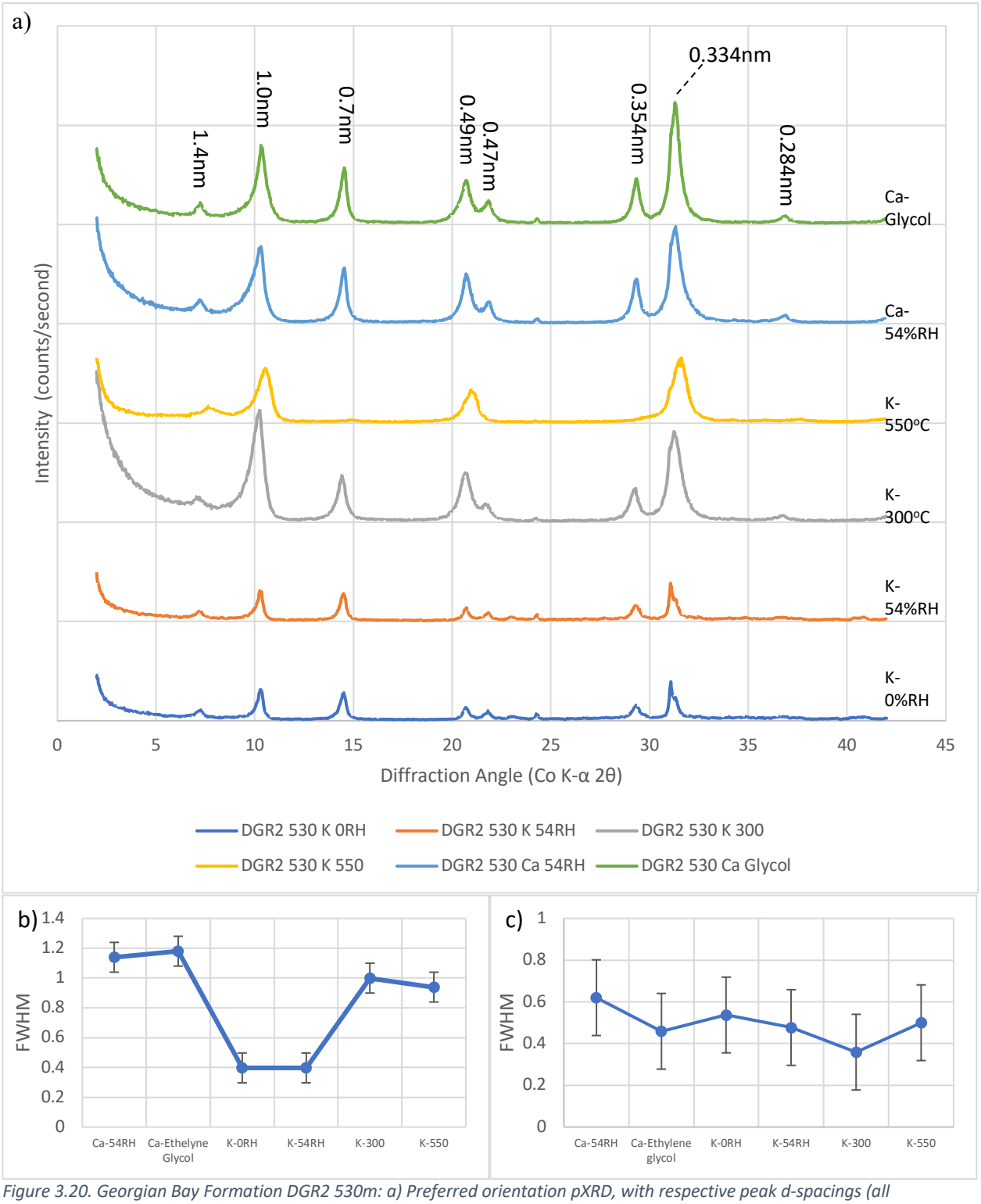

Figure 3.20. Georgian Bay Formation DGR2 530m: a) Preferred orientation pXRD, with respective peak d-spacings (all treatments are displayed at the same relative intensity enabling direct comparison); b) FWHM of illite (001) (error bars represent standard deviation of FWHM of quartz (101) within each sample set); c) FWHM of chlorite (001) (error bars represent standard deviation of FWHM of quartz (101) within each sample set).

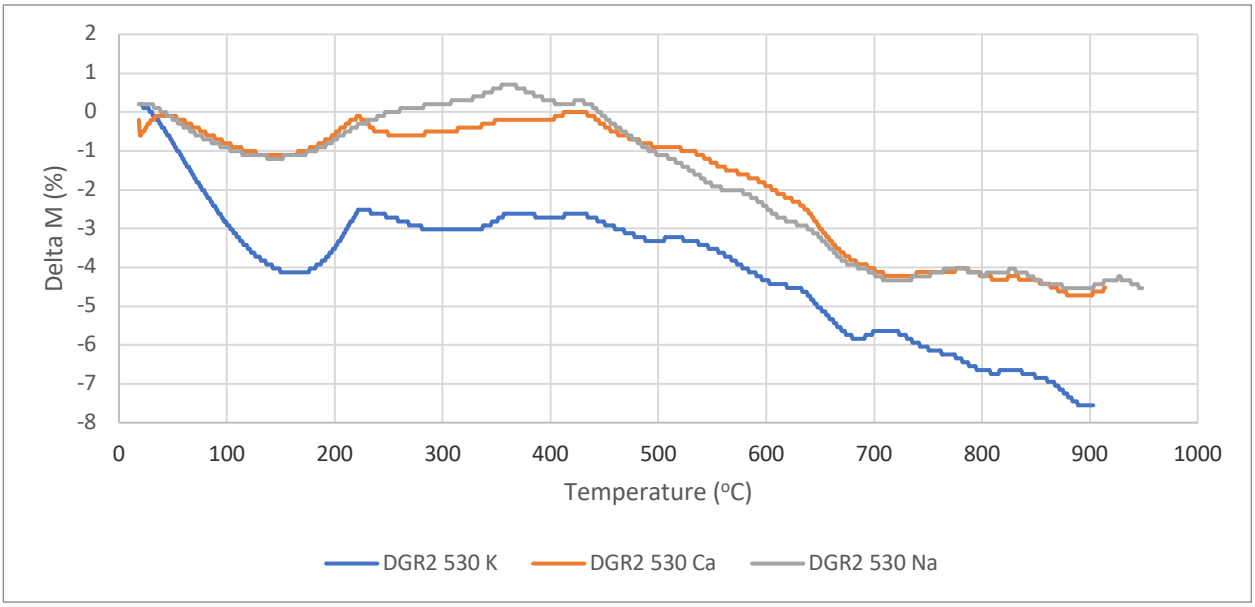

Figure 3.21. Georgian Bay Formation DGR2 530m: In vacuo TGA patterns air-dried <2µm K-, Ca- and Na- saturated DGR2 530m heated at a rate of 10°C/minute.

Blue Mountain Formation – OGS SG11-02 327m, NWMO DGR2 616m

The clay mineral assemblage (<2μm) of the Blue Mountain Formation is dominated by illite followed by kaolinite and then chlorite (Table 3.1). The pXRD 06 band patterns of randomly oriented samples confirmed the presence of kaolinite (0.149nm), illite (0.150nm) and trioctahedral chlorite (0.152nm). Non-clay minerals include quartz, gypsum and trace amounts of plagioclase, calcite and dolomite.

The pXRD and TGA patterns for Blue Mountain Formation samples OGS-SG11-02 327m and DGR2 616m are illustrated in Figures 3.22 and 3.23, and 3.24 and 3.25, respectively. None of the Ca-saturated samples showed significant swelling upon hydration at 54% RH or during EG treatment, nor was there any change upon rehydration of K-saturated aliquots from 0 to 54% RH, all properties signaling low levels of swelling clay interstratification. Heating to 300°C of the K-saturated sample caused an increase in the illite (001) intensity. Heating of the K-saturated samples to 550°C resulted in the typical loss of kaolinite and/or chlorite clay basal

diffractions at 0.7, 0.47, and 0.354nm. Degradation of the illite and chlorite structures is also indicated by lower illite basal diffraction intensities, and a lowering and shift of the chlorite 1.4nm diffraction to 1.3nm.

For sample OGS SG11-02 327m, the illite (001) FWHM for the Ca-54% RH sample (~1.3) lies within the shallow diagenetic zone but near the boundary with the deep diagenetic zone. The FWHM decreases sharply (to ~0.3) upon treatment with EG (Figure 3.22b), suggesting that swelling layers have moved to higher two-theta positions, thus reducing the illite (001) FWHM. The FWHM of K-saturated aliquots vary from ~0.7 to 1.3, which may indicate a less well organized illite, in which the K was not able to fully penetrate vacant interlayer or octahedral sheet positions. The FWHM of the chlorite (001) ranges widely across treatments (~0.1 to 0.6), but these differences are not significant given the large errors associated with these measurements (Figure 3.22c).

For Blue Mountain Formation sample DGR2 616m, the illite (001) FWHM of the Ca-54% RH aliquot (~0.6) lies within the deep diagenetic zone but near the boundary with the low anchizone, and does not change significantly across treatments (Figure 3.24b). The chlorite (001) FWHM trends slightly downwards across all treatments from its value of ~0.45 for the Ca-54% RH sample (middle anchizone?) but the differences are not significant (Figure 3.24c).

In air TGA of OGS SG11-02 327m showed 5, 8 and 10% loss by weight for the Ca-, K-, and Na-saturations, respectively, within the first 200°C. The Ca- and K- saturated aliquots then lost ~7% by weight from 400-700°C, after which only minor weight loss occurred up to 950°C. The Na-saturated sample lost 10% by weight from 300-700°C after only minor weight loss occurred (Figure 3.23a). By comparison, *in vacuo* TGA (Figure 3.23b) produced 2, 3 and 5.5% loss by weight for air-dried K, Na- and Ca-saturated samples, respectively, within the first

200°C. Then, for Ca- and K-saturated samples no weight loss (and for K, some apparent weight gain) was observed from 200-500°C, followed by 5% weight loss from 500-700°C, after which sample weights more or less stabilized for the remaining 200°C of heating. The Na-saturated sample displayed no weight change from 200-400°C, followed by 7% by weight loss from 400-700°C, after which sample weight stabilized for the remainder of the heating.

During TGA, Blue Mountain sample DGR2 616m showed *in vacuo* weight loss followed by minor weight gain for all saturations up to 200°C, by which temperature the K-, Na- and Ca-saturated samples had lost 1, 2, and 4% of their original weight, respectively (Figure 3.25). From ~200-400°C, there was little weight change for all saturations. This was followed by weight losses of 5% by 700°C, after which only minor further changes occurred (Figure 3.25).

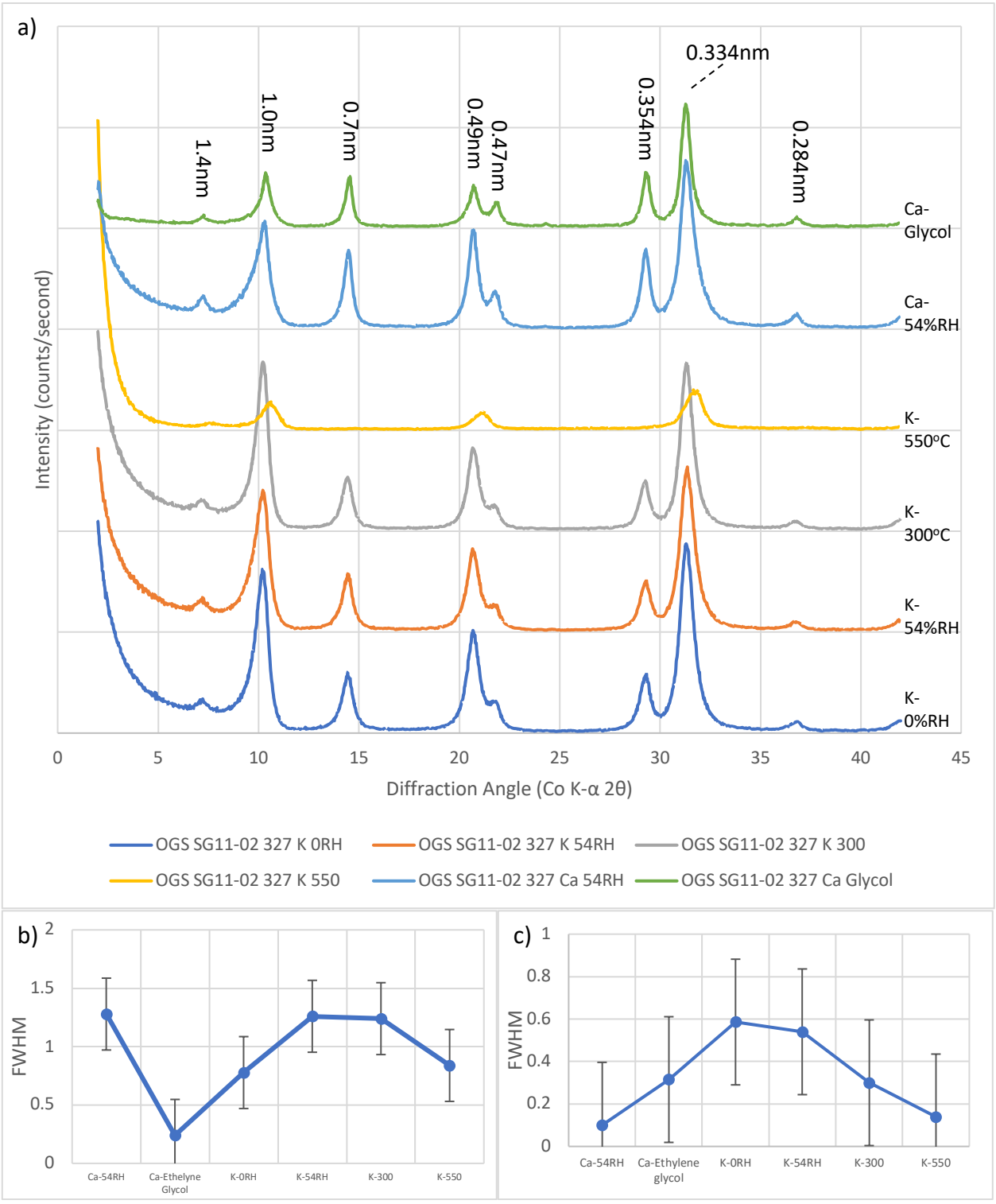

Figure 3.22. Blue Mountain Formation OGS SG11-02 327m: (a) Preferred orientation pXRD, with respective peak d-spacings (all treatments are displayed at the same relative intensity); (b) FWHM of illite (001) (error bars represent standard deviation of FWHM of quartz (101) within each sample set); (c) FWHM of chlorite (001) (error bars represent standard deviation of FWHM of quartz (101) within each sample set).

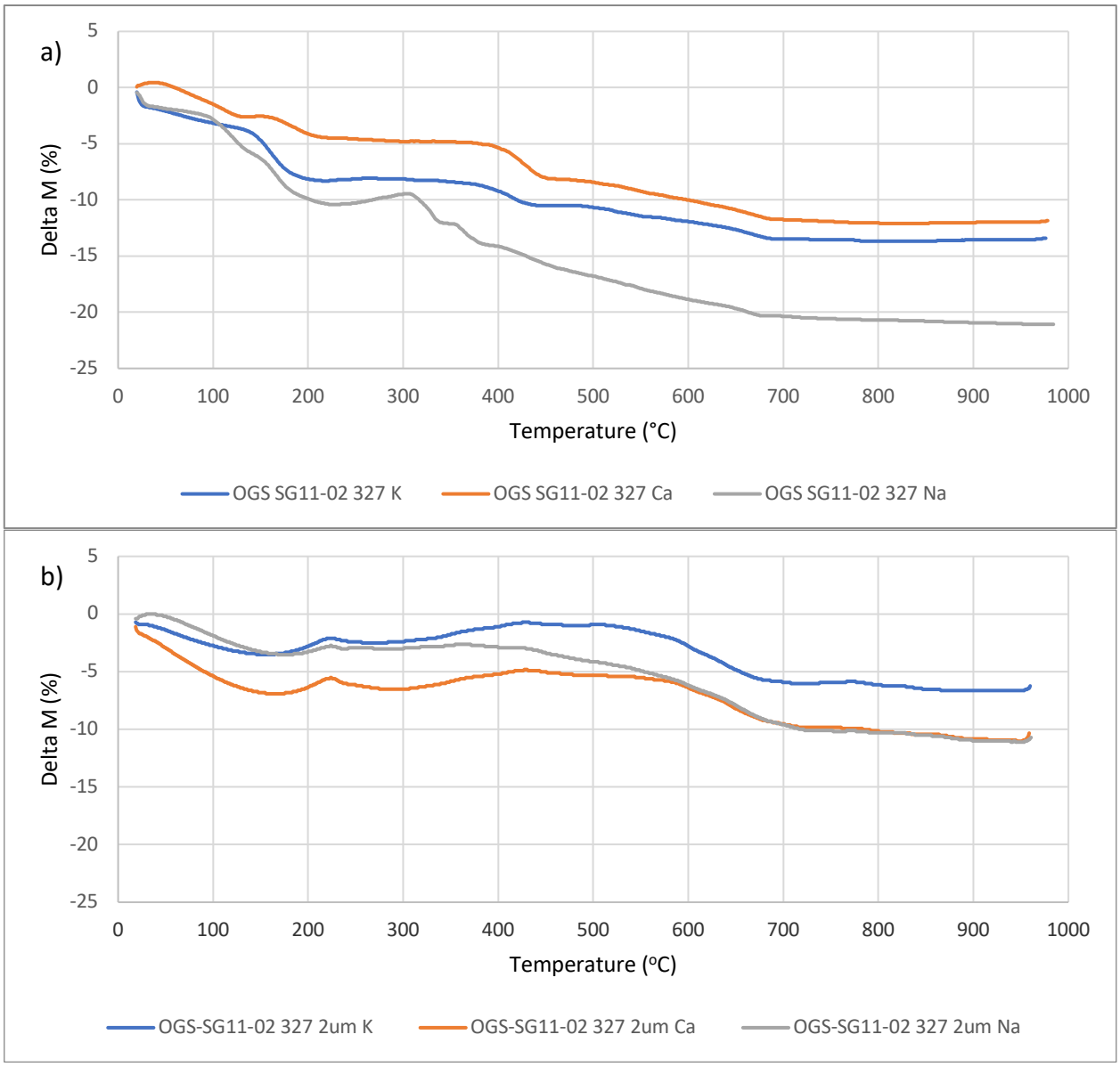

Figure 3.23. Blue Mountain Formation OGS SG11-02 327m: (a) In air and (b) in vacuo TGA patterns of air-dried <2µm K-, Ca- Na-saturated samples heated at a rate of 10°C/minute.

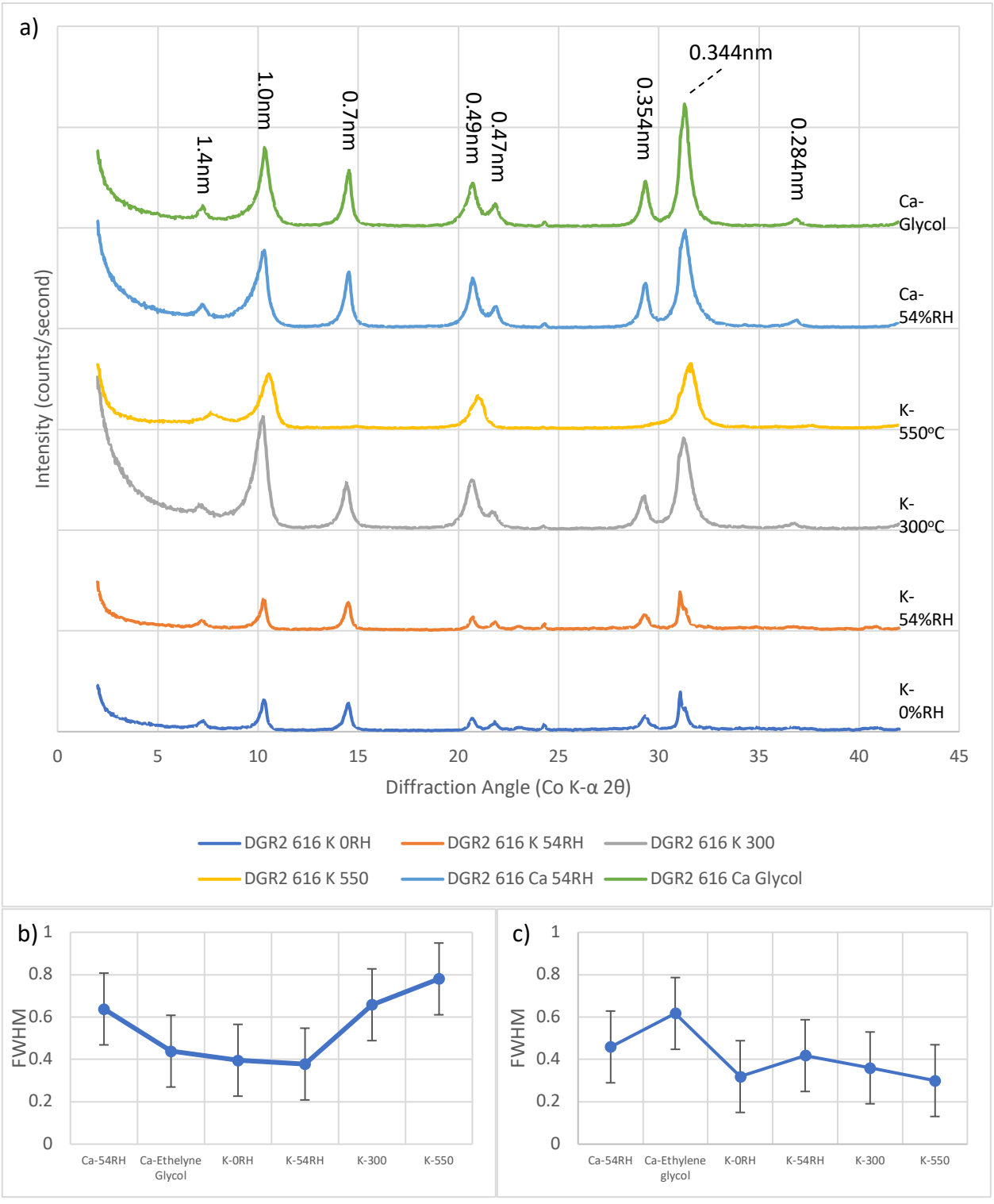

Figure 3.24. Blue Mountain Formation DGR2 616m: (a) Preferred orientation pXRD, with respective peak d-spacings (all treatments are displayed at the same relative intensity enabling direct comparison); (b) FWHM of illite (001) (error bars represent standard deviation of FWHM of quartz (101) within each sample set); (c) FWHM of chlorite (001) (error bars represent standard deviation of FWHM of quartz (101) within each sample set).

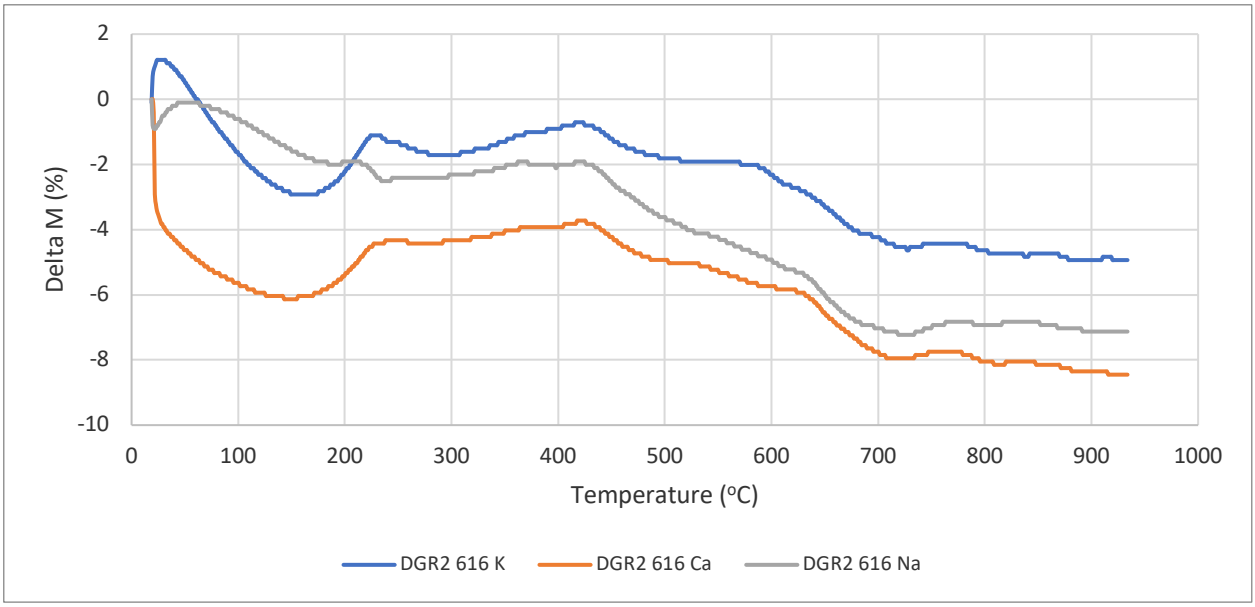

Figure 3.25. Blue Mountain Formation DGR2 616m: In vacuo TGA patterns of air-dried <2µm K-, Ca- and Na- saturated samples, heated at a rate of 10°C/minute.

Collingwood Member – OGS SG11-02 477m

The clay mineral assemblage (<2μm) in the Collingwood Member is dominated by illite, followed by kaolinite and then chlorite (Table 3.1; Figure 3.26a). The pXRD 06 band patterns of the randomly oriented sample confirmed the presence of illite (0.150nm) and trioctahedral chlorite (0.153nm). Non-clay minerals include quartz, calcite, gypsum, plagioclase and dolomite (Table 3.1). Abundant calcite was removed from the Ca- and K-saturated <2μm size-fractions using HCl prior to further examination, which led to an overall reduction in pXRD peak intensities in this sample, relative to most others.

None of the Ca-54% RH and EG-treated or heated K-saturated samples showed changes in pXRD basal spacings attributable to smectite group minerals (Figure 3.26a). Also, as is typical of kaolinite and chlorite, basal diffractions at 0.7, 0.47, and/or 0.354nm were lost upon heating to 550°C. The illite 1.0nm (001) diffraction displayed no significant change upon heating to 550°C, consistent with minimal interstratification. Upon heating to 550°C, the 1.4nm chlorite (001)

diffraction displayed a minor shift to a lower d-spacing, which is characteristic of heating-related degradation (Figure 3.26a). The Ca-54% RH illite (001) FWHM (~0.45) lies within the low anchizone, near the boundary with the deep diagenetic zone; the FWHM varied little (0.4-0.5) across all subsequent treatments (Figure 3.26b). The Ca-54% RH chlorite (001) FWHM is ~0.6 (Figure 3.26c). A decrease in FWHM following treatment with EG, and a further decrease following K-saturation at 0 and then 54% RH, suggests that peak sharpness was increased by these treatments. Heating to 550°C, however, produced a higher FWHM, consistent with heating-related degradation (Figure 3.26c)

In air TGA for Ca- and K-saturated, <2μm samples of OGS SG11-02 477m, both of which had been treated with HCl to remove carbonate, displayed almost smooth, continuous weight loss patterns. There was steady weight loss (12%) up to 425°C (12%) followed by a lower but still steady pattern of weight loss from 425-950°C (8%) (Figure 3.27a). By comparison, *in vacuo* TGA of the same HCl-treated samples showed clearer weight loss steps. Air-dried K- and Ca-saturated <2μm fractions showed 4 and 7% weight loss within the first 375°C. Both fractions then lost 11% by weight from 375-700°C after which there was only minor further weight loss (Figure 3.27b). In contrast, the TGA for the Na-saturated sample, which was not treated with HCl, was dominated by decarboxylation, losing 17% by weight from 425-700°C after which further weight loss was minor (Figure 3.27b).

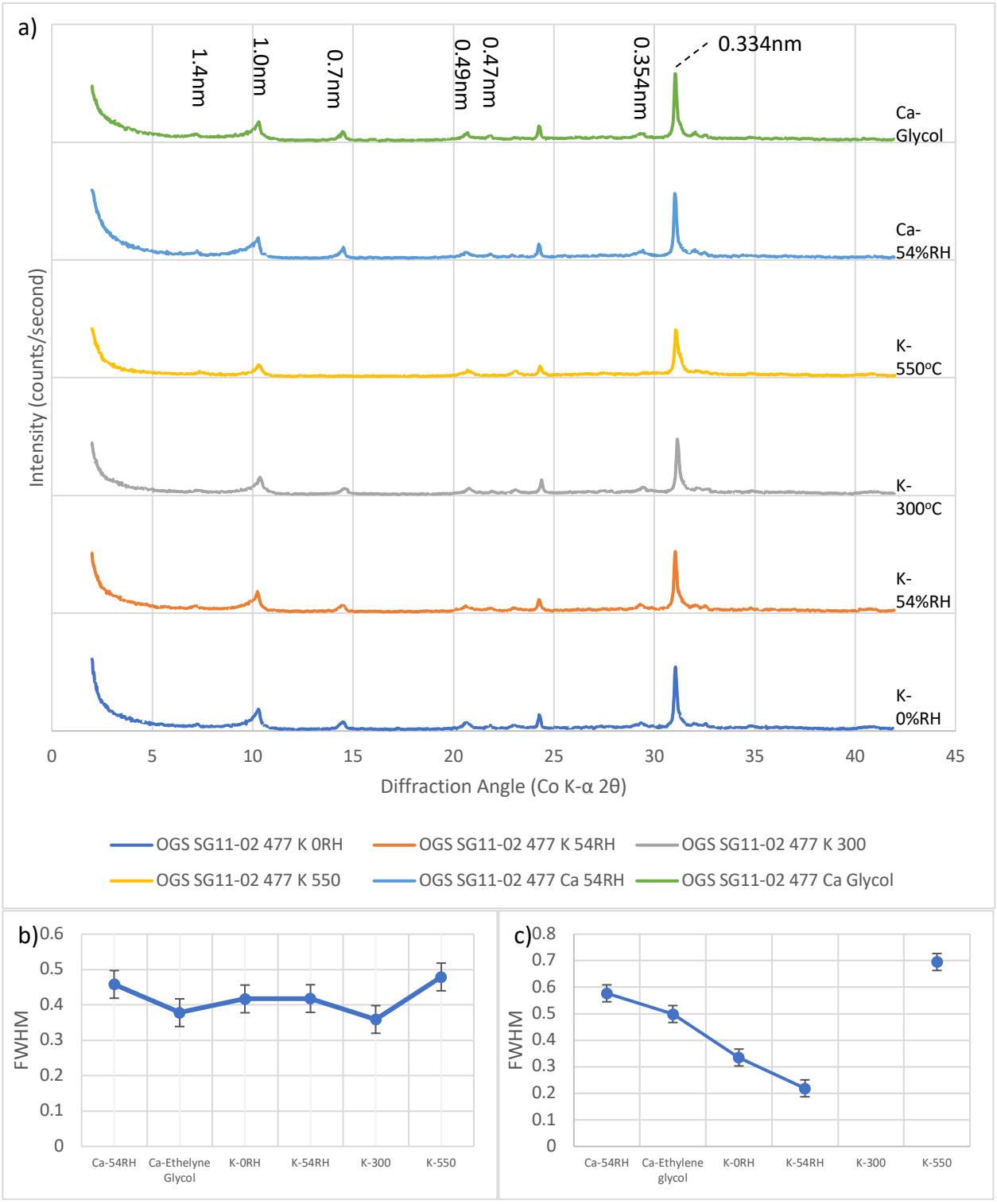

Figure 3.26. Collingwood Member OGS-SG11-02 477m: (a) Preferred orientation pXRD, with respective peak d-spacings (all treatments are displayed at the same relative intensity); (b) FWHM of illite (001) (error bars represent standard deviation of FWHM of quartz (101) within each sample set); (c) FWHM of chlorite (001) peak (error bars represent standard deviation of FWHM of quartz (101) within each sample set). Anomalous data for the K-saturated 300°C treatment is not shown.

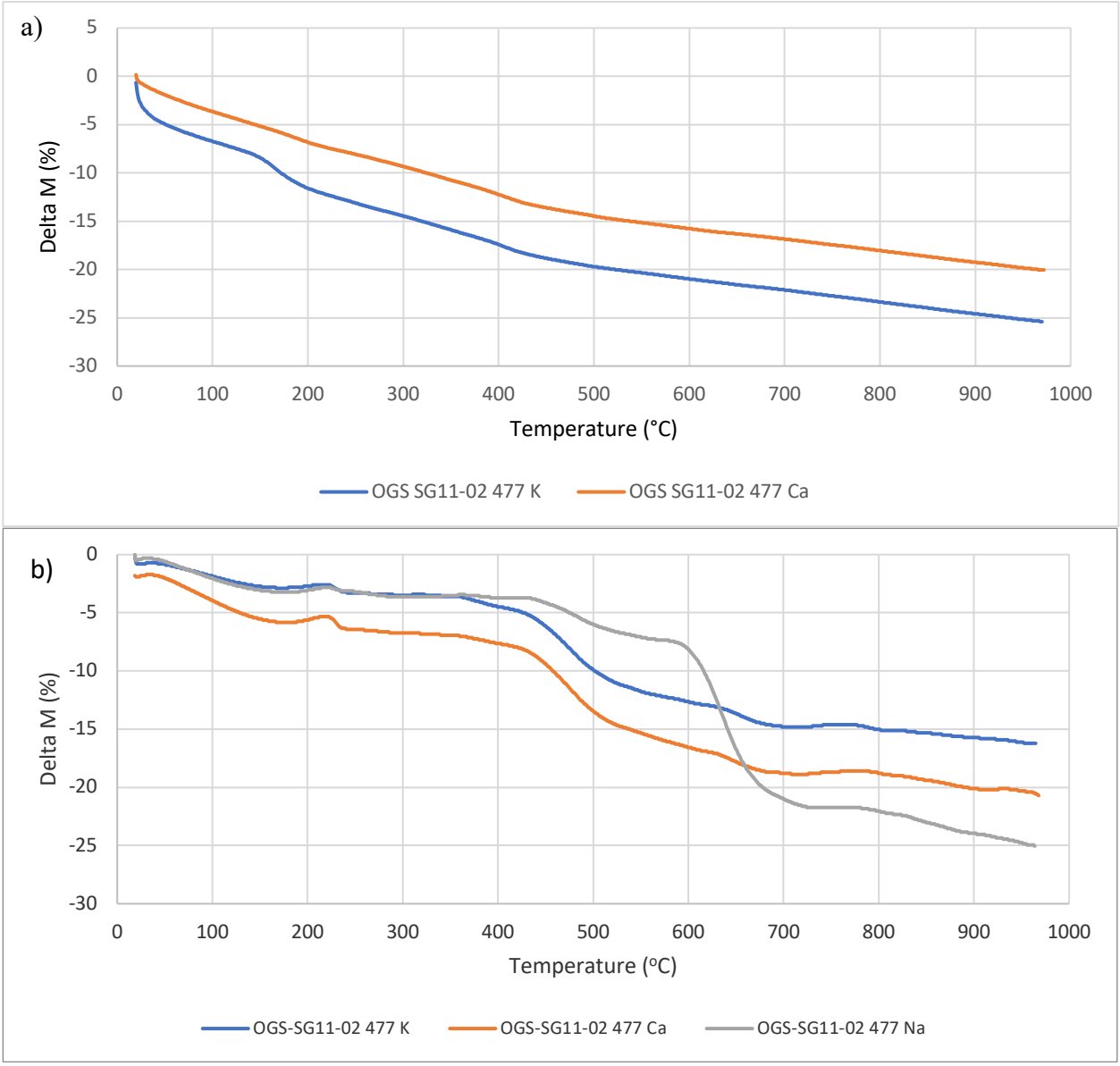

Figure 3.27. Collingwood Member OGS-SG11-02 477m: (a) In air and (b) in vacuo TGA patterns of <2µm HCl-treated K- and Ca -saturated OGS SG11-02 477m, and for in vacuo treatment, also Na-saturated sample (not treated with HCl),all heated at a rate of 10°C/minute.

Cobourg Formation – OGS SG11-02 491m

The clay mineral assemblage (<2μm) of the Cobourg Formation is dominated by illite, followed by kaolinite and then chlorite (Table 3.1; Figure 3.28a). The pXRD 06 band patterns of randomly oriented samples confirm the presence of dioctahedral (0.150nm; illite) and trioctahedral (0.153nm; chlorite) clay minerals. Non-clay minerals include quartz, calcite,

gypsum and dolomite (Table 3.1). Abundant calcite was removed using HCl prior to further examination of the Ca- and K-saturated <2μm size-fractions, which led to a reduction in pXRD peak intensities in this sample, relative to most others.

Low angle asymmetry is evident on the pXRD illite (001) in all treatments, but most pronounced for the Ca-saturated 54% RH sample; this feature suggests intercalation with other layer types (Figure 3.28a). Some of these layers are swelling in nature, as reflected in a decrease in the illite (001) low angle asymmetry for the Ca-saturated EG-solvated sample (see the reduced FWHM, Figure 3.28b). The additional presence of hydroxy-interlayer material is suggested by the continued asymmetry observed for the K-saturated 0% RH, 300°C and 550°C samples (Figure 3.28a). Complete loss of kaolinite and/or chlorite basal diffractions at 0.7, 0.47, and 0.354nm occurred upon heating to 550°C, as is typical of these phases. The illite (001) diffraction displayed no significant change in intensity upon heating to 550°C but some low angle asymmetry persisted. Upon heating to 550°C, the 1.4nm chlorite (001) diffraction shifted to a slightly lower d-spacing and broadened (Figure 3.28a).

The very large FWHM (~1.25) of the Ca-54% RH illite (001), which lies well within the shallow diagenetic zone, quantifies the low angle asymmetry described above (Figure 3.28b). The lower FWHM for all other treatments (K-saturated 300°C treatment excepted) mark the reduction in low angle asymmetry produced by adding K to the interlayer and perhaps also by partial removal of hydroxy-interlayer material. The chlorite (001) FWHM is variable (<0.1 to >0.5), in part because of the low intensity of this peak makes FWHM measurements subject to large errors. The rise in FWHM upon heating, however, may suggest structural degradation at higher temperatures (300°C and 550°C) (Figure 3.28c).

In air TGA of air-dried K- and Ca-saturated <2μm fractions of sample OGS SG11-02 491m, both of which had been treated with HCl to remove carbonate, displayed identical patterns of continuous weight loss of 12% up to 450°C and a further 6% from 450-950°C (Figure 3.29a). I*n vacuo* TGA of the same air-dried, Ca- and K-saturated, <2μm fractions exhibited 2 and 4% weight loss, respectively within the first 250°C of heating (Figure 3.29b). Further minor weight loss occurred up to 600°C, followed by additional weight loss of 2% up to 700°C, after which weight loss was insignificant. The Na-saturated sample, which had not been treated with HCl, lost 5% by weight up to 200°C. Its weight remained invariant between 200-600°C followed by a further weight loss of 20% by 700°C, after which weight loss was minor (Figure 3.29b).

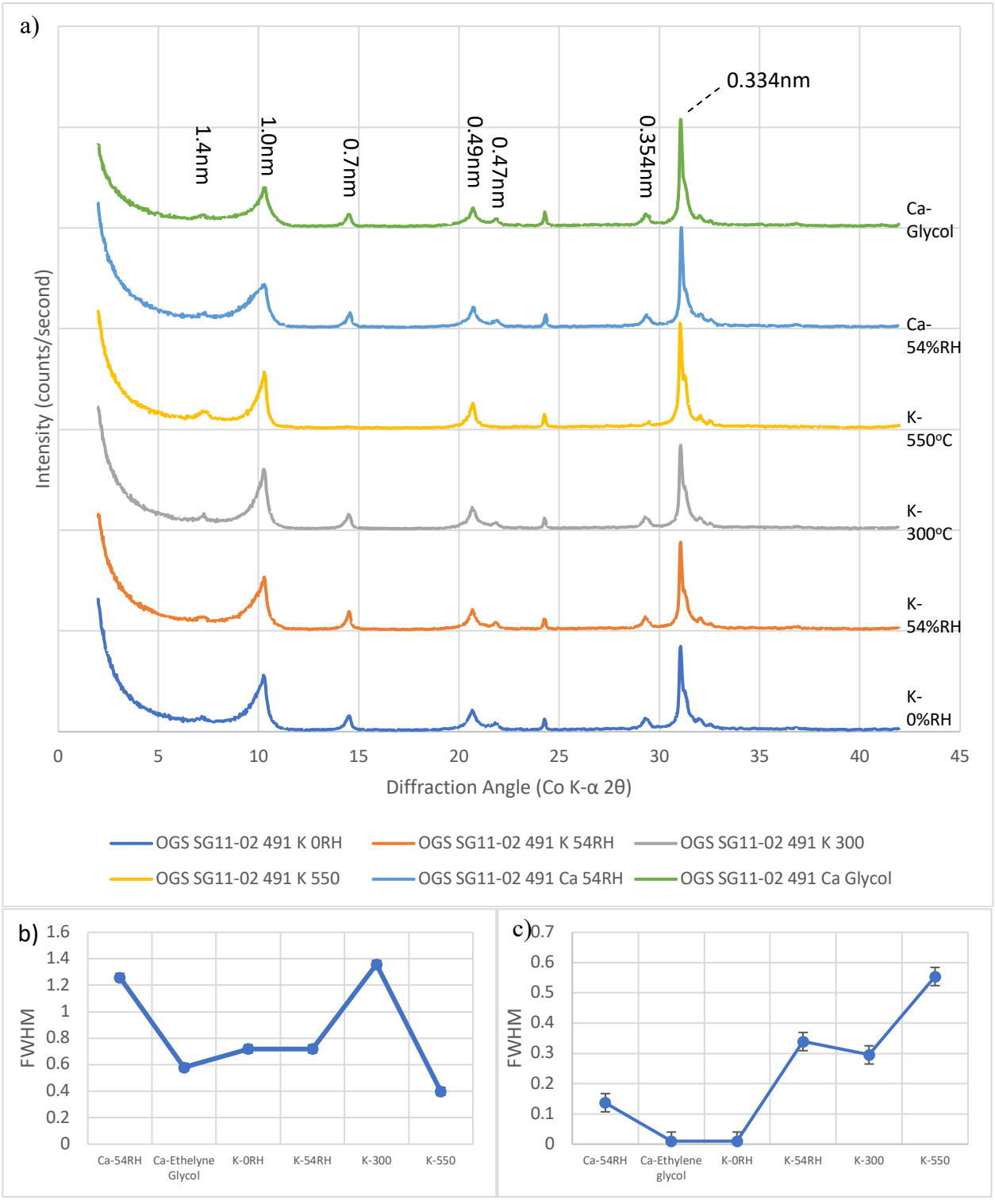

Figure 3.28. Cobourg Formation OGS-SG11-02 491m: (a) Preferred orientation pXRD, with respective peak d-spacings (all treatments are displayed at the same relative intensity); (b) FWHM of illite (001) (error bars represent standard deviation of FWHM of quartz (101) within each sample set); (c) FWHM of chlorite (001) peak (error bars represent standard deviation of FWHM of quartz (101) within each sample set).

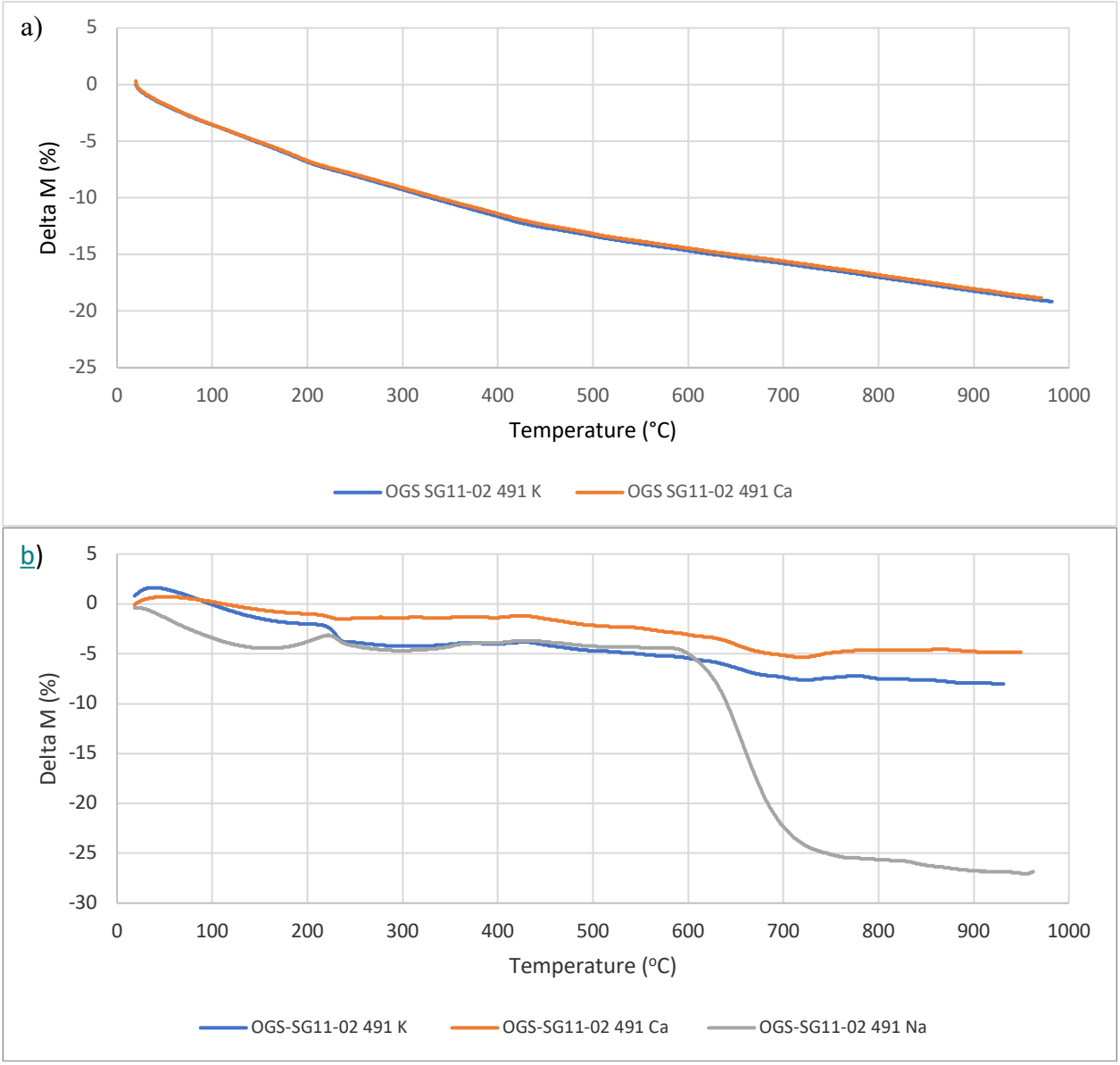

Figure 3.29. Cobourg Formation OGS-SG11-02 491m: (a) In air and b) in vacuo TGA patterns of <2µm HCl-treated K- and Ca – saturated, and Na-saturated samples (not treated with HCl), all heated at a rate of 10°C/minute.

3.3. Stable Isotopes

3.3.1. Clay Mineral Structural Oxygen and Hydrogen Isotopes – Conventional Analysis

The average hydrogen and oxygen isotope results obtained for the <2μm size-fractions obtained using conventional methods are listed in Table 3.2. Data for individual samples are tabulated in Appendix D (Tables D.1 and D.2). In $\delta^{2}H$ and $\delta^{18}O$ space, all Ordovician <2μm clay

fractions plot to the left the clay weathering lines first described by Savin (1967) and Savin and Epstein (1970) (Figure 3.30). The theoretical hydrogen and oxygen isotope compositions of the water from which the clays formed were calculated for 25, 70-90 and 150°C (assuming equilibrium) using clay-water isotope geothermometers summarized by Ziegler & Longstaffe (2000a,b) and described by Graham et al. (1984, 1987). These temperatures were chosen to model, respectively, surficial weathering, the range of burial diagenesis temperatures known for the study area (Al et al., 2011; Al-Aasm & Crowe, 2018), and the temperatures used during porewater extraction from these samples (Clark et al., 2013).

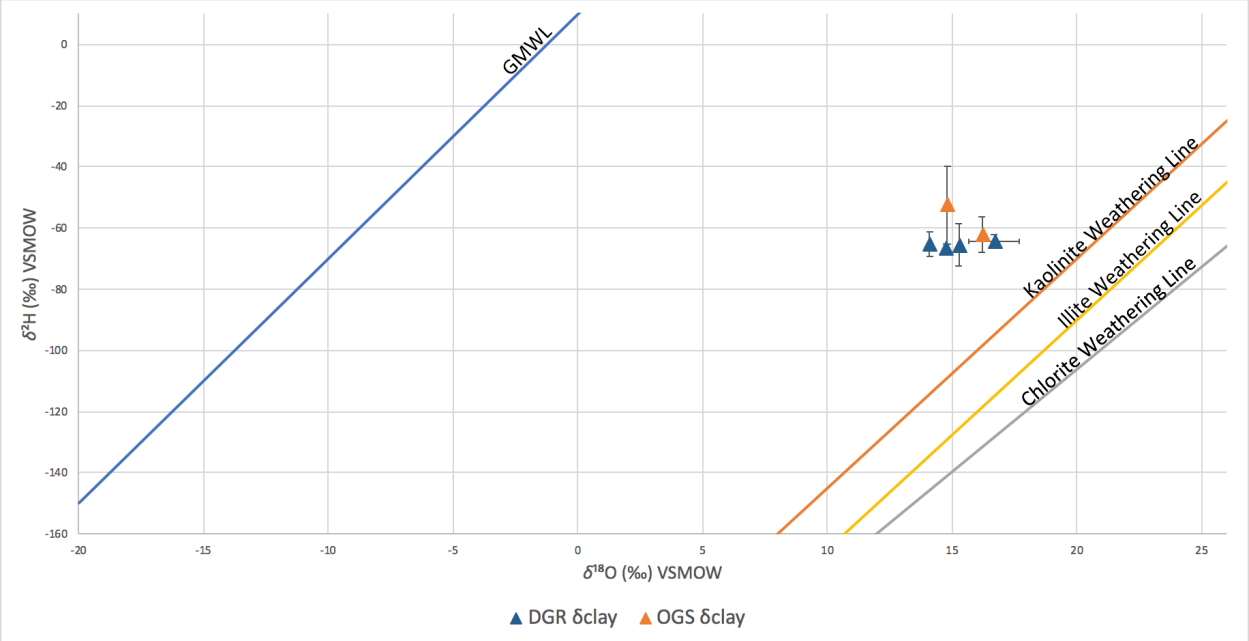

Figure 3.30. δ^2H versus $\delta^{18}O$ for NWMO and OGS Ordovician <2µm clay samples. The Global Meteoric Water Line (GMWL) of Craig (1961) and clay weathering lines of Savin (1967) and Savin and Epstein (1970) are also shown. Errors bars = replicate SD

3.3.2. Clay Mineral Hydrogen Isotopes via Thermal Combustion-Elemental Analyzer (TC-EA)

Table 3.3 compares the hydrogen isotope compositions acquired using the gas-fueled torch method to those acquired using the new (to our laboratory) TC-EA method (see Chapter 2). Appendix D (Table D.2) tabulates all individual analyses.

Table 3.2. Oxygen and hydrogen isotope compositions of <2μm clay size-fractions.

Sample	Unit	N	Average $\delta^{18}O$ (‰, VSMOW)	SD (‰)	Average Yield (μmoles/mg)	N	Average* $\delta^{2}H$ (‰, VSMOW)	SD (‰)	Yield (μmoles/mg)
KGa-1 K <2μm		4	**+20.67**	0.61	18.11	2	**–56.9**	2.19	6.65
IMt-1 K <2μm		4	**+14.43**	0.49	15.28	2	**–99.2**	1.98	2.06
CCa-1 K <2μm		4	**+3.53**	0.36	14.95	1	**–83.9**	n/a	4.49
OGS DHN1 129m K <2μm	Queenston	4	**+15.97**	0.16	14.96	2	**–62.1**	5.67	2.04
OGS SG11-02 327m K <2μm	Blue Mountain	3	**+15.06**	0.51	15.33	2	**–52.5**	12.66	2.28
OGS SG11-02 477m K <2μm	Collingwood	1	**+13.82**	n/a	13.54	1	–28.6	n/a	1.14
OGS SG11-02 491m K <2μm	Cobourg	1	**+15.31**	n/a	15.71	1	n/a	n/a	n/a
NWMO DGR3 459m K <2μm	Queenston	4	**+16.68**	0.45	15.25	2	**–64.3**	1.98	1.71
NWMO DGR3 523m K<2μm	Queenston	4	**+15.27**	0.46	14.93	4	**–65.6**	4.97	1.93
NWMO DGR2 530m K <2μm	Georgian Bay	4	**+14.74**	0.12	15.43	3	**–66.7**	4.82	2.33
NWMO DGR2 616m K <2μm	Blue Mountain	3	**+14.11**	0.11	15.29	4	**–65.3**	4.27	2.13

*n/a = not available. Data shown in red are unreliable because of a low hydrogen yield. *Only hydrogen isotope results obtained using the conventional off-line extraction method – without exchange -– are reported here.*

Table 3.3. Average stable isotope compositions of clay mineral structural hydrogen obtained using torch and TC-EA methods.

Methodology	Torch			TC-EA			Torch			TC-EA			Torch			TC-EA		
Sample	*Untreated δ^2H (‰, VSMOW)	N	SD (‰)	Untreated δ^2H (‰, VSMOW)	N	SD (‰)	**Light Water δ^2H (‰, VSMOW)	N	SD (‰)	Light Water δ^2H (‰, VSMOW)	N	SD (‰)	***Heavy Water δ^2H (‰, VSMOW)	N	SD (‰)	Heavy Water δ^2H (‰, VSMOW)	N	SD (‰)
KGa-1 K <2μm	–56.9	2	2.19	–48.0	2	0.85	n/a	n/a	n/a	n/a	n/a	n/a	n/a	n/a	n/a	n/a	n/a	n/a
IMt-1 K <2μm	–99.2	2	1.98	–102.7	3	2.22	–93.2	3	3.23	–104.0	2	0.35	n/a	n/a	n/a	n/a	n/a	n/a
Cca-1 K <2μm	–83.9	1	n/a	n/a	n/a	n/a	n/a	n/a	n/a	n/a	n/a	n/a	n/a	n/a	n/a	n/a	n/a	n/a
DHN1 129 K <2μm	–62.1	2	5.67	–56.4	2	2.62	n/a	n/a	n/a	n/a	n/a	n/a	n/a	n/a	n/a	n/a	n/a	n/a
SG11-02 327 K <2μm	–52.5	2	12.66	–57.4	2	0.78	n/a	n/a	n/a	n/a	n/a	n/a	n/a	n/a	n/a	n/a	n/a	n/a
SG11-02 477 K <2μm	–28.6	1		–73.5	1	n/a	n/a	n/a	n/a	n/a	n/a	n/a	n/a	n/a	n/a	n/a	n/a	n/a
SG11-02 491 K <2μm	n/a	n/a	n/a	–67.7	2	1.48	n/a	n/a	n/a	n/a	n/a	n/a	n/a	n/a	n/a	n/a	n/a	n/a
NWMO DGR3 459m K <2μm	–64.3	2	1.98	–55.8	1	n/a	–58.5	5	8.82	–62.8	2	0.14	–64.3	2	1.84	–46.1	2	0.21
NWMO DGR3 523m K <2μm	–65.6	4	4.97	–61.6	2	0.99	–68.5	2	1.06	–68.1	2	0.64	–58.6	3	2.17	–34.4	2	4.24
NWMO DGR2 530m K <2μm	–66.7	3	4.82	–58.6	3	1.27	–59.1	3	7.15	–57.0	2	0.71	–62.2	3	0.23	–47.2	2	0.78
NWMO DGR2 616m K <2μm	–65.3	4	4.27	–56.1	2	0.57	–62.7	2	0.21	–65.9	2	0.35	–58.4	3	9.55	–46.8	2	0.35

*SD based on replicate samples. n/a= not available. *Untreated = samples not exposed to isotopically labelled water before extraction. **Light Water = samples treated with δ^2H water = –309±5‰. ***Heavy Water = samples treated with δ^2H = +810±3‰.*

3.3.3. Clay-Water Hydrogen Isotope Exchange Experiments

As described in Chapter 2, some <2μm size-fractions were exposed to isotopically labelled waters (Light = samples treated with δ^2H water = –309±5‰; Heavy = samples treated with δ^2H = +810±3‰) to test for hydrogen isotope exchangeability at 68°C; these are henceforth referred to as 'treated' samples. The exchange experiments were conducted in initially evacuated vessels. Experimental difficulties were encountered for some samples, which likely affected the results. First, vacuum was lost for the fraction of sample NWMO DGR2 530m exposed to Light water, causing evaporative ^{2}H-enrichment of the latter. Second, samples NWMO-DGR3 523m (exchange with Light water) and NWMO-DGR2 616m (exchange with Light and Heavy water) came into direct contact with liquid exchange water rather than only vapour produced from the exchange water.

Using the torch method, there were no significant differences in δ^2H between untreated and treated <2μm clay fraction from the NWMO DGR samples (Table 3.3; Figure 3.31a). CMS illite IMt-1 also showed no significant change in δ^2H between untreated samples and aliquots treated with Light water. Using the TC-EA method, only small differences in δ^2H among treatments were observed for the standard illite (IMt-1) (Figure 3.31b). The DGR <2μm clay assemblages, however, systematically showed enrichments in ^{2}H when exposed to Heavy water and depletions of ^{2}H when exposed to Light water, relative to the δ^2H obtained for untreated samples using this method. It appears that the much greater precision of the TC-EA method allows these differences to be measured reproducibly.

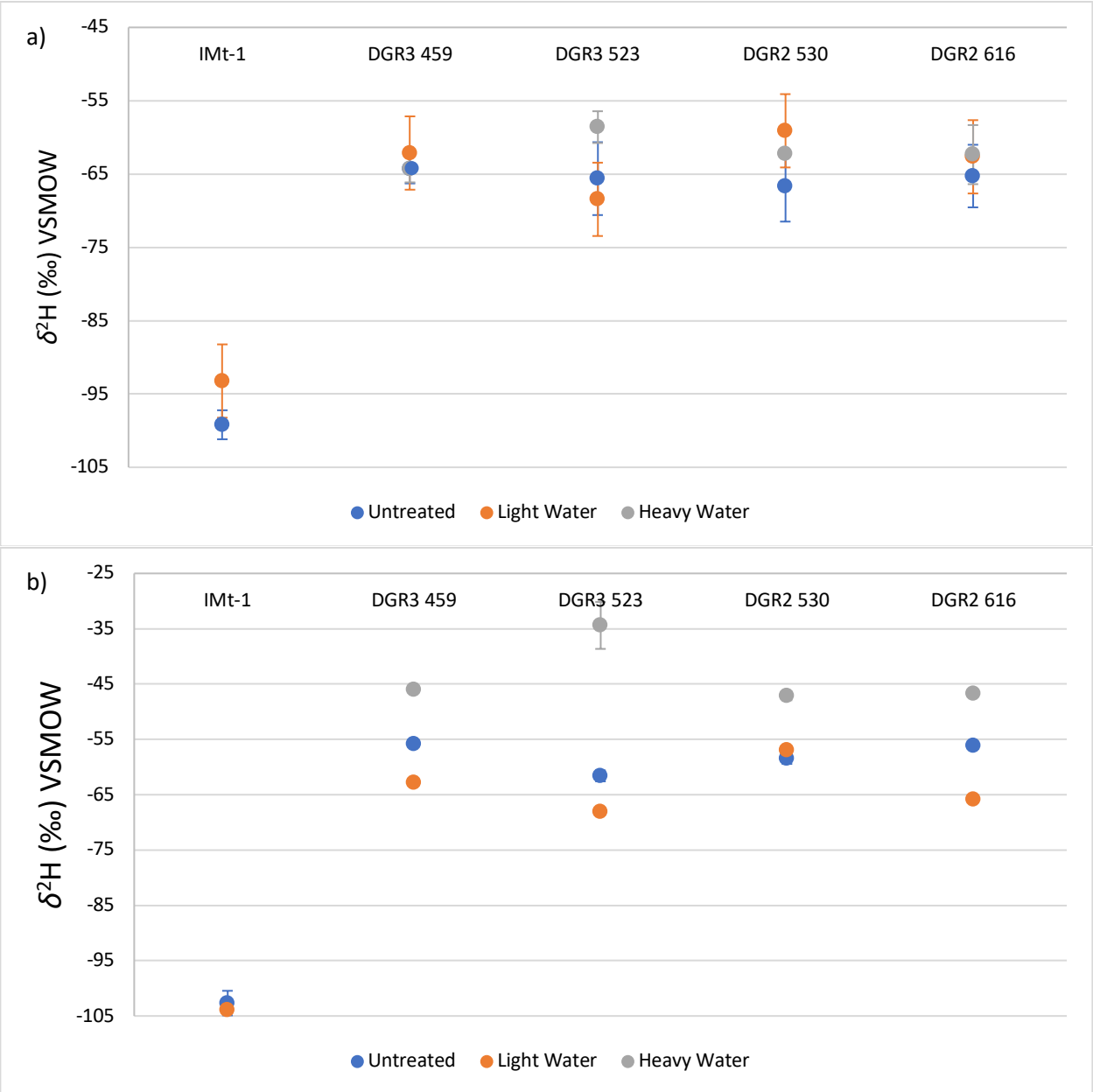

Figure 3.31. δ^2H of NWMO DGR2, NWMO DGR3 and reference clay IMt-1 <2µm size-fractions before and after exposure to isotopically labelled Light (–309±5‰) and Heavy (+810±3‰) water at 68°C for 70 days, except for sample DGR2 530 treated with Heavy water, which was exposed for 63 days. Results are illustrated for the (a) gas-fueled torch method, and (b) TC-EA method. Note that in figure a) the results of DGR3 459 before and after exposure to isotopically labelled Heavy (+810±3‰) water overlap. Untreated = samples not exposed to isotopically labelled water before extraction. Error bars are standard deviation and may be smaller than the symbols in part (b) of the figure.

3.3.4. Stepwise Heating of Bulk KGa-1 and NWMO DGR 523 K<2µm (Heavy)

Results for the stepwise heating experiments are listed in Table 3.4. For bulk KGa-1, only trace amounts of hydrogen were released at the low-temperature steps (<300°C), and had δ^2H

that decreased from –30 to –46‰ with increasing temperature. A small amount of hydrogen was released at the 300-400°C step, which had a much lower δ^2H (–68‰). Most hydrogen (–55‰) was released between 400-1000°C, as expected for dehydroxylation.

For NWMO DGR 523 K<2μm (Heavy), only traces of hydrogen were released at each temperature step up to 300°C. These steps had δ^2H that progressively increased from –11‰ at 19°C to +77‰ at 300°C (Table 3.4). Slightly more hydrogen was released at 400°C, which had a slightly lower δ^2H (+57‰) than the previous step. The bulk of the hydrogen was released between 400-1000°C and had a somewhat lower δ^2H (+20‰). This latter fraction should represent hydrogen released by dehydroxylation of this sample. Its δ^2H, however, was much higher than measured for hydroxyl hydrogen from this sample by conventional (torch, –58.6‰) or TC-EA (–34.4‰) methods (Table 3.3). This unusual result prompted testing of the stepwise-heating extraction line for contamination (memory effect) by ^{2}H-rich hydrogen, the most likely source of which would be the Heavy water (+810‰) to which this sample had been exposed. Water standards analyzed between 17 and 22 hours after active heating and pumping of the extraction line to remove contamination were still enriched in ^{2}H by ~10-20‰ relative to accepted values (Table 3.4). The problem persisted for much longer periods of time (86-171 hours), albeit at lower ^{2}H enrichments (Table 3.4). Dismantlement and cleaning of the line and replacement of all chemicals was necessary to eliminate this memory effect.

Table 3.4. H-isotope Results for Stepwise Heating of Bulk Kaolinite (KGa-1) and NWMO DGR3 523 K<2µm - Heavy

Sample	Temperature (°C)	δ^2H (‰, VSMOW)	H_2 yield (μmoles/mg)	Gas Evolution Time (min)
	20			10
KGa-1	20-100	**–30.2**	0.02	50
KGa-1	100-200			34
KGa-1	100-300	**–46.0**	0.02	30
KGa-1	300-400	**–67.8**	0.17	30
KGa-1	400-1000	**–55.0**	5.77	72
NWMO DGR3 523m K<2μm - Heavy	19	**–11.0**	0.02	15
NWMO DGR3 523m K<2μm - Heavy	19-100	**+33.4**	0.02	33
NWMO DGR3 523m K<2μm - Heavy	100-200	**+53.5**	0.02	44
NWMO DGR3 523m K<2μm - Heavy	200-300	**+76.9**	0.02	33
NWMO DGR3 523m K<2μm - Heavy	300-400	**+56.5**	0.03	36
NWMO DGR3 523m K<2μm - Heavy	400-1000	**+20.2**	0.46	78
	Accepted δ^2H (‰, VSMOW)	**Measured δ^2H (‰, VSMOW)**	**Time elapsed *since analysis of NWMO DGR 523m K<2μm - Heavy**	
EDT Laboratory Water Standard	-56	**–37.3**	17 hours	
EDT Laboratory Water Standard	-56	**–43.4**	18 hours	
EDT Laboratory Water Standard	-56	**–43.1**	19 hours	
Heaven Laboratory Water Standard	+88.7	**+98.6**	22 hours	
EDT Laboratory Water Standard	–56	**–50.5**	86 hours	
EDT Laboratory Water Standard	–56	**–48.3**	87 hours	
LSD Laboratory Water Standard	–161.8	**–155.8**	170 hours	
LSD Laboratory Water Standard	–161.8	**–156.3**	171 hours	

**Time elapsed since analysis of sample NWMO DGR3 523 K<2µm – Heavy while line was under active evacuation.*

Chapter 4. Discussion

This study set out to examine whether clay minerals in the Ordovician shales of southern Ontario, and particularly those associated with the proposed Deep Geologic Repository (DGR) for nuclear waste at the Bruce Nuclear Generating Station, have played a role in determining the present isotopic composition of porewater within these low water content and low permeability formations. Of particular interest was whether hydrogen isotope exchange has occurred between porewater and the hydroxyl groups of the clay minerals contained in these shales. Of interest also was whether fractionation between porewater bound to clay mineral surfaces and the remaining 'free' (i.e., mobile) porewater had a measurable effect on the latter's isotopic composition.

Understanding whether such processes have affected isotope composition of porewater in these Ordovician shales is important because such data are generally accepted as tracers of the water's origin. In particular, post-depositional incursions of meteoric water can be identified if the entrapped porewaters have been unaffected by shale-water interaction. If the Ordovician shales have remained impermeable to meteoric water influx over millions of years, the safety case for these rocks as a barrier to radionuclide migration is greatly strengthened.

4.1. Clay Mineralogy

Accurate measurement of the isotopic compositions of structural oxygen and hydrogen in clay minerals is prerequisite to evaluation of the possibility of clay-water exchange. However, such analyses, particularly for hydrogen, can be strongly affected by a clay mineral's tendency to retain residual bound water despite normal dehydration protocols in the laboratory (Marumo et al., 1995; McKay et al., 2013). The extent of this analytical challenge

depends in large part on the varieties of clay minerals present, especially their swelling versus non-swelling character. Of equal importance is the potential for post-depositional isotopic exchange between clay minerals and pore fluids through hydroxyl exchange and/or protonation reactions. The potential for isotopic exchange is dependent on clay mineral type, clay mineral transformation and/or neoformation during diagenesis, and clay crystallinity and grain size (Savin & Epstein, 1970a,b; Savin & Lee, 1988; Longstaffe & Ayalon, 1990; Sheppard & Gilg, 1996; Longstaffe, 2000, He et al., 2019, and references therein).

The results of the current study, as summarized in Table 3.1, show that the clay mineralogy (<2μm), as determined by pXRD, of all five Ordovician units examined (Queenston Formation, Georgian Bay Formation, Blue Mountain Formation, Collingwood Member, Cobourg Formation) is remarkably similar. Abundances of illite are much greater than those of kaolinite, which in turn are much more abundant than chlorite. This pattern for the <2μm size-fraction holds both for the NWMO samples obtained from the Bruce site and for the OGS samples obtained from cores located ~100km to the east (Figure 1.2). At the latter location, however, samples from the Collingwood Member and the Cobourg Formation are much richer in carbonate, which substantially dilutes the overall abundance of clay minerals in these rocks (Table 3.1).

The pXRD patterns obtained for the <2μm size-fractions of the shale samples across the series of humidity, glycolation and heat treatments closely correspond to the type patterns obtained for the CMS Source Clay illite (IMt-1), kaolinite (KGa-1) and chlorite (CCa-1). There is no indication of discrete swelling clays in any of these shale samples. In addition, illite in all samples has full width half maximum (FWHM) values for the Ca-saturated, 54% relative humidity (RH) pXRD patterns that are always lower than measured for the CMS Source Clay

IMt-1 illite (FWHM = 1.38). This points to a very low percentage of swelling clay interstratification in illites from the Ordovician shale samples.

Illite from the Queenston Formation in both NWMO and OGS cores has FWHM values typical of the deep diagenetic zone or low anchizone. This is also the case for the Collingwood Member sample from the OGS core suite. The illites from both the Georgian Bay and Blue Mountain formations have higher FWHM values, which are typical of shallower burial (i.e., mid to deep diagenetic zones) but again there are no pXRD indications of significant smectitic interstratification. Only the Cobourg sample from the OGS SG11-02 core, located ~100 km from the Bruce site (Figure 1.2), contains illite with a FWHM characteristic of the very shallow diagenetic zone. This illite also exhibits pXRD behaviour consistent with significant interstratification of both swelling clay layers and hydroxy-interlayer material.

Chlorite in the Ordovician shales examined here typically has FWHM values for the Ca-saturated, 54% RH, <2μm size-fraction ranging from ~0.4 to 0.7[1]. These values are significantly higher than the CMS Source Clay chlorite CCa-1 (~0.2). Only the Cobourg Formation's chlorite has a comparable FWHM (~0.15). The generally greater sharpness of the CCa-1 (001), however, is not surprising; it is the product of greenschist facies metamorphism, which should impart a much higher crystallinity than would be expected for chlorite from the Ordovician shales.

Some of the chlorites examined here show a growth in intensity of the (001) upon heating to 550°C; this is typical behaviour of well crystallized, Fe-rich chlorites. In others of poorer crystalline nature, heating to 550°C leads to structural damage resulting from structural reorganization of the brucite-like or hydroxy-interlayer sheets filling the interlayer position.

[1] Results for the Blue Mountain Formation OGS SG11-02 327m sample have been set aside given the large errors associated with this particular set of measurements.

That said, there are no systematic variations in diffraction positions, diffraction peak heights or FWHM across the pXRD treatments (hydration, EG-solvation, dehydration and heating to 300°C and 550°C) attributable to addition or loss of interstratified material of a swelling nature. The response of the chlorite FWHM to these treatments, in particular, is quite variable. It is more or less constant in some instances, sharpens slightly in others, or broadens as the (001) moves to somewhat lower d-spacings. The first behaviour indicates no change in chlorite pXRD characteristics attributable to an ability to uptake fluids into the interlayer. The second behaviour describes the expected increase in crystallinity that arises from structural rearrangement associated with heating to higher temperatures. The third behaviour is common in Fe-rich chlorites in which the brucite-like sheet/hydroxy-interlayer material that fills the interlayer begins to degrade with heating, particularly at >500°C. In short, while chloritic phases have the potential to be interstratified with swelling clay material, there is little evidence for significant interlayering of this sort in the Ordovician chlorites examined in this study (Schandl , 2009; Skowron & Hoffman, 2009).

4.2. Thermogravimetric Behaviour

The thermogravimetric (TG) examination of the <2μm size-fraction of the CMS source clays and the southern Ontario's Ordovician clays offers three kinds of information that are important to the current investigation. First, it provides insight into the crystallinity of the clay minerals and potential for isotopic exchange of structural hydrogen and oxygen with porewaters by defining the nature of the dehydroxylation step (temperatures of initiation and completion). Second, it defines the dehydration characteristics of the clay mineral, in particular the temperature range over which bound water is lost, the amount of that water, and an indication of organic matter sorbed on the clays. Third, this information can be used to design the most

appropriate analytical protocols for capturing structural and bound (hydroxyl groups, interlayer water, outer surface-sorbed water) water for hydrogen and oxygen isotope analysis. This latter information is best collected by conducting TG analyses *in vacuo*, under conditions as close as possible to those used during water extraction for isotopic analysis.

4.2.1. Source Clays (<2μm)

Analysis of the CMS Source Clays provides baseline information on the dehydration and dehydroxylation behaviour that might be predicted for the Ordovician shale <2μm size-fractions examined here. This information can then be used to shape the protocols for isotopic analysis.

For the air-dried illite (IMt-1) (Figure 3.8a), the considerable weight loss from room temperature to ~175°C for all saturations during 'in air' analysis (i.e., at atmosphere), reflects dehydration of surface water. Continued dehydration-related weight loss to >200°C for the Na- and Ca-saturated samples reflects the greater water-binding potential of these cations. The overall greater weight loss of the Na-saturated sample also reflects its much greater propensity to attract water. The major stage of dehydroxylation begins at ~300°C and reaches completion between 500-650°C, depending again on cation saturation (Ca>K≈Na). Further weight loss at much higher temperatures (>850°C) reflects final devolatilization associated with phase transformations.

The quite different patterns for air-dried, '*in vacuo*' illite samples (Figure 3.8b) reflect loss of most surface water during evacuation of the TG chamber prior to analysis. That said, Ca-saturated samples retained a greater fraction of residual surface water to higher temperatures, or perhaps even appear to have taken up moisture from the chamber, which may reflect the especially hygroscopic nature of Ca-saturated samples. Na-saturated illite appears to lose sorbed water more readily than the other saturations, and hence likely retains less residual surface water

prior to onset of dehydroxylation. Dehydroxylation for all cation saturations appears to go largely to completion between ~420-750°C. Cation saturation appears to make a big difference in the ability to achieve a clean separation between surface-sorbed water and water derived from loss of hydroxyl groups.

For the air-dried chlorite (CCa-1) (Figure 3.10a), the large weight loss from room temperature to ~200°C for all saturations during 'in air' analysis results from dehydration of surface water. The K-saturated sample's notably steeper gradient of weight loss from 150-200°C reflects the lower potential of K-saturated chlorite for retaining residual surface water above 150°C. All saturations, nonetheless, continue to lose considerable quantities of residually bound surface water, until a plateau is reached at ~450°C. The dehydroxylation temperature range for CCa-1, which is initiated at ~500°C and largely completed by 625-650°C, however, appears to be independent of cation saturation. The very limited further weight loss at higher temperatures is unlikely to have significant consequences for the isotopic results obtained for bound or hydroxyl water isotopic compositions.

There are instructive differences in the patterns for the air-dried, '*in vacuo*' chlorite samples (Figure 3.10b). The minor weight losses for all saturations up to ~200°C are consistent with the earlier removal of much of the surface water as the TG chamber is evacuated prior to initiation of the analysis. This reflects the very loosely bound nature of such water on chlorite. Whereas the Na- and K-saturated samples then maintain more or less a constant weight until dehydroxylation is initiated, however, the Ca-saturated sample undergoes a further sharp loss of bound water from ~180-245°C. This is indicative of the tendency of Ca-saturated samples to retain residual bound water to higher temperatures than is the case for Na- or K-saturated samples. These weight losses are followed by dehydroxylation, which for all saturations may

have occurred in two steps, first a minor weight loss at ~425-500°C followed by the major loss of hydroxyls from ~540-560°C to ~720-730°C. It cannot be ruled out, however, that the first minor weight loss represents final removal of bound water that was trapped in the interlayer octahedral sheet of the chlorite.

For the air-dried kaolinite (KGa-1) (Figure 3.12a), the limited weight loss for the Na- and K-saturated samples up to ~200°C during the 'in air' analysis indicates only minor sorption of water. In contrast, the weight gain of the Ca-saturated sample between ~100-180°C is unexpected, and suggestive of adsorption of water from the TG chamber during this time-temperature interval. This water is then lost, beginning at ~375°C and continuing up to the initiation of dehydroxylation. The steep weight loss for all saturations from ~475-575°C indicates dehydroxylation, which is also likely the cause of further, very minor weight loss up to ~800°C, when the final recalcitrant hydroxyl groups are removed.

The variable behaviour of the air-dried '*in vacuo*' KGa-1 samples up to initiation of dehydroxylation at ~425°C (Figure 3.12b) is curious. The K-saturated sample is best behaved, showing little gain or loss of water over this temperature interval. Such consistency again points to the value of using K-saturated samples for isotopic analysis when the goal is to analyze only structural oxygen and hydrogen. The initial loss of water up to ~150°C for the Ca-saturated sample is consistent with removal of surface water that was retained during initial evacuation of the chamber, based on the tendency of Ca-saturation to increase water retention on clay surfaces. The subsequent gain in weight starting at ~150°C and ending at ~225°C, however, is unexplained, as is the pattern of weight gain that was observed for the Na-saturated sample up to near the initiation of dehydroxylation. The temperature range of dehydroxylation, however, was the same for all saturations, beginning at ~425°C, which is lower than for analyses conducted *in*

air. Significant weight loss arising from dehydroxylation during *in vacuo* analyses also extended to higher temperatures (~650-700°C) than for KGa-1 samples analyzed *in air*.

4.2.2. Southwestern Ontario Ordovician Clay Minerals (<2μm)

The TGA patterns obtained for the <2μm size-fractions are broadly similar across all of the Ordovician shale units examined, consistent with the clay mineralogy obtained by pXRD. The dehydration and dehydroxylation patterns were similar to those of the CMS Source clays, illite in particular, which comprises the bulk of the <2μm size-fractions. Only samples containing substantial carbonate <2μm failed to follow the TGA pattern of illite because of overprinting of the TGA signal by decarboxylation reactions.

We comment here in more detail only on the *in vacuo* samples, as this is the condition under which isotopic analysis of structural water and bound water was attempted in this study. For almost all Ordovician <2μm samples analyzed *in vacuo*, small amounts of weight loss occur for each of the K-, Ca- and Na-saturations by 150-200°C. This weight loss is attributed to dehydration of clay surface-bound water. In the Queenston Formation, some Ca-saturated samples also gained water in the early stages of heating, likely because of formation of salt hydration complexes. By comparison, Na-saturated samples lost more surface-bound water, and commonly did so at lower temperatures than for other saturations. K-saturated sample weight change curves lie in between the patterns obtained for Ca- and Na-saturated samples. In contrast, a much higher surface-bound water related weight loss was obtained for the Georgian Bay K-saturated sample than for its Ca- or Na-saturated counterparts. In the Blue Mountain Formation, the Ca-saturated sample lost surface-bound water at lower temperatures and/or in greater amounts than either of the K- or Na-saturated samples. In the Cobourg Formation, similar to the Queenston Formation, the Na-saturated sample lost surface-bound water in greater quantities and

at lower temperatures than the other cation saturations. This variability among samples of very similar clay mineralogy points to the complexity of clay-water interactions associated with the electric double layer, depending on clay type and formation water chemistry. There is potential for significant variation in the amounts and temperatures at which clay surface-bound water is released, even for non-swelling clays. This has the potential to affect the isotopic compositions of the clay-associated water, depending on the method by which it is sampled.

The majority of weight loss for all *in vacuo* samples occurred at much higher temperatures and is attributed to dehydroxylation. Dehydroxylation patterns were similar, but not identical for each sample, as befits the measured variation in relative abundances of illite, chlorite and kaolinite among samples of the <2μm size-fraction, albeit all within the framework that illite abundance is always greater than that of kaolinite, which in turn is more abundant than chlorite. Dehydroxylation typically began at ~430°C and was almost entirely completed by 710-730°C, although very minor weight losses continued to higher temperatures. Within this temperature range, it was common to observe a relatively smaller rate of weight loss from 430°C to 550-580°C (and occasionally higher, i.e. to 640°C), followed by a larger rate of weight loss from 550-580°C to 710-750°C. This two-step process is consistent with the differences in dehydroxylation temperature ranges for illite, chlorite and kaolinite, as well as for variations within each mineral species depending on the grain-size distribution within each <2μm size-fraction, clay structure (i.e. 1:1 versus 2:1 versus 2:2 layers), and the crystallinity each clay phase.

In general, there was no consistent relationship observed between cation saturation and the temperature range for dehydroxylation. However, in the Queenston Formation, Na-saturated samples did not show the generally observed, two-step dehydroxylation pattern. In the Georgian

Bay Formation, K-saturated samples continued to show significant weight loss from 710-890°C, much higher than the typical end of dehydroxylation. In the Blue Mountain Formation, weight loss associated with dehydroxylation for one sample began at temperatures ranging from 425-580°C, rather than the more typical 430°C. In another K-saturated, Blue Mountain Formation sample, the earlier period of dehydroxylation began at 430°C but ended at ~520°C, with no further weight loss until temperatures exceeded 590°C. These features again point out that cation saturation can affect the thermal behaviour of the clay minerals in these Ordovician formations. Controlling that cation saturation will be important for the establishment of systematic analytical schemes for extracting hydroxyl oxygen and hydrogen. Likewise, understanding the control of formation water chemistry on the natural state of these Ordovician clays will be important for assessing their ability to retain surface-bound water as well as give up hydroxyl groups upon exposure to higher temperatures during natural (or human-induced) processes.

Following removal of the high carbonate content that characterizes the Cobourg Formation, its clay pXRD demonstrated the greatest potential for illite and chlorite interstratification. The <2μm size-fraction remaining after carbonate removal, however, was insufficient and/or somehow chemically modified such that high-resolution TGA patterns could not be obtained. Hence examination of this sample's TGA pattern for a signal of the putative presence of swelling clay layers was not possible.

4.3. Hydrogen and Oxygen Isotope Clay-Water Systematics

4.3.1. Controls on the $\delta^{18}O$ and $\delta^{2}H$ of Southwestern Ontario Ordovician Clays Minerals (<2μm)

The siliciclastic sediments comprising much of the Ordovician shales of southwestern Ontario originated from the east coast Appalachian highlands of proto-North America (Irving, 1979; Ziegler & Longstaffe, 2000; Ziegler & Longstaffe, 2000). The $\delta^{18}O$ and $\delta^{2}H$ of the detrital

clay minerals present in these sediments would originally have been established during weathering. Clay oxygen and hydrogen isotope compositions are controlled, for the most part, by temperature and the isotopic composition of the water from which they formed. As such, clays formed during terrestrial weathering closely track the $\delta^{18}O$ and $\delta^{2}H$ of the Global Meteoric Water Line (GMWL) (Savin, 1967; Savin & Epstein, 1970; Lawrence & Taylor, 1971; Longstaffe, 1987, 1989, 2000; McKay & Longstaffe, 2013). Other factors that also affect clay mineral $\delta^{18}O$ and $\delta^{2}H$, but usually to a lesser extent, include clay chemical composition and crystal-chemistry (Yang et al., 2017; Suzuoki & Epstein, 1976; O'Neil J. R., 1987), water salinity (Horita et al., 1995; Horita et al., 1999; Horita et al., 2002; McKay & Longstaffe, 2013), and in rare cases, pressure (Horita et al., 1999; Horita et al., 2002).

Figures 3.30 and 4.1a show that the Ordovician <2μm clay separates analyzed in the present investigation do not plot on or near the weathering lines known for any of their major clay mineral phases. Three possible explanations for this observation are considered here: (1) contamination by non-hydrous oxygen-bearing phases in the <2μm size-fractions lowered the $\delta^{18}O$ of these separates; (2) the <2μm size-fractions have undergone isotopic re-equilibration during burial diagenesis, and (3) post-formation hydrogen isotope exchange occurred between the <2μm clay minerals and porewater.

Concerning the first possibility (contamination), comparison of clay mineral content (Table 3.1) and $\delta^{18}O$ (Table 3.2) shows no correlation between the two parameters. In addition, the non-clay mineral content in <2μm separates, as determined by pXRD, is commonly overestimated, making their potential impact less than might be suggested by Table 3.1. Oxygen from non-clay mineral contamination is unlikely to be a major control on the $\delta^{18}O$ of the <2μm clay size-fraction.

Concerning the second possibility (isotopic re-equilibration), Figure 4.1a illustrates the porewater $\delta^{18}O$ and $\delta^{2}H$ at isotopic equilibrium with the <2μm size-fractions under three conditions: (i) terrestrial weathering (25°C), (ii) burial diagenesis (70-90°C), and (iii) Vacuum Distillation Extraction (VDE) (150°C) (Clark et al., 2010b, 2013; Murseli et al., 2017). The oxygen and hydrogen isotope geothermometers used to make these calculations were as follows.

Illite – water. The equation of Lee (1984), as presented in Savin & Lee (1988) and previously used by Ziegler & Longstaffe (2000a,b) for southwestern Ontario Paleozoic clay minerals, was employed for oxygen isotopes:

$$10^3 \ln \alpha^{Ox}_{illite-water} = -2.87 + \left(1.83 \times \frac{10^6}{T^2}\right) + (0.0614 \times \frac{10^6}{T^2})^2 \times -(0.0015 \times \frac{10^6}{T^2})^3 \quad \text{(Eq. 4.1)}$$

The equation of Capuano (1992), as previously used by Ziegler & Longstaffe (2000a,b) for southwestern Ontario Paleozoic clay minerals, was employed for hydrogen isotopes:

$$10^3 \ln \alpha^{hy}_{illite-water} = -45.3 \times \frac{10^3}{T} + 94.7 \quad \text{(Eq. 4.2)}$$

Kaolinite – water. The equation of Sheppard and Gilg (1996), as previously used by Ziegler & Longstaffe (2000a,b) for southwestern Ontario Paleozoic clay minerals, was employed for oxygen isotopes:

$$10^3 \ln \alpha^{Ox}_{kaolinite-water} = 2.76 \times \frac{10^6}{T^2} - 6.75 \quad \text{(Eq. 4.3)}$$

The equation of Sheppard & Gilg (1996) equation, as previously used by Ziegler & Longstaffe (20001,b) for southwestern Ontario Paeozoic clay minerals, was used for hydrogen isotopes:

$$10^3 \ln \alpha^{hy}_{kaolinite-water} = -2.2 \times \frac{10^6}{T^2} - 7.7 \quad \text{(Eq. 4.4)}$$

Chlorite-water. The equation of Sheppard & Gilg (1996), as previously used by Ziegler & Longstaffe (2000a,b) for southwestern Ontario Paleozoic clay minerals, was employed for oxygen isotopes:

$$10^3 \ln \alpha^{Ox}_{chlorite-water} = \left(3.47 \times \frac{10^6}{T^2}\right) + \left(-5.79 \times \frac{10^3}{T}\right) \quad \text{(Eq. 4.5)}$$

For hydrogen isotopes, the equation of Graham et al. (1984) was used, in the absence of chlorite Fe/(Fe+Mg) ratios that would have made possible use of the Marumo et al. (1980) geothermometer previously employed by Ziegler & Longstaffe (2000a,b) for southwestern Ontario clay minerals:

$$10^3 \ln \alpha^{hy}_{chlorite-water} = -3.7 \times \frac{10^6}{T^2} - 24 \quad \text{(Eq. 4.6)}$$

Using these geothermometers, weighted according to the amount of each clay phase in the <2μm size-fraction (Table 3.1), the calculated porewater isotopic compositions at 25°C plot well to the left of the GMWL (Figure 4.1a), which is most unlikely for fresh waters involved in the weathering to produce clay minerals. Scenarios for porewater isotopic compositions in equilibrium with the <2μm clay size-fractions at higher temperatures plot to the right of the GMWL, with the clay-water isotopic fractionation decreasing as temperature increases (Figure 4.1a).

To assess whether any of these scenarios are realistic, it is instructive to examine some of the isotopic data available for porewater from these rocks (e.g., Hobbs et al., 2011; Clark et al., 2010a; Mazurek et al., 2013, 2015). Figure 4.1a shows that the δ^{18}O and δ^{2}H of the water samples form a trajectory from the GMWL (generally younger and more porous and permeable portions of the Paleozoic section) towards the calculated isotopic compositions of porewater in equilibrium with the <2μm clay size-fraction at ~90°C. The latter samples represent the lower portion of the Paleozoic stratigraphic section, specifically Ordovician shales of the Queenston Formation, Georgian Bay Formation, Collingwood Member and Cobourg Formation; these units are characterized by high salinity, and substantial decreases in permeability, hydraulic

conductivity and water content relative to much of the Paleozoic section (Hobbs et al., 2011; Clark et al., 2010a, 2013, and references therein).

Figure 4.1b focuses on the $\delta^{18}O$ and $\delta^{2}H$ of porewaters obtained for the Queenston Formation, Georgian Bay Formation, Collingwood Member and Cobourg Formation from the proposed Bruce site of the Deep Geological Repository (DGR). Samples analyzed using Vacuum Distillation Extraction (VDE) (Clark et al., 2010a) lie near the end of this porewater isotopic trajectory ($\delta^{18}O$ = –5.71 to –2.57‰; $\delta^{2}H$ = –59.5 to –45.3‰; n = 16). Perhaps of even more significance is that almost all porewater $\delta^{18}O$ and $\delta^{2}H$ obtained using Adaptive Isotope Diffusive Exchange (AIDE) for the Queenston and Cobourg Formations (Hobbs et al., 2011; $\delta^{18}O$ = +0.2 to +1.7‰; $\delta^{2}H$ = –39.3 to –38.0‰; n = 2), and high-pressure squeezing for the Blue Mountain and Cobourg Formation (Mazurek et al., 2013, 2015; $\delta^{18}O$ = +1.18 to +3.32‰; $\delta^{2}H$ = –-35.6 to – 32.1‰; n = 3) plot in the region predicted for isotopic equilibrium between the <2μm clay size-fraction and associated porewater at 90°C. A sample from the Blue Mountain Formation is the only exception; it was diluted with a water of a known and contrasting isotopic composition in an attempt to improve analytical precision by increasing sample size. Its $\delta^{18}O$ plots in a higher temperature region on Figures 4.1a,b but carries a large error and is considered an analytical outlier.

There are several implications of these observations. First, the small difference in the water compositions measured by VDE versus AIDE or high-pressure squeezing may reflect a difference in the water sampled by the respective methods. As discussed earlier in this thesis, the latter two methods may be capturing more bound water than the former, which is anticipated to be enriched in both ^{18}O and ^{2}H relative to fully mobile porewater. This speculation, however, is founded on the assumption that both oxygen and hydrogen isotope equilibrium was established

at 90°C between the <2μm size-fraction and porewater. For this outcome, traditional theory would require the <2μm size-fraction to have undergone dissolution-reprecipitation reactions in order to establish both oxygen and hydrogen isotope equilibrium. As such, the bulk of these illite-dominated <2µm size-fractions should then be considered diagenetic in origin, rather than detrital, at least from an isotopic point-of-view. This observation is counter to the largely detrital origin of the clays suggested by Bouchard et al. (2019) on the basis of $^{87}Sr/^{86}Sr$ ratios of both porewater and leached solid residues. Resolution of these different interpretations will likely require detailed examination of the clays using electron microscopic techniques.

That said, if the Kübler Index data for the illite samples are accepted at face value, temperatures of ~200°C for the Queenston Formation (DRG and OGS sites) and Collingwood Member (OGS site), ~100°C for the Georgian Bay Formation (DGR site), ~100-175°C for the Blue Mountain Formation (lowest at OGS site; highest at the DGR site), and <100°C for the Cobourg Formation (OGS site) are indicated based on the thermal boundaries between shallow diagenesis, deep diagenesis and the low anchizone (Abad, 2007) The ~100°C estimate for the Georgian Bay Formation is consistent with the generally accepted maximum burial temperature for these shales at the DGR site (70-90°C: Al et al., 2011; Al-Aasm et al., 2018). The ~175-200°C estimates for the Queenston and Blue Mountain formation sites, however, are too high. These initial results may point to a scenario in which – prior to transport – the clays originated from physical erosion of previously more deeply buried sedimentary rocks to the east in the Appalachian Orogen. Alternatively, these results may indicate the need for recalibration of the Kübler Index for use with the equipment employed by Western's Laboratory for Stable Isotope Science. The Kübler Index is well known for being instrument and laboratory sensitive (Warr & Ferrerio Mählmann, 2015).

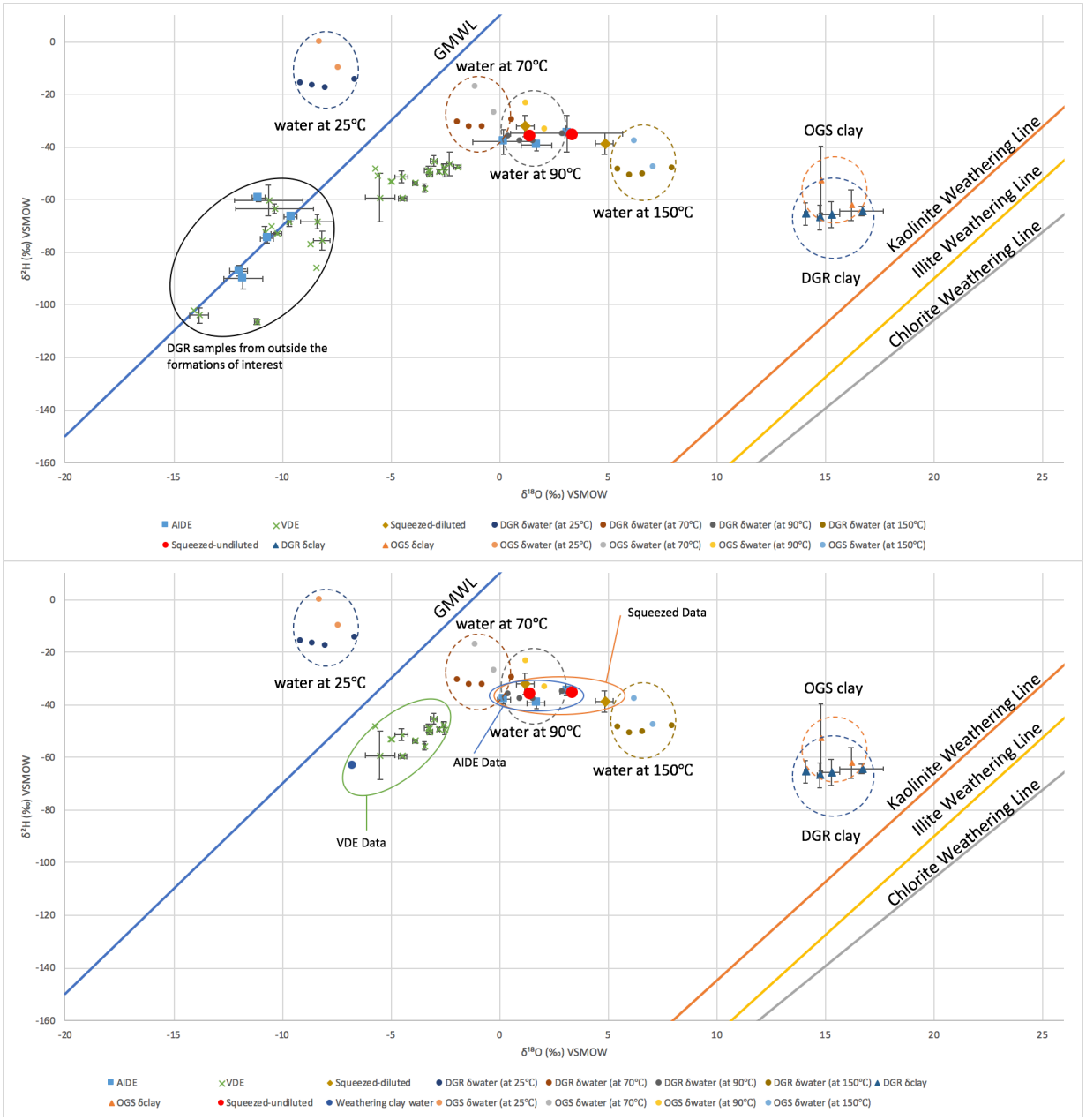

Figure 4.1. δ^2H vs. $\delta^{18}O$ of NWMO DGR2 and DGR3, and OGS Ordovician <2µm clay samples compared to the illite, kaolinite and chlorite clay weathering lines of Savin (1967). Also shown are the Global Meteoric Water Line (GMWL) and calculated porewater δ^2H and $\delta^{18}O$ (δ_{water}) assuming isotopic equilibrium with the Ordovician <2µm clay samples at 70°, 90° and 150°C (see text). ***Part (a)*** *also shows the δ^2H and $\delta^{18}O$ of water samples obtained by various methods (Adapted Isotope Diffusive Exchange, AIDE, Hobbs et al., 2011; Vacuum Distillation Extraction, VDE, Clark et al., 2010a; high-pressure squeezing, Mazurek et al., 2013) from the Paleozoic stratigraphic section.* ***Part (b)*** *shows only the δ^2H and $\delta^{18}O$ of water samples from the Queenston Formation, Georgian Bay Formation, Blue Mountain Formation, Collingwood Member and Cobourg Formation. These are the units from which the <2µm clay size-fractions have been analysed. Errors bars = replicate SD.*

Consideration of the third possibility (post-formation hydrogen isotope exchange), clay mineral isotopic compositions can be modified by exchange after crystallization (Longstaffe, 1987, 1989, 2000; Longstaffe & Ayalon, 1990; Sheppard & Gilg, 1996). As discussed earlier, however, clay mineral $\delta^{18}O$ is not significantly affected by post-formation exchange at <300°C in the absence of dissolution-reprecipitation reactions (Savin & Epstein, 1970; Coplen & Hanshaw, 1973; Longstaffe, 1987, 1989, 2000; Zheng, 1993; Delgado & Reyes, 1996). In contrast, it is increasingly well accepted that post-formation proton exchange can significantly affect clay mineral δ^2H at <100°C, given sufficient time and/or sufficiently high water-rock (w/r) ratios (O'Neil & Kharaka, 1976; Bird & Chivas, 1988; Longstaffe & Ayalon, 1990; Mizota & Longstaffe, 1996; McKay & Longstaffe, 2013). Post-formation hydrogen isotope exchange at 90°C between initially low δ^2H clays and higher δ^2H porewater could produce the δ^2H measured for the <2μm clay size-fraction.

Consideration of the role of w/r ratios in this system can provide some further insight into the observed isotopic systematics of both the <2μm clay size-fraction and the associated porewater. Figures 4.2a and 4.2b illustrate two scenarios for isotopic re-equilibration at 90°C for a range of water/rock ratios and starting water isotopic compositions. This approach is based on Equation 4.7, first presented by Taylor (1974) and rearranged by Faure et al. (2002). Figures 4.2a,b show how the initial δ-values of water change for various water/rock ratios (calculated by weight), assuming isotopic equilibrium is reached at 90°C:

$$\delta^f_{water} = \frac{w}{w+zr}\delta^i_{water} + \frac{zr}{w+zr}(\delta^i_{rock} - \Delta) \qquad \text{(Eq. 4.7)}$$

where f = final, i = initial, r = rock and w = water in weight units, z = amounts of hydrogen and oxygen per weight unit in water and rock, Δ = permill rock-water fractionation factor for either hydrogen or oxygen, and $\delta = \delta^2H$ or $\delta^{18}O$. Faure et al. (2002) note that z-values of 0.5 for oxygen

and 0.01 for hydrogen are typically assigned to sedimentary rocks containing 10% water. Higher average values of z (oxygen, 1.82; hydrogen, 0.036) were calculated here given the lower volumetric water contents (converted here to weight units) reported for the nearest samples in DGR cores #2 and #3 by Clark et al. (2010a).

An initial $\delta^{18}O$ of +16.68‰ was selected for the <2μm size-fraction, which is the highest value measured in this study. This choice assumes that there was only modest ^{18}O-depletion of the *<2μm* clay size fraction (average $\delta^{18}O$ = +15.1±0.9‰, Table 3.2) during isotopic exchange with porewater at 90°C. Assuming that the $\delta^{18}O$ (average = +15.1‰) of the <2μm size-fraction was entirely unaffected by oxygen isotope exchange or assuming a ~1‰ further increase in original $\delta^{18}O$ of the <2μm clay size-fraction shifts the water-rock curves shown in Figures 4.2a.b only slightly. The initial $\delta^{2}H$ assumed for the <2μm clay size-fraction (–115‰) represents the intersection of the assumed initial clay $\delta^{18}O$ (+16.68‰) with the illite weathering line of Savin (1967) (Figures 4.2a,b), and presumes a weathering origin for the <2μm size-fraction.

Two different initial water compositions were tested using Equation 4.7. In the first scenario (Figure 4.2a), the initial water compositions of $\delta^{18}O$ = –6.8‰ and $\delta^{2}H$ = –63‰ are those associated with a weathering origin for the illite-dominated <2μm clay size-fraction at 25°C. These values plot slightly off the GMWL, typical of slightly evaporated fresh water (Figures 4.1a,b; 4.2a). Perhaps of interest is that this water's $\delta^{2}H$ and $\delta^{18}O$ plot along the Paleozoic formation water trend defined by Clark et al. (2010a), filling the gap between higher values for porewater in units considered here and formation waters from higher in the Paleozoic section (Figures 4.1a, 4.2a). At w/r ratios of ≤0.1 and lower, a significant lowering of water $\delta^{2}H$ is observed. This also provides a reasonable explanation for the elevated $\delta^{2}H$ measured for the <2μm size-fraction relative to that expected for clays of weathering origin. The predicted water

δ^2H at any w/r ratio, however, do not match the isotopic compositions measured for any of the porewaters by VDE, AIDE or high-pressure squeezing, or those predicted for clay-porewater equilibration at 90°C. A w/r ratio >5 is also needed to explain the measured porewater δ^{18}O.

In the second scenario, values of δ^{18}O = –5.5‰ and δ^2H = –34‰ were selected for the initial water isotopic composition. These choices are based on (i) the lowest average δ^{18}O obtained by Clark et al. (2010a, 2015) among the Ordovician shales examined in the current study (in this case, the Cobourg Formation) and (ii) the calculated δ^2H that places this water on the GMWL. This approach assumes that this porewater evolved from originally fresh water and that the currently measured δ^2H of this sample (–59.25‰, Clark et al., 2010c) has been shifted to a lower value by some process that did not affect its original δ^{18}O. Figure 4.2b shows that at low w/r ratios (<0.1) the water δ^2H is substantially lowered by isotopic exchange. Also, at w/r ≈ 0.1, the water δ^2H bracket those measured for these units by VDE (Clark et al., 2010a). To match the measured porewater δ^{18}O by any method – and the δ^2H obtained by AIDE – however, requires a substantially higher w/r ratio (≥5).

In short, isotopic re-equilibration at a burial temperature of 90°C remains the simplest explanation for the match between the porewater isotopic compositions measured by AIDE and high-pressure squeezing, and those calculated for equilibrium with the measured isotopic compositions of the <2μm size-fraction 90°C. This scenario suggests that both water and clay isotope compositions were shifted from original values at w/r ratios higher than might initially be assumed for rocks currently of such low water content.

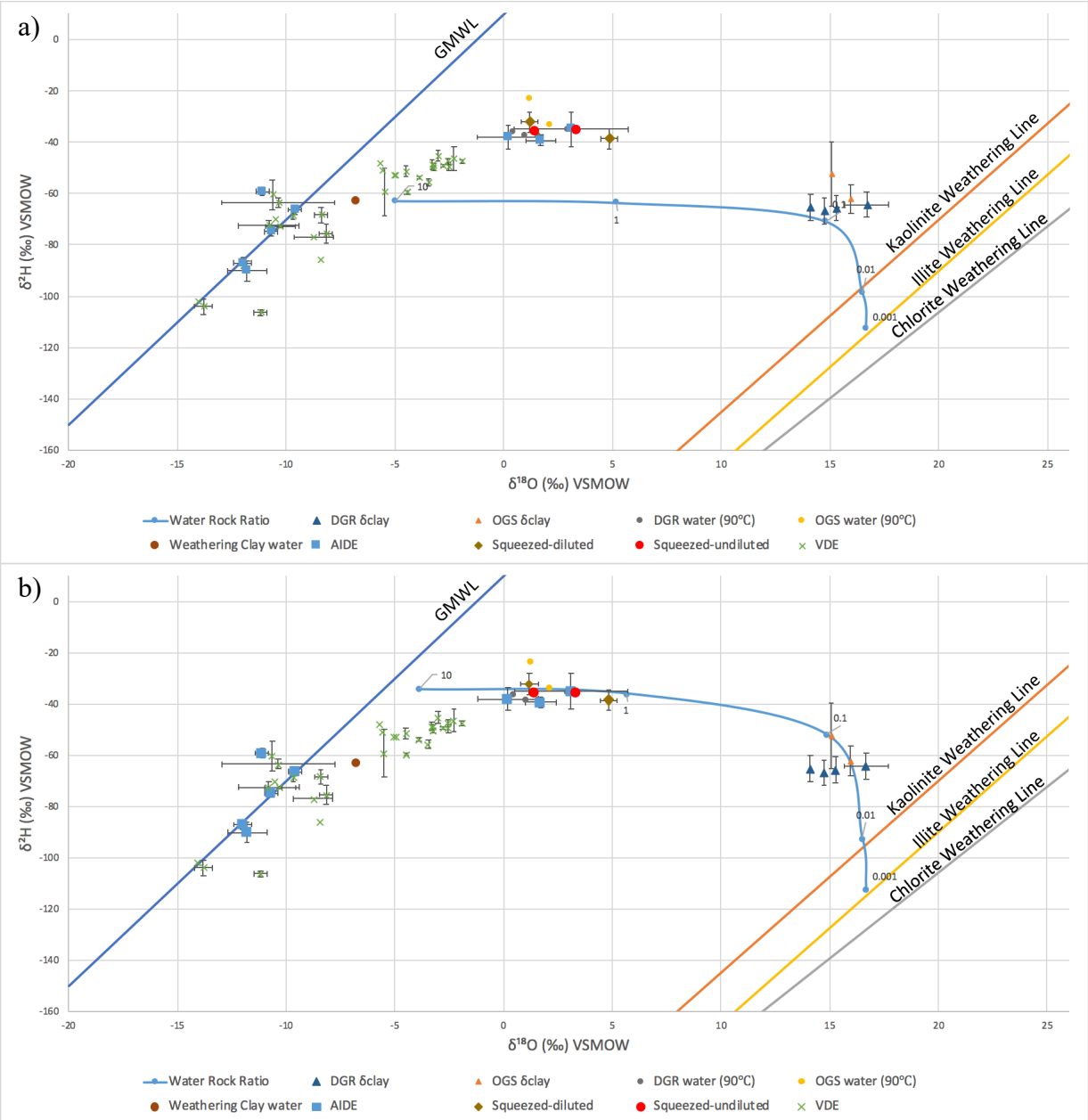

Figure 4.2. Data as shown in Figure 4.1b for the Global Meteoric Water Line (GMWL), clay weathering lines of Savin (1967), the NWMO DGR2, NWMO DGR3 and OGS Ordovician <2µm clay size-fractions, and calculated water isotopic compositions in equilibrium with these clays at 90°C. The blue line shows the trajectory of the <2µm clay size-fraction for various water/rock ratios: a) with an initial water composition of $\delta^{18}O = -6.8‰$ and $\delta^{2}H = -63‰$ and b) initial water compositions of $\delta^{18}O = -5.5‰$ and $\delta^{2}H = -34‰$. See text for discussion.

4.3.2. Clay-Water Hydrogen Isotope Exchange Experiments

Section 3.3.2 describes how development of the TC-EA method enabled more precise and accurate hydrogen isotope analysis of the <2μm size-fractions. This enabled the precision and accuracy needed to test whether hydrogen isotope exchange had affected the four DGR samples and the CMS Source Clay illite (IMt-1) over the 9-10 weeks that they were exposed to two different isotopically labelled waters at 68°C. As documented in Table 3.3, illustrated in Figure 3.31b and summarized in Table 4.1, this experiment suggests that the DGR <2μm size-

Table 4.1. Hydrogen isotope exchange between <2µm size-fractions and ^{2}H-depleted and ^{2}H-enriched water

Sample	δ^2H ‰ VSMOW Exchanged Value	δ^2H ‰ VSMOW Unexchanged Value	δ^2H ‰ VSMOW Exchange Water	% Exchange*	Conditions
DGR3 459 K <2µm L	-62.80	-55.80	-309.00	2.76%	68°C, 10 weeks
DGR3 459 K <2µm H	-46.05	-55.80	810.00	1.13%	68°C, 10 weeks
				1.95%	*average*
DGR3 523 K <2µm L	-68.05	-61.60	-309.00	2.61%	68°C, 10 weeks
DGR3 523 K <2µm H	-34.40	-61.60	810.00	3.12%	68°C, 9 weeks
				2.86%	*average*
DGR2 530 K <2µm L	-57.00	-58.60	-309.00	-0.64%	68°C, 10 weeks
DGR2 530 K <2µm H	-47.15	-58.60	810.00	1.32%	68°C, 10 weeks
				0.34%	*average*
DGR2 616 K <2µm L	-65.9	-56.1	-309.0	3.86%	68°C, 10 weeks
DGR2 616 K <2µm H	-46.8	-56.1	810.0	1.08%	68°C, 10 weeks
				2.47%	*average*
IMt-1 K <2µm Light	-104.0	-102.7	-309.0	0.61%	68°C, 10 weeks

L = Light water, δ^2H = –309±5‰; H = Heavy water, δ^2H = +810±3‰
*amount of water (ml) to clay (mg)approximates an infinite water/clay ratio

fraction is susceptible to post-formation isotopic exchange, attaining higher δ^2H when exposed to ^{2}H-enriched water and lower δ^2H when exposed to ^{2}H-depletd water, both at very high w/r ratios.

Over the short period of the experiment at a relatively low temperature, the amount of exchange exhibited by the DGR <2μm samples varied from 0.3 to 3%, and limited hydrogen isotope exchange (0.6%) was also observed for the CMS Source Clay illite (IMt-1). Whether oxygen isotope exchange occurred during this experiment, however, was not tested. Such testing would require doubly-labelled exchange waters, in which a large contrast in both δ^{18}O and δ^2H was present. Isotopic analysis would also require either a much greater quantity of the <2μm size-fraction sample of the Ordovician shales or a method for analyzing the oxygen isotope composition of much smaller quantities of sample, as was developed for the hydrogen isotope measurements. Both approaches are currently being developed at Western's Laboratory for Stable Isotope Science by other researchers.

4.3.3. Stepwise Heating of CMS Source Clay Kaolinite (KGa-1) and NWMO DGR 523 K<2μm exchanged with 'Heavy' Water

As described in section 3.3.4, *in vacuo* stepwise heating of the <2μm size-fraction was undertaken to assess whether bound water on clay surfaces was enriched in ^{2}H relative to the mobile porewater associated with these clays. In particular, these experiments were designed to test whether the differences encountered between porewater hydrogen isotope compositions made by VDE versus AIDE or high-pressure squeezing might arise from such isotopic partitioning between bound and mobile phases of porewater.

The proof-of-principle test performed on CMS Source Clay kaolinite KGa-1 was promising. This clay sample was exposed to ambient water vapour at ~20°C, which had a δ^2H of ~ –120‰ and a condensed δ^2H of ~ –45‰ (Longstaffe, unpublished data). As summarized in

Table 3.4 and illustrated in Figure 4.3a, the first very small volume of H_2 (0.02μmoles/mg of clay) evolved between 20-100°C had δ^2H (–30‰) enriched in ^{2}H by 15‰ relative to the ambient condensed water with which the sample was in contact. This hydrogen is attributed to sorbed water on the kaolinite surfaces. Progressively lower δ^2H were then obtained for the small aliquots of H_2 released at still higher temperature steps (100-300°C: –46‰, 0.02μmoles/mg H_2; 300-400°C: –68‰, 0.17μmoles/mg H_2). The hydrogen released at 300-400°C is attributed to loosely bound kaolinite hydroxyl groups. Most hydrogen was released between 400-1000°C (5.77μmoles/mg), which is the typical temperature interval over which kaolinite dehydroxylation occurs. The δ^2H (–55‰) of this step is very close to the accepted value for structural hydrogen in KGa-1 (–57‰; He et al., 2019). The lower δ^2H for the more loosely bound hydroxyls released between 300-400°C is also expected as larger fractionations between clay hydroxyl groups and water can be expected for more weakly held moieties. More broadly, McKay & Longstaffe (2013) reported similar patterns for bound water – hydroxyl hydrogen release for smectite and hydroxy-interlayer smectite from Alberta oil sands.

As described in section 3.3.4, however, application of this approach to the DGR samples failed. As summarized in Table 3.4 and illustrated in Figure 4.3b for the test case of DGR 523 K<2μm (Heavy), progressively higher δ^2H was obtained for the small fractions of hydrogen released up to 400°C, as might be expected for release of increasingly tightly bound water. However, none of these compositions approached the δ^2H of the 'Heavy' water (+810‰) with which this sample was treated. Moreover, for the temperature interval (400-100°C) during which dehydroxylation should occur, the measured δ^2H (+20.2‰) is substantially higher that the known value for this sample (–34.4‰) as measured using the TC-EA method. Subsequent analysis of water standards, as described in section 3.3.4 (see also Table 3.4), suggests that 'Heavy' water –

loosely held on the sample – contaminated the vacuum system in which the sample was placed, likely during initial evacuation. The presence of this memory effect made it clear that the true δ^2H of hydrogen released during stepwise heating of the clay was overprinted by ^{2}H-rich hydrogen originating from the 'Heavy' water released at earlier stages of the experimental process.

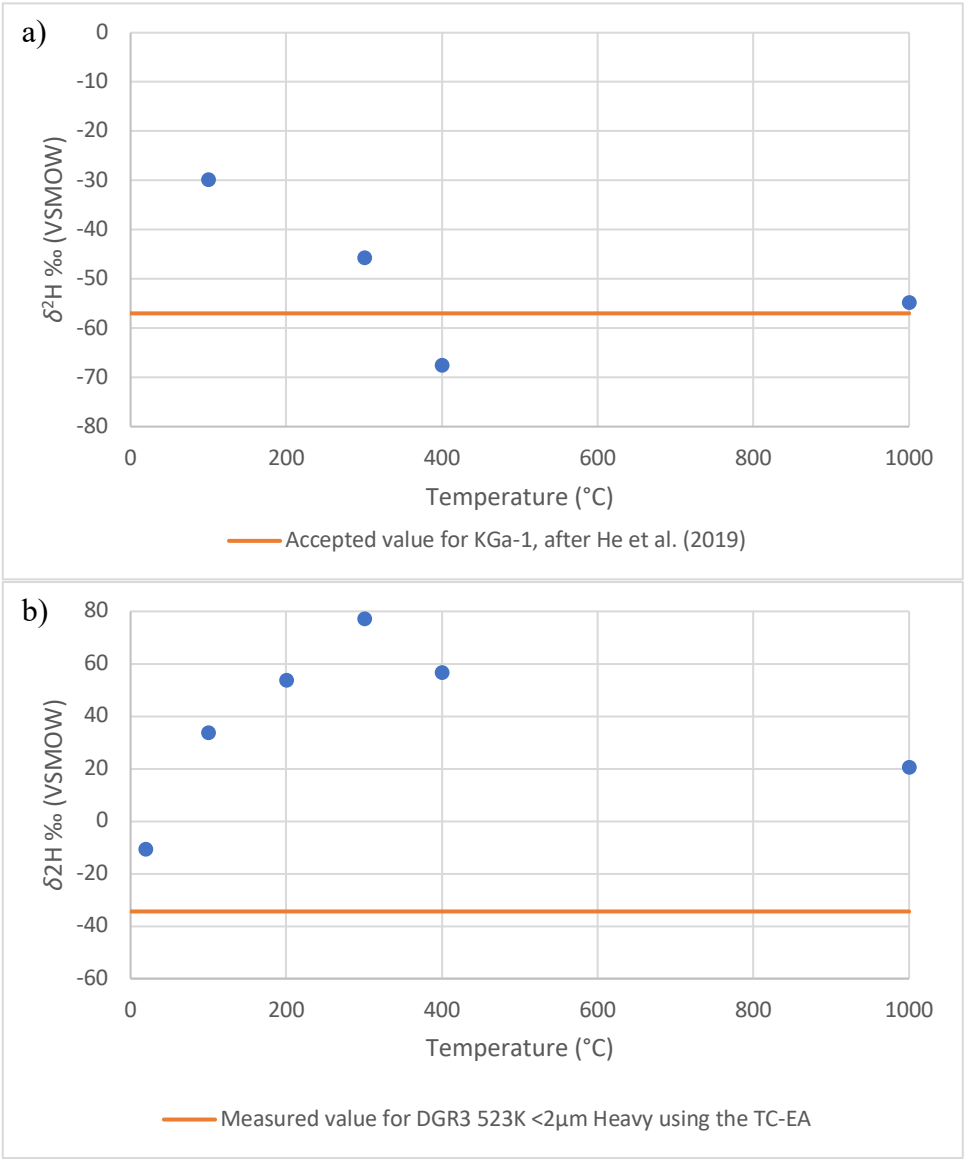

Figure 4.3. δ^2H versus stepwise-heating temperature for (a) bulk KGa-1, and (b) DGR 523 K<2µm (Heavy).

Because of this memory effect, further experiments of this nature were discontinued. Efforts to develop a different means of securely measuring the hydrogen (and oxygen) isotope

composition of bound versus mobile water in illite, kaolinite, chlorite and smectite systems are currently being developed by other researchers at Western's Laboratory for Stable Isotope Science.

Chapter 5. Conclusion

This study set out to examine whether clay minerals in Ordovician shales from southern Ontario played a role in determining the present isotopic composition of porewater within these low water content and low permeability formations. A particular effort was made to examine shale units located within the stratigraphic section of the proposed Deep Geologic Repository (DGR) for nuclear waste at the Bruce Nuclear Generating Station. Of specific interest was whether hydrogen (and oxygen) isotope exchange had occurred between porewater and clay mineral hydroxyl groups in these shales. Also of interest was whether partitioning between clay mineral surface-bound water and remaining 'free' (i.e., mobile) porewater had a measurable effect on the latter's isotopic composition. The ability to accurately measure the isotopic compositions of structural oxygen and hydrogen in clay minerals is prerequisite to evaluating the possibility of clay-water, post-formation isotopic exchange. Particularly for hydrogen, however, the accuracy of analyses can be strongly affected by a clay mineral's tendency to retain residual bound water. This thesis also set out to examine this possibility. The major conclusions concerning these three main points are summarized below.

The clay mineralogy (<2μm) determined by pXRD for all Ordovician units examined (Queenston Formation, Georgian Bay Formation, Blue Mountain Formation, Collingwood Member) is remarkably similar. The clay mineral assemblage of each unit is dominated by illite, with lower amounts of kaolinite and still lower quantities of chlorite. Across the series of humidity, glycolation and heat treatments used in the pXRD analysis, the results for each clay

mineral in the shale samples closely corresponded to patterns obtained for the Clay Mineral Society (CMS) Source Clay illite (IMt-1), kaolinite (KGa-1) and chlorite (CCa-1). Discrete swelling clays were not present in any shale samples. The latter finding is significant; the amount of porewater immobilized through binding to clay surfaces is likely to be limited in the absence of inner surface areas associated with swelling clay minerals.

Thermogravimetric (TGA) examination of the <2μm size-fraction of the CMS Source Clays and the southern Ontario's Ordovician clays offered three important kinds of information. First, TGA defined the dehydration characteristics of the clay minerals including the temperature range and amount of bound-water loss. Second, TGA provided insight into the clay minerals' potential for isotopic exchange of structural hydrogen and oxygen with porewaters by defining the temperatures for initiation and completion of dehydroxylation. Third, the TGA information provided the basis for designing analytical protocols for capturing only structural water for hydrogen and oxygen isotope analysis.

The TGA patterns of the <2μm size-fractions were broadly similar across all Ordovician shale units examined, consistent with the clay mineralogy obtained by pXRD. Dehydration and dehydroxylation patterns were also similar to those obtained for the CMS Source clays, illite in particular, which comprised most of the <2μm size-fractions.

The possibility existed for significant variation in the amounts and temperatures at which clay surface-bound water was released during dehydration. In such a scenario, there would be potential to affect the isotopic compositions of the clay-associated water, depending on analytical method. Variations in the dehydration patterns of the Ordovician <2μm clay size-fraction, however, were quite limited, albeit apparently dependent on exchangeable cation (Na, Ca, K). No consistent pattern, however, in the temperature and/or amount of water loss during

dehydration could be discerned among the Ordovician shale units analyzed. This variability among samples of similar clay mineralogy points to the complexity that can be expected from clay-water interactions, depending on clay type and formation water chemistry. Testing for dehydration behaviour, and in particular retention of residual bound water at higher-than-expected temperatures should likely be monitored on a case-by-case basis, given its potential to affect mobile water isotopic compositions.

The majority of weight loss for all samples analyzed using *in vacuo* conditions on the TGA occurred at higher temperatures, as a result of dehydroxylation. Dehydroxylation began at as low as ~300°C and reached completion between ~420-750°C, depending clay mineral type and exchangeable cation saturation. A relatively smaller rate of weight loss from 430°C to 550-580°C (and occasionally higher, i.e. to 640°C) was common, followed by a larger rate of weight loss from 550-580°C to 710-750°C. A two-step weight loss process is consistent with differences in the expected dehydroxylation behaviour of illite, kaolinite and chlorite, and with species-dependent variations arising from clay structure (2:1, 1:1; 2:2), crystallinity and grain size. It can be anticipated that samples in which dehydroxylation begins at lower temperatures may be more susceptible to isotopic exchange, given the inferred weaker bonding of hydroxyl groups and hydrogen within those hydroxyl groups.

The *in vacuo* TGA patterns overall, and their variability among <2μm size-fractions, also indicate the need to assess on an individual basis, the best temperature at which to remove bound water from clay samples, and the temperature at which to begin collection of hydroxyl-bound water. Such data will also help identifying clay mineral assemblages with the potential for cross-contamination between the mostly tightly bound surface water and the most loosely bound hydroxyl-group water.

The siliciclastic sediments comprising much of the Ordovician shales of southwestern Ontario originated from the east-coast Appalachian highlands of proto-North America. The $\delta^{18}O$ and $\delta^{2}H$ of their clay minerals should therefore have been established during the weathering that produced them. As such, their $\delta^{18}O$ and $\delta^{2}H$ should closely track clay weathering lines related to the Global Meteoric Water Line (GMWL) by temperature- and clay-dependent fractionations. The <2μm clay separates analyzed in the present investigation, however, do not plot on or near these weathering lines. Instead there is an apparent match between water in isotopic equilibrium at 90°C (maximum burial temperature at the DGR) with clay structural oxygen and hydrogen isotope compositions and currently available porewater isotopic compositions for these shales produced by Adaptive Isotope Diffusive Exchange (AIDE) and high-pressure squeezing (HPS). This scenario, however, suggests that both water and clay isotope compositions were shifted from original values during post-formation exchange at w/r ratios higher than might initially be expected for rocks of such low water content.

The porewater hydrogen isotope compositions calculated from hydroxyl group measurements versus those currently available from Vacuum Distillation Extraction (VDE) can also be matched through a process of post-formation clay-water hydrogen isotope exchange. Preliminary experiments using DGR <2μm size-fractions and CMS illite IMt-1 showed that hydrogen isotope exchange can be detected in as little as nine-ten weeks at 68°C. Detection of exchange was made possible by a newly developed approach to hydrogen isotope analysis of clay minerals via Thermal Combustion Elemental Analyzer (TC-EA).

Future work should focus on development of methods to accurately separate and isotopically analyze as discrete entities: (i) bound water from clay surfaces, and (ii) structurally bound hydroxyl groups. The coupling in continuous flow mode of a modern TGA with a laser

water isotope analyzer could achieve this goal. Successful development of such a methodology would resolve the question of whether isotopic fractionation between clay bound water and mobile porewater can affect the isotopic composition of: (i) structural oxygen and hydrogen in a clay mineral, and (ii) remaining mobile porewater. In the former case, contamination by residual bound water could cause the process controlling a clay mineral's isotopic composition to be misidentified. In the latter case, a change in isotopic composition of mobile porewater could cause its source to be misinterpreted, with attendant implications for the nuclear repository safety case.

Chapter 6. References

Al, T., Beauheim, R., Crowe, R., Diederichs, M., Frizzell, R., Kennell, L., Lam, T., Parmenter, A., & Semec, B. (2011). DGR-TR-2011-11. *Geosynthesis.* Nuclear Waste Management Organization, 1-418.

Al-Aasm, I. S., & Crowe, R. (2018). Fluid compartmentalization and dolomitization in the Cambrian and Ordovician successions of the Huron Domain, Michigan Basin. *Marine and Petroleum Geology, 92*, 160-178.

Alvarez-Puebla, R. A., dos Santos, D. S., Blanco, C., Echeverria, J. C., & Garrido, J. J. (2005). Particle and surface characterization of a natural illite and study of its copper retention. *Journal of Colloid and Interface Science, 285*(1), 41-49.

Armstrong, D. K., & Carter, T. R. (2010). *The subsurface Paleozoic stratigraphy of southern Ontario* (Ontario Geological Survey Special Volume 7), 301p.

Ayalon, A., & Longstaffe, F. J. (1988). Oxygen isotope studies of diagenesis and pore-water evolution in the Western Canada sedimentary basin; evidence from the Upper Cretaceous basal Belly River Sandstone, Alberta. *Journal of Sedimentary Research, 58*(3), 489-505.

Bahri, M. H., Wardana, I., Hamidi, N., & Wijayanti, W. (2017). Combustion Characteristic of Albizia falcataria using Thermogravimetry. *Proceedings "The 1st UMM International Conference on Pure and Applied Research (UMM-ICOPAR2015)"*, 103-107.

Bauer, K. K., & Vennemann, T. W. (2014). Analytical methods for the measurement of hydrogen isotope composition and water content in clay minerals by TC/EA. *Chemical Geology, 363*, 229-240.

Bird, M. I., & Chivas, A. R. (1988). Stable-isotope evidence for low-temperature kaolinitic weathering and post-formational hydrogen-isotope exchange in Permian kaolinites. *Chemical Geology: Isotope Geoscience Section, 72*(3), 249-265.

Biscaye, P. E. (1964). Distinction between kaolinite and chlorite in Recent sediments by x-ray diffraction. *American Mineralogist, 49*, 803-832.

Biscaye, P. E. (1965). Mineralogy and sedimentation of recent deep-sea clay in the Atlantic Ocean and adjacent seas and oceans. *Geological Society of America Bulletin, 76*(7), 803-832.

Borthwick, J., & Harmon, R. S. (1982). A note regarding CIF 3 as an alternative to BrF 5 for oxygen isotope analysis. *Geochimica et Cosmochimica Acta, 46*, 1665-1668.

Bouchard, V. L., Kennell-Morrison, L., Jensen, M., Raven, K. G., & Clark, I. D. (2018). Origin and 87Rb–87Sr age of porewaters in low permeability Ordovician sediments on the eastern flank of the Michigan Basin, Tiverton, Ontario, Canada. *Canadian Journal of Earth Science, 56*(3), 201-208.

Brown, G., & Brindley, G. W. (1980). *Crystal structures of clay minerals and their X-ray identification* (Vol. 5). London: Mineralogical Society.

Capuano, R. M. (1992). The temperature dependence of hydrogen isotope fractionation between clay minerals and water: Evidence from a geopressured system. *Geochimica et Cosmochimica, 56*(6), 2547-2554.

Carlsson, H. (1986). Update: The internation Stripa project. *IAEA Bulletin*, 25-28.

Cases, J. M., Berend, I., & Francois, M. (1992). Mechanism of adsorption and desorption of water vapor by homoionic montmorilloonite. 1. The sodium-exchanged form. *Langmuir , 8*(11), 2730-2739.

Chipera, S. J., & Bish, D. L. (2001). Baseline studies of the clay minerals society source clays: powder X-ray diffraction analyses. *Clays and Clay Minerals, 49*(5), 398-409.

Clark, I. (2015). *Groundwater geochemistry and isotopes.* CRC press.

Clark, I. D., Al, T., Jensen, M., Kennell, L., Mazurek, M., Mohapatra, R., & Raven, K. G. (2013). Paleozoic-aged brine and authigenic helium preserved in an Ordovician shale aquiclude. *Geology, 41*(9), 951-954.

Clark, I. D., Ilin, D., Jackson, R. E., Jensen, M., Kennell, L., Mohammadzadeh, H., . . . Raven, K. G. (2015). Paleozoic-aged microbial methane in an Ordovician shale and carbonate aquiclude of the Michigan Basin, southwestern Ontario. *Organic Geochemistry, 83*, 118-126.

Clark, I. D., Liu, I., Mohammadzadeh, H., Mohapatra, R., Zhang, P., & Wilk, M. (2010a). *Porewater and gas analyses in DGR-3 and DGR-4 Core.* Ottawa, Canada: Intera Engineering Ltd.

Clark, I., Jackson, R., Liu, I., & Heagle, D. (2010b). *Vacuum Distillation Experiments on DGR Core.* Ottawa, Canada: Intera Engineering Ltd.

Clayton, R. N., & Mayeda, T. K. (1963). The use of bromine pentafluoride in the extraction of oxygen from oxides and silicates for isotopic analysis. *Geochimica et Cosmochimica Acta, 27*(1), 43-52.

Cole, D. R., Mottl, M. L., & Ohmoto, H. (1987). Isotopic exchange in mineral-fluid systems. II. Oxygen and hydrogen isotopic investigation of the experimental basalt-seawater system. *Geochimica et Cosmochimica Acta, 51*, 1523-1538.

Coplen, T. B. (1996). New guidelines for reporting stable hydrogen, carbon and oxygen isotope-ratio data. *Geochimica et Cosmochimica Acta, 60*, 3359-3360.

Coplen, T. B., & Hanshaw, B. B. (1973). Ultrafiltration by a compacted clay membrane—I. Oxygen and hydrogen isotopic fractionation. *Geochimica et Cosmochimica Acta, 37*(10), 2295-2310.

Craig, H. (1961). Isotopic variations in meteoric waters. *Science, 133*(3465), 1702-1703.

Davidson, A. (1995). A review of the Grenville orogen in its North American type area. *AGSO Journal of Australian Geology and Geophysics, 16*(1), 3-24.

De Haller, A., Hobbs, M., & Spangenberg, J. E. (2016). Adapting the diffusive exchange method for stable isotope analysis of pore water to brine-saturated rocks. *Chemical Geology, 444*, 37-48.

Delgado, A., & Reyes, E. (1996). Oxygen and hydrogen isotope compositions in clay minerals: A potential single-mineral geothermometer. *Geochimica et Cosmochimica Acta, 60*(21), 4285-4289.

Derkowski, A., Drits, V. A., & McCarty, D. K. (2012). Nature of rehydroxylation in dioctahedral 2:1 layer clay minerals. *American Mineralogist, 97*(4), 610-629.

Dickinson, W. R., Beard, L. S., Brakenridge, G. R., Erjavec, J. L., Ferguson, R. C., Inman, K. F., Knepp, R. A., Lindberg, A. F., & Ryberg, R. T. (1983). Provenance of North American Phanerozoic sandstones in relation to tectonic setting. *Geological Society of America Bulletin, 94*(2), 222-235.

Facella, J., Belfadhel, B., & Patton, P. (2012). *Process for selecting a site for Canada's deep geological repository for used nuclear fuel.* Toronto, ON: Nuclear Waste Management Organization.

Fagan, R. (2001). *Oxygen- and hydrogen- isotope study of hydroxyl group behavior in standard smectite and kaolinite.* PhD Thesis, The University of Western Ontario, Canada, London.

Faure, K., Matsuhisa, Y., Metsugi, H., Mizota, C., & Hayashi, S. (2002). The Hishikari Au-Ag epithermal deposit, Japan: oxygen and hydrogen isotope evidence in determining the source of paleohydrothermal fluids. *Economic Geology, 97*(3), 481-498.

Folk, R. L. (1980). *Petrology of sedimentary rocks.* Austin, Texas: Hemphill Publishing Company.

Frakes, L. A., Francis, J. E., & Syktus, J. I. (2005). *Climate modes of the Phanerozoic.* Cambridge University Press.

Graham , C. M., Atkinson, J., & Harmon, R. S. (1984). Hydrogen isotope fractionation in the system chlorite-water. *NERC 6th Progress Report of Research 1981-1984*, 1-139.

Guggenheim, S., & Van Groos, K. A. (2001). Baseline studies of the clay minerals society source clays: thermal analysis. *Clays and Clay Minerals, 49*(5), 433-443.

Guggenheim, S., Bain , D. C., Bergaya, F., Brigatti, M. F., Drits, V. A., Eberl, D. D., . . . Stanjek, H. (2002). Order, disorder and crystallinity in phyllosilicates and the use of the "crystallinity index". *Report of the association Internationale pour l'Etude des Argiles (AIPEA) Clay Min, 37*, 389-393.

Guillet, G. R. (1977). *Clay and Shale Deposits of Ontario; Ontario Division of Mines, Map 2358, 1:2 000 000.*

Hamblin, A. P. (1999a). Lower Silurian Medina Group of Southwestern Ontario: Summary of literature and concepts. *Geological Survey of Canada*, Open File 3468.

Hamblin, A. P. (1999b). Upper Ordovician strata of southeastern Ontario: synthesis of literature and concepts. *Geological Survey of Canada*, Open File 3729.

He, S., Longstaffe, F. J., & Zhou, Z. (2019). Stable isotopes of clay minerals from autoclave tests of oil sands: Implications for clay formation during steaming of Alberta Clearwater oil sands. *Applied Geochemistry, 104*, 202-209.

Hendricks, S. B. (1942). Lattice structure of clay minerals and some properties of clays. *The Journal of Geology, 50*(3), 276-290.

Hendry, J. M., & Wassenaar, I. L. (2000). Controls on the distribution of major ions in pore waters of a thick surficial aquitard. *Water Resources Research, 36*(2), 503-513.

Hendry, J. M., Kelln, C. J., Wassenaar, L. I., & Shaw, J. (2004). Characterizing the hydrogeology of a complex clay-rich aquitard system using detailed vertical profiles of the stable isotopes of water. *Journal of Hydrology, 293*(1-4), 47-56.

Hendry, M. J., & Wassenaar, L. I. (1999). Implications of the distribution of δD in pore waters for groundwater flow and the timing of geologic events in a thick aquitard system. *Water Resources Research, 35*(6), 1751-1760.

Hobbs, M. Y., Frape, S. K., Shouakar-Stash, O., & Kennell, L. R. (2008). *Supporting Technical Report Phase I Regional Hydrogeochemistry, Southern Ontario.*

Hobbs, M., de Haller, A., Koroleva, M., Mazurek, M., Spangenberg, J. E., Mäder, U., & Meier, D. (2011). *Borehole DGR-3 and DGR-4 porewater investigations.* Geogirma Engineering Ltd.

Horita, J., Cole, D. R., & Wesolowski, D. J. (1995). The activity-composition relationship of oxygen and hydrogen isotopes in aqueous salt solutions: III. Vapor-liquid water equilibration of NaCl solutions to 350 C. *Geochimica et Cosmochimica Acta, 59*(6), 1139-1151.

Horita, J., Cole, D. R., Polyakov, V. B., & Driesner, T. (2002). Experimental and theoretical study of pressure effects on hydrogen isotope fractionation in the system brucite-water at elevated temperatures. *Geochimica et Cosmochimica Acta, 66*(21), 3769-3788.

Horita, J., Driesner, T., & Cole, D. R. (1999). Pressure effect on hydrogen isotope fractionation between brucite and water at elevated temperatures. *Science, 286*(5444), 1545-1547.

Howell, P. D., & van der Pluijm, B. A. (1999). Structural sequences and styles of subsidence in the Michigan basin. *Geological Society of America Bulletin, 111*(7), 974-991.

Huddlestun, P. F., & Summerour, J. H. (1996). *The lithostratigraphic framework of the uppermost Cretaceous and lower Tertiary of eastern Burke County, Georgia.* Georgia Department of Natural Resources Environmental Protection Division Georgia Geologic Survey, Atlanta.

Huggett, J., Adetunji, J., Longstaffe, F., & Wray, D. (2017). Mineralogical and geochemical characterisation of warm-water, shallow-marine glaucony from the Tertiary of the London Basin. *Clay Minerals, 52*(1), 25-50.

Ignasiak, T. M., Kotlyar, L., Longstaffe, F. J., Strausz, O. P., & Montgomery, D. S. (1983). Separation and characterization of clay from Athabasca asphaltene. *Fuel, 62*(3), 353-362.

Independent Electricity System Operator (IESO). (2018). *Supply Overview*. Retrieved January 11, 2018, from Power Data: http://www.ieso.ca/power-data/supply-overview/transmission-connected-generation

INTERA. (2011b). *Hydrogeological Modelling.* Ottawa, ON.

INTERA. (2017). *Method Develoment: Micro Vacuum-distilation Experiments (µVDE).* Ottawa, ON.

Irving, E. (1979). Paleopoles and paleolatitudes of North America and speculations about displaced terrains. *Canadian Journal of Earth Sciences*, 669-694.

Jackson, M. L. (1979). *Soil chemical analysis - Advanced course, 2nd edition.* Madison, Wisconsin, U.S.A.: Published by the Author.

King, T. V., & Clark, R. N. (1989). Spectral characteristics of chlorites and Mg-serpentines using high-resolution reflectance spectroscopy. *Journal of Geophysical Research:Solid Earth, 94*(B10), 13997-14008.

Lawrence, J. R., & Taylor Jr., H. P. (1971). Deuterium and oxygen-18 correlation: Clay minerals and hydroxides in Quaternary soils compared to meteoric waters. *Geochimica et Cosmochimica Acta, 35*(10), 993-1003.

Lee, M. (1984). *Diagenesis of the Permian Rotliegendes Sandstone, North Sea: K/Ar, O18/O16 and petrologic evidence.* PhD thesis, Case Western Reserve University , Cleveland, Ohio, USA.

Libbey, R. B., Longstaffe, F. J., & Flemming, R. L. (2013). Clay mineralogy, oxygen isotope geochemistry, and water/rock ratio estimates, Te Mihi area, Wairakei geothermal field, New Zealand. *Clays and Clay Minerals, 61*(3), 204-217.

Linseis. (2018). *Thermo-gravimetric Analyzer-TGA 1600.* Linseis.

Liu, Z. (2016). *Stable Isotope Paleolimnology of Barry Lake, Ontario, Canada Since AD-1268.* The University of Western Ontario, Graduate Program in Geology. London, Ontario: The University of Western Ontario.

Longstaffe, F. J. (1987). Stable isotope studies of diagenetic processes. In T. Kyser (Ed.), *Stable Isotope Geochemistry of Low Temperature Fluids*. Mineralogical Association of Canada Short Course. 13, 187-257.

Longstaffe, F. J. (1989). Stable isotopes as tracers in clastic diagenesis. In I. Hutcheon (Ed.), *Burial Diagenesis*. Mineralogical Association of Canada Short Course. 15, 201-277.

Longstaffe, F. J. (2000). An introduction to stable oxygen and hydrogen isotopes and their use as fluid tracers in sedimentary systems. In T. Kyser (Ed.), *Fluids and Basin Evolution*. Mineralogical Association of Canada Short Course. 28, 115-162.

Longstaffe, F. J., & Ayalon, A. (1990). Hydrogen-isotope geochemistry of diagenetic clay minerals from Cretaceous sandstones, Alberta, Canada: evidence for exchange. *Applied Geochmistry, 5*(5-6), 657-668.

Longstaffe, F. J., Clark, I. D., & Chauvin, S. (2017). Investigation of Clay-Water H- & O-Isotope Interactions in Fine-Grained Sedimentary Rocks. *NWMO 15th Annual Geoscience Seminar, June 7-8.* Toronto, Canada.

Low Level Radioactive Waste Management Office (LLRWMO). (2012). *Inventory of Radioactive Waste in Canada.* Low-Level Radioactive Waste Management Office, Ottawa, Canada.

Mäder, U. K., Waber, H. N., & Gautschi, A. (2014). New method for porewater extraction from claystone and determination of transport properties with results for Opalinus Clay (Switzerland). *Proceedings of the 11th International Symposium on Water-Rock Interaction, WRI, 11*, 445-448.

Marumo, K., Longstaffe, F. J., & Matsubaya, O. (1995). Stable isotope geochemistry of clay minerals from fossil and active hydrothermal systems, southwestern Hokkaido, Japan. *Geochimica et Cosmochimica Acta, 59*(12), 2545-2559.

Marumo, K., Nagasawa, K., & Kuroda, Y. (1980). Mineralogy and hydrogen isotope geochemistry of clay minerals in the Ohnuma geothermal area, northeastern Japan. *Earth and Planetary Science Letters, 47*(2), 255-262.

Mazurek, M., & De Haller, A. (2017). Pore-water evolution and solute-transport mechanisms in Opalinus clay at Mont Terri and Mont Russelin (canton Jura, Switzerland). *Swiss Journal of Geosciences, 110*(1), 129-149.

Mazurek, M., Al, T., Celejewski, M., Clark, I. D., Fernandez, A. M., Kennell-Morrison, L., . . . Yu, C. (2016). *: Mont Terri Project: Comparison of pore-water investigations conducted by several laboratories on materials from the BDB-1 borehole.* St. Ursanne, Switzerland (in press): Mont Terri Consortium.

Mazurek, M., Oyama, T., Eichinger, F., & De Haller, A. (2013). *Squeezing of Porewater from Core Samples of DGR Boreholes: Feasibility Study.* Toronto, Ontario: Nuclear Waste Management Organization.

Mazurek, M., Oyama, T., Wersin, P., & Alt-Epping, P. (2015). Pore-water squeezing from indurated shales. *Chemical Geology, 400*, 106-121.

McKay, J. L., & Longstaffe, F. J. (2013). Tracking fluid movement during cyclic steam stimulation of Clearwater Formation oil sands using stable isotope variations of clay minerals. *Clays and Clay Minerals, 61*(5), 440-460.

McLelland, J. M., Selleck, B. W., & Bichford, M. E. (2010). Review of the Proterozoic evolution of the Grenville Province, its Adirondack outlier, and the Mesoproterozoic inliers of the Appalachians. In R. P. Tollo, M. J. Bartholomew, J. Hibbard, & P. M. Karabinos, *From Rodinia to Pangea: The Lithotectonic Record of the Appalachian Region: Geological Society of America Memoir 206* pp. 21-49.

Mitchell, J. K., & Soga, K. (2005). *Fundamentals of soil behavior* (Vol. 3). New York: John Wiley & Sons.

Mizota, C., & Lonsgtaffe, F. J. (1996). Origin of Cretaceous and Oligocene kaolinites from the Iwaizumi clay deposit, Iwate, northeastern Japan. *Clays and Clay Minerals, 44*(3), 408-416.

Moll, W. F. (2001). Baseline studies of the clay minerals society source clays: Geological origin. *Clays and Clay Minerals, 49*(5), 374-380.

Moore, D. M., & Reynolds, R. C. (1989). *X-ray Diffraction and the Identification and Analysis of Clay Minerals* (Vol. 332). New York: Oxford Univeristy Press.

Moreau-Le Golvan, Y., Michelot, J.-L., & Boisson, J.-Y. (1997). Stable isotope contents of porewater in a claystone formation (Tournemire, France): assessment of the extraction technique and preliminary results. *Applied Geochemistry, 12*(6), 739-745.

Murseli, S., St-Jean, G., Hanna, D., & Clark, I. (2017). *Method Development: Micro Vacuum-distillation Experiments (µVDE).* Toronto, Ontario: Nuclear Waste Management Organization.

Newman, A., & Brown, G. (1987). The Chemical Constitution of Clays. In *Chemistry of Clays and Clay Minerals*. Mineralogical Society Monograph. 6, 1-128.

Noronha, J. (2016). *Deep Geological Repository Conceptual Design Report Crystalline / Sedimentary Rock Environment.* Toronto, ON: Nuclear Waste Management Organization.

Oerter, E., Singleton, M., & Davisson, L. (2017). Hydrogen and oxygen stable isotope signatures of goethite hydration waters by thermogravimetry-enabled laser spectroscopy. *Chemical Geology, 475*, 14-23.

O'Neil, J. R. (1987). Preservation of H, C, and O isotopic ratios in the low temperature environment. *Stable Isotope Geochemistry of Low Temperature Processes, 13*, 85-128.

O'Neil, J. R., & Kharaka, Y. K. (1976). Hydrogen and oxygen isotope exchange reactions between clay minerals and water. *Geochimica et Cosmochimica, 40*(2), 241-246.

Pavlides, L., Boucot, A. J., & Skidmore, W. B. (1968). Stratigraphic Evidence for the Taconic Orogeny in the Northern Appalachians. In E.-a. Zen, W. S. White, J. B. Hadley, & J. B. Thompson, *Studies of Appalachian Geology: Northern and Maritime* pp. 61-82. Interscience Publishers.

Pearson, F., Arcos, D., Bath, A., Boisson, J., Fernandez, A., Gaebler, H., . . . Waber, H. N. (2003). Geochimistry of water in the Opalinus Clay formation at the Mont Terri Rock Laboratory–Synthesis Report. *Geology Series No. 5*.

Pearson, R. C., Berger, B. R., Kaufmann, H. E., Hanna, W. F., & Zen, E. A. (1988). *Mineral Resources of the Eastern Pioneer Mountains, Beaverhead County, Montana.* United States Geological Survey , Department of the interior. Denver: United States Government Printing Office.

Percival, J. A., & Easton, R. M. (2007). Geology of the Canadian Shield in Ontario: an update. *Ontario Geological Survey*. Open File Report 6196.

Petts, D. C., Saso, J. K., Diamond, L. W., Aschwanden, L., Al, T. A., & Jensen, M. (2017). The source and evolution of paleofluids responsible for secondary minerals in low-permeability Ordovician limestones of the Michigan Basin. *Applied Geochemistry, 86*, 121-137.

Pitts, M. (2017). *Thermal properties of the Cobourg Limestone.* MSc Thesis. Kingston, ON: Queen's University.

Post, J. L., & Plummer, C. C. (1972). The chlorite series of Flagstaff Hill area, California: A preliminary investigation. *Clays and Clay Minerals, 20*(5), 271-283.

Pruett, R. J., & Webb, H. L. (1993). Sampling and analysis of KGa-1 B well-crystallized kaolin source clay. *Clays and Clay Minerals, 41*(4), 514-519.

Qi, H., Coplen, T. B., Gehre, M., Vennemann, T. W., Brand, W. A., Geilmann, H., . . . Longstaffe, F. J. (2017). New biotite and muscovite isotopic reference materials, USGS57 and USGS58, for *δ*2H measurements–A replacement for NBS 30. *Chemical Geology, 467*, 89-99.

Rübel, A. P., Sonntag, C., Lippmann, J., Pearson, F. J., & Gautschi, A. (2002). Solute transport in formations of very low permeability: Profiles of stable isotope and dissolved noble gas contents of pore water in the Opalinus Clay, Mont Terri, Switzerland. *Geochimica et Cosmochimica Acta, 66*(8), 1311-1321.

Reed, S. J. (2005). *Electron microprobe analysis and scanning electron microscopy in geology.* Cambridge University Press, 1-189.

Rivers, T. (1997). Lithotectonic elements of the Grenville Province: review and tectonic implications. *Precambrian Research, 86*(3-4), 117-154.

Rodgers, J. (1971). The Taconic Orogeny. *Geological Society of America Bulletin, 82*(5), 1141-1178.

Rowley, D. B., & Kidd, W. F. (1981). Stratigraphic relationships and detrital composition of the medial Ordovician flysch of western New England: Implications for the tectonic evolution of the Taconic orogeny. *The Journal of Geology, 89*(2), 199-218.

Rule, A. C., & Bailey, S. W. (1987). Refinement of the crystal structure of a monoclinic ferroan clinochlore. *Clays and Clay Minerals, 35*(2), 129-138.

Sacchi, E., Michelot, J. L., Pitsch, H., Lalieux , P., & Aranyossy, J. F. (2001). Extraction of water and solutes from argillaceous rocks for geochemical characterisation: methods, processes and current understanding. *Hydrogeology Journal, 9*(1), 17-33.

Savin, S. M. (1967). *Oxygen and hydrogen isotope ratios in sedimentary rocks and minerals.* PhD Thesis. Calif. Inst. of Tech.

Savin, S. M., & Epstein, S. (1970). The oxygen and hydrogen isotope geochemistry of clay minerals. *Geochimica et Cosmochimica Acta, 34*(1), 25-42.

Savin, S. M., & Lee, M. (1988). Isotopic studies of phyllosilicates In: Hydrous Phyllosilicates. (S. W. Bailey, Ed.) *Reviews in Mineralogy , 19*, 189-223.

Savoye, S., Michelot , J. L., Wittebroodt, C., & Altinier, M. V. (2006). Contribution of the diffusive exchange method to the characterization of pore-water in consolidated argillaceous rocks. *Journal of Contaminant Hydrology, 86*(1-2), 87-104.

Schandl , E. (2009). *Petrography of DGR-1 and DGR-2 Core.* Intera.

Seal, R. R., & Rye, R. O. (1992). Stable isotope study of water-rock interaction and ore formation, Bayhorse base and precious metal district, Idaho. *Economic Geology, 87*(2), 271-287.

Shafer, Z. (2014). *Use of X-Ray Diffraction to Identify and Quantify Soil Swelling Potential.* MSc Thesis. Tempe, AZ: Arizona State University.

Sharp, Z. D., Atudorei, V., & Durakiewicz , T. (2001). A rapid method for determination of hydrogen and oxygen isotope ratios from water and hydrous minerals. *Chemical Geology, 178*(1-4), 197-210.

Sheppard, S. F., & Gilg, H. A. (1996). Stable isotope geochemistry of clay minerals. *Clay Minerals, 31*, 1-24.

Skowron, A., & Hoffman, E. (2009). *XRD Mineralogical Analysis of DGR-1 and DGR-2 Core.* Activation Laboratories Ltd. Ancaster, Ontario: Intera.

Stott, D. F., & Aitken, J. D. (1993). Sedimentary cover of the craton in Canada. *Geological Survey of Canada. Geology of North America no.* 5, 1-826.

Suzuoki, T., & Epstein, S. (1976). Hydrogen isotope fractionation between OH-bearing minerals and water. *Geochimica et Cosmochimica Acta, 40*, 1229-1240.

Swanson, S. (2013). *Deep Geologic Repository Project for Low and Intermediate Level Waste - Submission of Responses to the First Sub-set of Package #8 Information Requests.* Toronto, Ontario: Ontario Power Generation, 1-189.

Tan, K. H., Hajek, B. F., & Barshad, I. (1986). Thermal analysis techniques. In *Methods of Soil Analysis, Part 1 - Physical and Mineralogical Methods* (pp. 151-183).

Taylor, H. P. (1974). The application of oxygen and hydrogen isotope studies to problems of hydrothermal alteration and ore deposition. *Economic Geology, 69*(6), 843-883.

U.S. Dept. of Energy. (2000). *Pioneering, nuclear waste disposal.* Carlsbad, NM, 1-11.

Van Staal, C. R., Whalen, J. B., McNicoll, V. J., Pehrsson, C. J., Zagorevski, A., Van Breemen, O., & Jenner, G. A. (2007). The Notre Dame arc and the Taconic orogeny in Newfoundland *In 4-D Framework of Continental Crust. Hatcher, R. D.*, Carlson Jr., M. P., McBride, J. H., & Martínez Catalán J. R. (Eds), *Geological Society of America Memoirs, 200*, 511-552.

Warr, L. N., & Ferreiro Mählmann, R. (2015). Recommendations for Kübler index standardization. *Clay Minerals, 50*(3), 283-286.

Wells, F. G., Page, L. R., & James, H. L. (1940). *Chromite Deposits of the Pilliken Area, Eldorado County, California. US Geological Survey Mulletin 922-O,* Department of the Interior. Washington: US Government Printing Office, 1-31.

Williams, H. R., Surcliffe, R. H., & Stott, G. M. (1992). *Geology of Ontario.* (P. C. Thurston, Ed.) Ontario Geological Survey, Special Volume 4 (1), 239-277.

Yang, C., Yang, S., & Su, N. (2016). Stable hydrogen and oxygen isotopes in mineral-bound water and the indication for chemical weathering intensity. *Chemical Geology, 441*, 14-23.

Yang, C., Yang, S., & Su, N. (2017). The hydrogen and oxygen isotopic compositions of hydroxyl in clay mineral from a weathering profile: New proxies for paleo-climate change? *Acta Geochimica, 36*(3), 370-373.

Zheng, Y.-F. (1993). Calculation of oxygen isotope fractionation in hydroxyl-bearing silicates. *Earth and Planetary Science Letters, 120*(3-4), 247-263.

Ziegler, K., & Longstaffe, F. J. (2000). Clay mineral authigenesis along a mid-continental scale fluid conduit in Palaeozoic sedimentary rocks from southern Ontario, Canada. *Clay Minerals, 35*(1), 239-260.

Ziegler, K., & Longstaffe, F. J. (2000). Multiple episodes of clay alteration at the Precambrian/Paleozoic unconformity, Appalachian basin: isotopic evidence for long-distance and local fluid migrations. *Clays and Clay Minerals, 48*(4), 474-493.

Appendix A. Clay Size-Fractionation and Cation Saturation

Disaggregated samples were weighed and ~20g placed into a glass 250ml beaker. The beaker was then filled with distilled (DI) water up to the 200ml mark. The sample was then sonicated using a Sonics & Materials. Inc. Vibracell® ultrasonic probe set at 200 Hz for 3 minutes in order to suspend the <2μm size-fraction. Such ultrasonic treatments do not cause isotope exchange between water and clay (Fagan, 2001). Once the mixture was fully agitated, the supernate was decanted into a 1L settling column. This process was repeated 5 times, or until the supernate became clear. Residual material remaining in the beaker was dried at 65°C and archived.

The settling column was capped with a rubber cork and vigorously agitated to resuspend the ~<10μm sediment. It was then left for 22 hours and 11 minutes in order for the >2μm size-fraction to settle below 30cm from the column water surface. This time and distance were calculated using Stoke's Law for 20°C (Equations A.1 & A.2) (Jackson, 1979). These equations were developed for calculating settling time of a spherical object but they serve as an approximation for the settling time of various sizes of clay minerals, which typically have a platy habit (Fagan, 2001).

$$v = \frac{[g(sp-sl)D^2]}{18n} \qquad \text{(Eq. A.1)}$$

or

$$t = \frac{18nh}{g(sp-sl)D^2} \qquad \text{(Eq. A.2)}$$

where:

D= particle diameter (cm)

v= settling velocity (cm/sec) = $h \div t$ (h = height or settling depth, chosen to be 30cm, and t=time)

n= viscosity (poise)

g= gravitational constant (980 cm/s^2)

sp= specific gravity of the particle (2.65)

sl= specific gravity of the liquid (for water at 20°C it is 0.99823)

CMS KGa-1, as well as the OGSR samples from the Cobourg Formation (including the Collingwood Member), were initially difficult to disperse, flocculating readily upon addition to the distilled water in the settling columns. Thus, sodium hexametaphosphate (NaHMP) (40ml of a 0.08M solution) was added as a deflocculant (Chipera & Bish, 2001).

Once the allotted settling time for fully dispersed sample had passed, the <2μm size-fraction remaining in the top 30cm of the water column was siphoned into a 2L beaker using a hose and a U-shaped tube. Once in the 2L beaker, 50ml of bleach (6% sodium hypochlorite (NaClO)) was added to flocculate the <2μm sediment. Once flocculated, the clear bleach/water supernatant was decanted, with care taken not to decant any sediment. This flocculation time could take as long as 48 hours. DI water was then added to the settling column up to the 1L mark and the column again agitated to resuspend any remaining <2μm size-fraction. The process of size-separation was then repeated (typically five times) until the upper 30cm of the settling column became clear. About 150ml of commercial bleach was then added to the 2L beaker following addition of the final aliquot of <2μm material in order to flocculate the clay fraction and facilitate organic matter removal. The bleach/water/sediment (± NaHMP) mixture was then placed, covered, into a water bath at 65°C and left overnight in order to complete oxidation of any organic matter remaining in the sample. Any residue remaining in the settling column was dried (65°C) and archived.

Bleach, any NaHMP and dissolved compounds were then removed from the sediment samples by washing with DI water. To wash the samples, they were centrifuged 6 times at 18000 rpm for 18 minutes in 50ml centrifuge tubes using a Beckman fixed-rotor Avanti J25 centrifuge. Between centrifuge cycles, the supernatant was decanted, DI water was again added to the centrifuge tubes, and the samples sonicated to ensure sediments were thoroughly rinsed and agitated.

To ensure uniform behaviour during hydration of a specific mineral, the clay mixtures were made homoionic (Tan et al., 1986). To do so ~100mg of <2μm samples, once thoroughly cleaned of bleach (± NaHMP), were saturated with 15ml of either 2M $CaCl_2$ (to become Ca-saturated) or 2M KCl (to become K-saturated). After 24 hours, these samples were washed following the same centrifugation procedure used to remove bleach from the samples. An additional original aliquot of the <2μm size-fraction was left untreated, which because of the prior bleaching (±NaHMP), was assumed to be Na-saturated.

Due to elevated carbonate levels in the Cobourg Formation (including the Collingwood Member), as verified through pXRD, 15ml of 6M HCl was added to the samples for 10 minutes in order remove the carbonates (Oerter et al., 2017). Once samples contained little to no carbonates, as verified through pXRD, they were thoroughly cleaned of the HCl, again following the same washing procedures as described above. Due to cation exchange affinity, those clays thus became H-saturated.

Samples were then frozen and freeze-dried and the <2μm size-fraction was weighed. Approximately 15mg of Ca- and K-saturated samples were sonicated in a bath with 0.5 ml of DI water and subsequently deposited by pipette onto labeled glass slides to establish a preferred orientation of clay minerals for pXRD analysis. Likewise, ~30mg of Ca-saturated <2μm was

back-packed into an Al-sample holder to establish a random orientation of clay particles for pXRD analysis.

Appendix B. TGA Repairs

In June of 2006 the Linseis 81 Thermogravimetric Analyzer – Differential Thermal Analyzer (TGA-DTA) stopped displaying weight loss and DTA curves. Efforts to resolve these issues throughout July 2006 and again in February 2007 were unsuccessful. Ten years later, in May of 2016, I began my position of Research/Technical Support 1 at The University of Western Ontario (UWO). Part of my position included repairing the TGA-DTA. The first steps taken to solve the issue was to contract help from the Linseis directly. Graham Hughes, the Canadian Linseis representative came to the University of Western Ontario to replace the computer system that drove the TGA-DTA, transfer over the old software, and modify it to accommodate a newer version of Windows. Alas, these upgrades did not fix the system, and the TGA weight loss and DTA patterns continued to be unresponsive flat lines.

The following first steps were then taken in order to rejuvenate the system:

1. Re-reading all manuals for our specific system and newer ones, to establish proper familiarity with all circuitry and systems, and
2. Cleaning and dusting of all hardware (focusing on the amplifier), and re-plugging all circuitry.

The system remained unresponsive. The electronic recorders of the system did not display any movement at all even when the weighing arm was moved mechanically.

The following steps were taken next:

1. The unit's amplifier was sent to the Chemistry Department's Electronics Shop Manager for a closer look at the circuitry. The Electronics Shop identified a few issues: (a) a reversed circuit, leading to a setting to be on/off instead of off/on, and (b) a mis-

calibrated dial, which led to the display of one reading while the amplifier was actually at a different setting.

2. Once these issues were fixed, the amplifier was reconnected and more tests made. The first test done was gently lifting and lower the weighing arm to see if the computer cursor display recognized movement of the arm. The system now did recognize movement. However, this recognition was limited to only maximum and minimum weights. This meant that the system could identify beam movement but not any variations in the extent of that movement. This suggested that communication between the amplifier and the computer was flawed. This communication error could have been: (a) the message from the old amplifier was not being translated properly to the new computer and software, and/or (b) the message being sent from the old amplifier to the new computer and software was corrupted.
3. To identify which of these possibilities was the case, the amplifier was re-sent to the Electronics Shop Manager for a closer look at the circuitry. The Electronic shop identified a blown circuit. This blown circuit caused the weight loss signal to become destructive instead of constructive, therefore erasing the signal produced by the amplifier during analysis before it was sent to the computer software.
4. This circuit was replaced, and the amplifier was again re-connected to the system and tested. The system then displayed movement over the full range of positions from minimum to maximum.
5. The system was then manually re-calibrated for a new weight system. Custom-fabricated weights were placed on the counterbalanced weighing arm and the TGA portion of the system was able to tare properly. Using the old software for purposes of direct

comparison, test standards were then analyzed and the results matched well with the same material analyzed 10 years prior to the TGA-DTA failure (see Appendix C, Figure C.2).

6. The DTA signal unfortunately remains not fully operational, for reasons as yet not understood.
7. The original TGA-DTA system was purchased with the capability of analyzing samples under vacuum. Due to ageing and degradation of its O-rings and O-ring grease, this was no longer the case. Testing of the vacuum revealed that the system was fully open to the atmosphere. New O-rings were purchased, greased, and replaced. In addition, custom flanges were fabricated at Western's Earth Sciences Machine Shop in order to further limit the volume of the system and leaks at joints.
8. Vacuum was re-established in early 2018. For test samples analyzed under vacuum, the weight loss patterns were comparable to previous results, although there was a minor, previously unrecognized apparent weight loss trough in the first 200°C of each analysis when data was collected and processed using the old software. The cause of this small difference is still unclear, but it may be related to the age of the instrument (Linseis Thermal Analysis, 2018), and/or the repairs to the systems amplifier, which may have changed its signal linearity at low temperatures.
9. When data collection and processing were completed using the new software, the minor, apparent weight-loss trough in the first 200°C was greatly diminished. An explanation may be that background (null) weight calculations are more accurately performed using the new software, which can better account for fluctuations in the low-temperature signal linearity of the amplifier.

10. In February 2018, the quartz glass weighing arm was broken. The arm was repaired by in Western's Chemistry Department glass blowing shop. Test samples analyzed after the repair match those from before the breakage.

Appendix C. Introduction to Powder X-ray Diffraction (pXRD) and Thermogravimetric Analysis (TGA)

C.1.1. An Introduction to X-ray Diffraction Analysis

All atoms in a crystal are arranged in a definite three-dimensional manner; this theoretical, ordered arrangement of points in space, about which atoms or groups of atoms can be arranged, is called a lattice (Hendricks, 1942; and references therein). The location of the atoms within the lattice are called lattice points (Moore & Reynolds, 1989). Lattice points can then be arranged in a variety of way and form planes whose orientations and directions in the crystal system can be named using Miller indices (Shafer, 2014). The (001) Miller Indices are especially important to clay mineralogy because of their generally indicative nature of different clay mineral groups, which are characterized by the size of the spacing (in nm) between successive basal planes. The intensity of the basal diffraction (001) in oriented samples is also the largest due to close packing of atoms in such planes (Mitchell & Soga, 2005). This information is at the root of the classification and identification of clay minerals by X-ray diffraction (Moore & Reynolds, 1989).

X-ray diffraction analysis involves placing the sample in the path of an X-ray beam (incident beam) of a known radiation. The sample is situated on a stage that moves at a fixed rate (e.g., one-degree theta (θ) per minute) whereas the radiation counting device that measures the radiation scattered from the sample moves at twice the rate of the stage (e.g., 2θ per minute). During the analysis, the X-ray beam travels to each atomic plane in the sample, a portion of the beam is absorbed by the atoms, and subsequently re-radiated (scattered) in all directions (Shafer, 2014). Some of this scattered radiation is in phase with the source radiation and can be observed

as a diffraction of the incident beam; this in-phase ‘diffraction’ is then intercepted by a radiation counting device (Figure C.1).

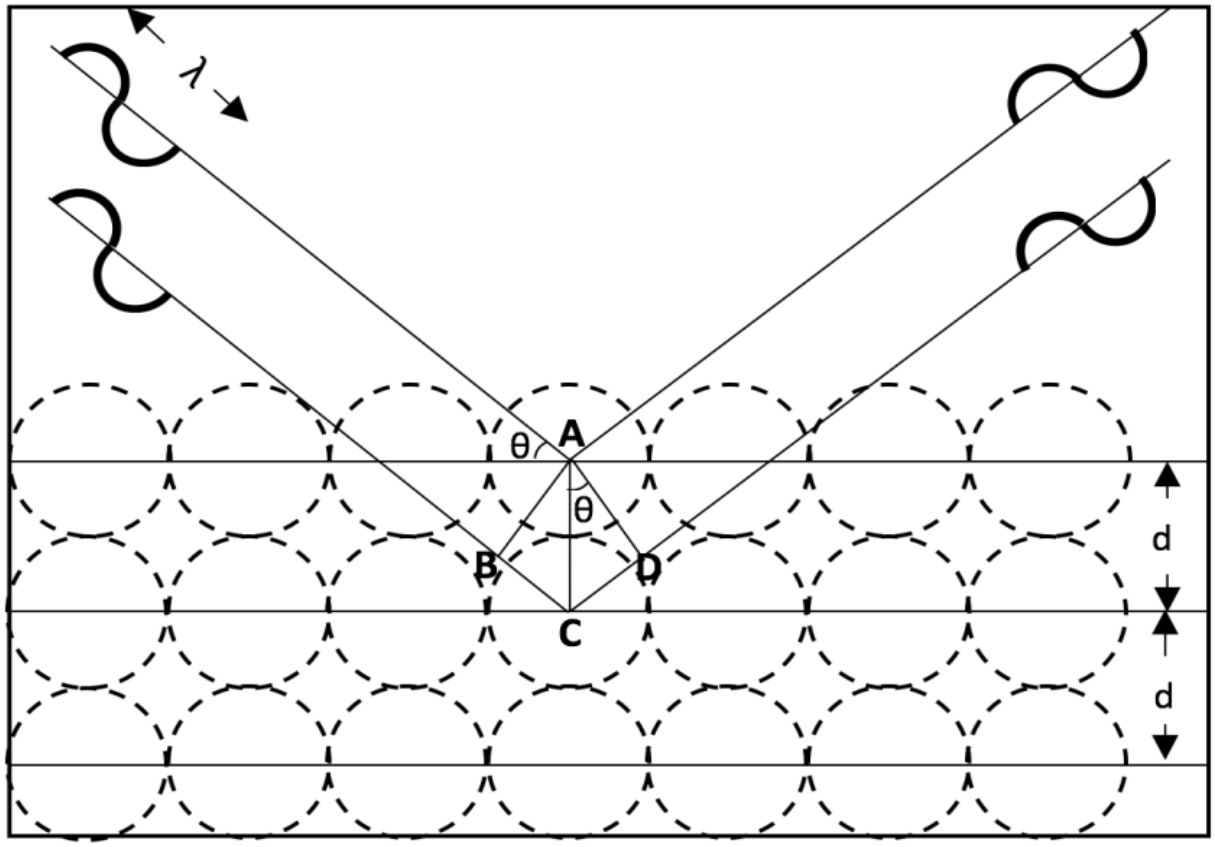

Figure C.1. Diagram of pXRD. Modified from Shafer (2014).

For incident and diffracted rays to be in phase depends on the wavelength of the incident X-rays, as well as the spacing between atomic planes (Eq. C.1-C.5) (Mitchell & Soga, 2005). Bragg’s Law relates the wavelength of the radiation (λ), the angle of the incident beam with respect to the parallel planes (which cause the diffraction) (θ), and the spacing between the two planes (d) (Moore & Reynolds, 1989). These parameters are illustrated in Figure C.1, where parallel beams of X-rays intersect parallel atomic planes. The wavelength of the incident and diffracted beams, when diffracted from two different parallel plans, can be in phase. This occurs,

if and only if, the added path distance between two-parallel rays differs by an integer number of wavelengths; that is to say, from Figure C.1:

$$\overline{BC} + \overline{CD} = n\lambda \quad \text{where n} \in \mathbb{N} \qquad \text{(Eq. C.1)}$$

Due to symmetry, we know:

$$\overline{BC} = \overline{CD} \qquad \text{(Eq. C.2)}$$

Following trigonometry, it can be further deduced that:

$$\overline{CD} = d \sin\theta \qquad \text{(Eq. C.3)}$$

Therefore:

$$2d \sin\theta = n\lambda \qquad \text{(Eq. C.4)}$$

Equation C.4 is also known as Bragg's Law.

Bragg's Law is at the center of mineral identification using X-ray diffraction, as every mineral has its own unique three-dimensional array of atomic spacings. As a result, the specific angles that cause in-phase diffraction, which is a measure of atomic spacing between parallel planes, can be used to differentiate and identify a particular crystal structure (Mitchell & Soga, 2005).

Due to the nanometer (nm) dimensions of most clay minerals, examining a single crystal is difficult and thus oriented aggregates of particles are typically used instead. This method capitalizes on the platy nature of clays, which facilitates efforts to created oriented samples for powder X-ray diffraction (pXRD) analysis. As stated above, Bragg's Law requires *n* to be any natural number. If $n = 1$ then the equivalent diffraction is termed the *first-order basal diffraction*. As an example, if the first order basal diffraction of a clay mineral is given by $d_{(001)} = 1.0$nm, then the second-order diffraction ($n = 2$) will be $d_{(002)} = 0.50$nm, followed by third-order

diffraction (n = 3) at $d_{(003)}$ = 0.333nm, and so on, as long as the intensity is detectable by the radiation counting device. When n > 1 the correlating diffractions are referred to as *higher-order diffractions*, although they do not realistically depict atomic spacing between planes. These orders simply represent values of:

$$\frac{d}{n} = \frac{\lambda}{2 \sin \theta} \quad \text{for n} > 1 \text{ where n} \in \mathbb{N}. \qquad \text{(Eq. C.5)}$$

C.1.2. An Introduction to Thermogravimetric Analysis

C1.2.1. Temperature-dependent Weight Losses and Phase Changes

Thermogravimetric analysis (TGA) is one within a broad category of measuring methods that determine physical parameters, including energy, weight, dimensions, and evolved volatiles, as a dynamic function of temperature (Tan et al., 1986). Most geologic samples show numerous reactions once heated, and the rates at which these reactions occur can be diagnostic. Lower temperature reactions include loss of adsorbed water (dehydration). Slightly higher temperatures reactions include oxidation of organic compounds and metallic ions originally occurring in a reduced state (Tan et al., 1986). Still higher temperature reactions include dehydroxylation (loss of crystal-structure hydroxyl groups [$(OH)^-$] as water) and devolatilization of carbonate minerals, which releases carbon dioxide (CO_2).

There are a variety of types of water in geologic samples in addition to free porewater. One of these varieties is adsorbed water. Water molecules are located either completely on the external surfaces of the clay layers (e.g., kaolinite) or on the external and internal surfaces of the clay layers (e.g., smectite). The majority of water molecules align themselves into a mono or di-molecular layers on the surface of the oxygen atoms on the clay surfaces, or they group around exchangeable ions. Minor amounts of water molecules may also be present in cavities in clay tetrahedral sheets. In clay minerals, adsorbed water is generally driven off within the first 200°C,

but for some phases, interlayer water is not lost completely until 400°C. Such removal of H_2O molecules is classified as dehydration. Depending on the type of clay mineral, dehydration may be reversible (Tan et al., 1986). Another type of water is 'structural' water, which occurs as hydroxyl groups ($(OH)^-$). Hydroxyl groups occur in fixed positions in clay minerals, as a part of continuous octahedral sheets (Tan et al., 1986). Upon hydroxyl removal (termed dehydroxylation) the clay mineral structure is irreversibly changed or destroyed in most instances. While dehydroxylation reactions generally occur between 500-1000°C. structural water can begin to be lost at or slightly below 400°C but is generally is not completely removed until >800°C (Mitchell & Soga, 2005).

New mineral phases can also form upon heating, either from structures previously destroyed during lower temperature heating or from amorphous material. These reactions typically occur at >800°C. Certain crystal structures can also change forms at specific temperatures. For example, when quartz is heated to 537°C it changes from its α form to its denser β form. The intensity of the peak at this temperature seen on thermograms is directly proportionate to the amount of quartz in the sample, which can be a helpful diagnostic when examining <2μm size-fractions dominated by clay minerals.

C1.2.2. Analytical Procedure for Thermogravimetric Analysis

TGA is performed by heating a sample, generally together with a thermally inert substance at a constant rate (commonly 10°C/min) to 900-1000°C or higher while continuously measuring weight loss. In the present study, an empty crucible was utilized in place of an inert substance (Brindley & Brown, 1980; Guggenheim & Van Groos, 2001; Mitchell & Soga, 2005). Also, in the present study, organic matter and carbonate minerals were removed from the clay size-fraction (<2μm) prior to TGA in order to focus on clay-related water-loss reactions.

TGA of Calcium Monohydrate Standard at Atmosphere (in air) and under vacuum (in vacuo)

During this research, TGA analyses were conducted both at atmosphere (in air) and also under vacuum (*in vacuo*). A reference calcium oxalate monohydrate ($CaC_2O_4 \bullet H_2O$) standard was analyzed several times under both conditions. Virtually identical patterns were obtained for this standard when analyzed in air before (e.g., 2006) and after the repairs (2016-2019) described in Appendix B. Figure C.2 illustrates results obtained for the $CaC_2O_4 \bullet H_2O$ standard during this project, once repairs had been completed to the TGA.

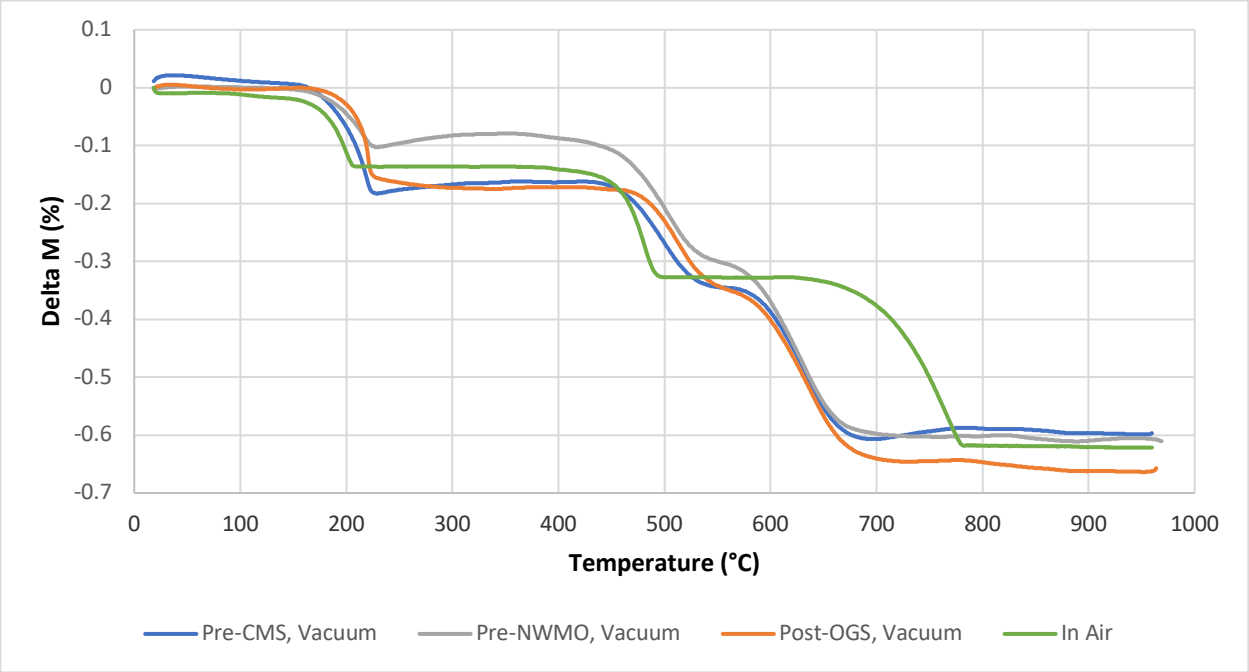

Figure C.2. TGA curves for the $CaC_2O_4 \bullet H_2O$ standard after repairs to the TGA. Change in sample weight is shown on the y-axis. The pattern labelled "Pre-CMS, Vacuum" was measured just prior to the analyses of the CMS Source Clays; the "Pre-NWMO, Vacuum" pattern was obtained just prior to analysis of the NWMO samples, and the "Post-OGS, Vacuum" pattern was obtained just after analysis of the OGS samples. The 'In Air' pattern demonstrates the difference in standard (and hence potentially sample) thermal behaviour, depending on the atmosphere in the TGA chamber.

Appendix D

Table D.1. Oxygen isotope results for structural oxygen in the <2µm samples.

Sample	$\delta^{18}O$ ‰ VSMOW	Yield µmoles/mg
KGa-1 K <2µm	+20.60	*17.33*
KGa-1 K <2µm	+20.36	*18.29*
KGa-1 K <2µm	+21.54	*18.44*
KGa-1 K <2µm	+20.18	*18.36*
IMt-1 K <2µm	+14.32	*14.76*
IMt-1 K <2µm	+13.78	*16.48*
IMt-1 K <2µm	+14.79	*14.88*
IMt-1 K <2µm	+14.81	*14.98*
CCa-1 K <2µm	+3.64	*15.45*
CCa-1 K <2µm	+3.19	*14.86*
CCa-1 K <2µm	+3.60	*14.59*
CCa-1 K <2µm	+3.67	*14.91*
NWMO DGR3 459m K <2µm	+16.60	*14.80*
NWMO DGR3 459m K <2µm	+17.03	*15.81*
NWMO DGR3 459m K <2µm	+17.00	*15.68*
NWMO DGR3 459m K <2µm	+18.71	*12.23*
NWMO DGR3 459m K <2µm	+16.07	*14.71*
NWMO DGR3 523m K <2µm	+15.57	*14.58*
NWMO DGR3 523m K <2µm	+15.75	*14.80*
NWMO DGR3 523m K <2µm	+15.00	*15.42*
NWMO DGR3 523m K <2µm	+14.77	*16.18*
NWMO DGR2 530m K <2µm	+14.73	*14.75*
NWMO DGR2 530m K <2µm	+14.58	*16.14*
NWMO DGR2 530m K <2µm	+14.79	*15.32*
NWMO DGR2 530m K <2µm	+14.85	*15.50*
NWMO DGR2 616m K <2µm	+14.17	*14.64*
NWMO DGR2 616m K <2µm	+13.98	*16.23*
NWMO DGR2 616m K <2µm	+14.96	*16.02*
NWMO DGR2 616m K <2µm	+14.17	*14.99*
OGS DHN1 129m K <2µm	+16.19	*15.07*
OGS DHN1 129m K <2µm	+16.04	*15.63*
OGS DHN1 129m K <2µm	+15.65	*14.78*
OGS DHN1 129m K <2µm	+15.98	*15.04*
OGS SG11-02 327m K <2µm	+14.81	*15.86*

OGS SG11-02 327m K <2μm	**+14.73**	*15.15*
OGS SG11-02 327m K <2μm	**+15.65**	*14.98*
OGS SG11-02 477 K HCl <2μm	**+13.82**	*13.54*
OGS SG11-02 491 K HCl <2μm	**+15.31**	*15.71*

Results in red are excluded from further consideration due to analytical challenges including overheating, underheating and/or system leaks during analysis

Table D.2. Hydrogen isotope composition of clay mineral structural hydrogen from torching and TC-EA methods.

Methodology	Torching *Untreated		TC-EA *Untreated	Torching **Light Water		TC-EA **Light Water	Torching ***Heavy Water		TC-EA ***Heavy Water
Sample	δ^2H (‰) VSMOW	Yield µmoles/mg	δ^2H (‰) VSMOW	δ^2H (‰) VSMOW	Yield µmoles/mg	δ^2H (‰) VSMOW	δ^2H (‰) VSMOW	*Yield µmoles/mg*	δ^2H (‰) VSMOW
KGa-1 K <2µm	–58.4	*6.58*	–47.4						
KGa-1 K <2µm	–55.3	*6.69*	–48.6						
IMt-1 K <2µm	–100.6	*2.12*	–103.3	–90.8	*1.57*	–103.7			
IMt-1 K <2µm	–97.8	*1.99*	–104.5	–96.9	*1.83*	–104.2			
IMt-1 K <2µm			–100.2	–92.0	*1.46*				
CCa-1 K <2µm	–83.9	*4.49*							
OGS DHN1 129m K <2µm	–58.1	*2.06*	–58.2						
OGS DHN1 129m K <2µm	–66.1	*2.01*	–54.5						
OGS SG11-02 327m K <2µm	–43.5	*2.27*	–57.9						
OGS SG11-02 327m K <2µm	–61.4	*2.28*	–56.8						
OGS SG11-02 477m K <2µm	–28.6	*1.14*	–73.5						
OGS SG11-02 477m K <2µm			–102.7						
OGS SG11-02 491m K <2µm			–68.7						
OGS SG11-02 491m K <2µm			–66.6						
NWMO DGR3 459m K <2µm	–62.9	*1.67*	–55.8	–62.0	*1.22*	–62.9	–65.6	*1.73*	–45.9
NWMO DGR3 459m K <2µm	–65.7	*1.75*		–70.0	*1.39*	–62.7	–63.0	*1.46*	–46.2
NWMO DGR3 459m K <2µm				–46.3	*1.43*				

NWMO DGR3 459m K <2μm				**–54.4**	*1.17*				
NWMO DGR3 459m K <2μm				–59.6	*0.32*				
NWMO DGR3 523m K <2μm	–78.9	*2.10*	**–60.9**	**–67.7**	*1.71*	**–68.5**	**–56.3**	*1.40*	**–31.4**
NWMO DGR3 523m K <2μm	**–61.3**	*2.04*	**–62.3**	–52.2	*1.73*	**–67.6**	**–58.9**	*1.42*	**–37.4**
NWMO DGR3 523m K <2μm	**–69.2**	*2.10*		**–69.2**	*1.35*		**–60.6**	*0.88*	
NWMO DGR3 523m K <2μm	–108.2	*1.61*					–55.6	*0.42*	
NWMO DGR3 523m K <2μm	**–70.6**	*2.04*							
NWMO DGR3 523m K <2μm	**–61.4**	*1.71*							
NWMO DGR2 530m K <2μm	**–70.3**	*2.62*	**–59.7**	**–53.3**	*1.93*	**–56.5**	**–62.5**	*1.92*	**–46.6**
NWMO DGR2 530m K <2μm	–52.5	*2.37*	**–57.2**	**–56.9**	*2.06*	**–57.5**	**–62.1**	*2.54*	**–47.7**
NWMO DGR2 530m K <2μm	**–68.5**	*2.34*	**–58.8**	**–67.1**	*1.74*		**–62.1**	*1.78*	
NWMO DGR2 530m K <2μm	**–61.2**	*2.02*							
NWMO DGR2 616m K <2μm	**–65.2**	*2.40*	**–56.5**	**–62.8**	*1.65*	**–65.6**	**–51.7**	*1.87*	**–46.5**
NWMO DGR2 616m K <2μm	**–59.8**	*2.30*	**–55.7**	**–62.5**	*1.53*	**–66.1**	**–65.2**	*1.60*	**–47.0**
NWMO DGR2 616m K <2μm	**–65.9**	*2.18*					**–59.5**	*1.85*	
NWMO DGR2 616m K <2μm	**–70.2**	*2.08*							

**Untreated: no isotopic exchange with water vapour attempted*
***Light Water: allowed to exchange with δ^2H water = –309±5‰*
****Heavy Water: allowed to exchange with δ^2H = +810±3‰*
Results in red are excluded from further consideration due to analytical challenges including overheating, underheating, incorrect yields, and/or system leaks during analysis.